GOLD MINERALIZATION AND PRECAMBRIAN GEOLOGY OF THE HOPEWELL AREA, RIO ARRIBA COUNTY, NEW MEXICO

by

ISAAC OPOKU BOADI

Thesis Submitted in Partial Fullfillment
of the Requirements for the Degree of
Masters of Science in Geology

New Mexico Institute of Mining and Technology
Socorro, New Mexico.

January, 1986

Dedicated to my brother

E. Oppong Dwamenah, and to my daughter

Barbara Sikayena Boadi.

ABSTRACT

The Moppin Metavolcanic Series, the Burned Mountain metarhyolite, and a succession of quartzose meta-sediments comprise the Precambrian supracrustal succession in the Hopewell area. The Moppin Metavolcanic Series is the oldest unit in the succession and consists mainly of a mixture of volcanic and volcaniclastic rocks that are interpreted, based on their composition, relict textures, and trace element chemistry, to constitute a continuous calcalkaline volcanic suite containing basalts, andesites, and dacite. The series is comparable to modern volcanic suites which form along converging plate margins.

The petrography and trace element chemistry of the next youngest unit, Burned Mountain metarhyolite suggest that it is an ash flow tuff with the composition of a rhyolite. The basal conglomeratic portion of the metasedimentary rocks which constitute the youngest supracrustal unit formed by accumulation of detrital material derived from the Burned Mountain metarhyolite and the uppermost, felsic portion of the Moppin Metavolcanic Series. Overlying the conglomerate is a 1 km-thick Ortega quartzite that was deposited during a long period of quiescence in a shallow marine environment.

The granite of Hopewell Lake, which intrudes the Moppin Metavolcanic Series, was derived either directly, from a depleted mantle source, or indirectly, from the partial

melting of a source rock that was, itself, originally derived from the mantle and which had experienced a short crutsal residence.

All of the Precambrian rocks have been regionally metamorphosed to the greenschist facies and have been subjected to polyphase deformation resulting in three generations of folds and related metamorphic fabrics.

Gold mineralization in the Hopewell area is hosted by both mafic and felsic members of the Moppin Series. Gold values in the altered Moppin rocks commonly range from 1 to 10 ppm; one sample from the intensely altered zone at the Croesus mine contained 1160 ppm of gold. In the unaltered rocks, values range from 0.1 to 4 ppb. The gold mineralization occurs in two forms: quartz and quartz - carbonate veins, and massive, sulphide-bearing veins and replacement bodies. Veins range from a few centimetres up to 30 cm in width and can be traced for several metres along strike; replacement bodies have similar dimensions. The quartz and quartz-carbonate veins generally occur in the the more felsic members of the series, and have limited alteration haloes. The massive, sulphide-bearing replacement bodies are restricted to the mafic (and typically more altered) rocks where they commonly display broad pyritic haloes.

Pyrite, chalcopyrite, sphalerite, galena, and specular hematite constitute the common assemblage in the ore zone. Minor amounts of arsenopyrite and stibnite are present, although they may not be visually discernible. Native gold is associated with the chalcopyrite and pyrite, and occurs either as disseminations or as microveinlets within these sulphide phases. Later hypogene hematite commonly mantles grains of chalcopyrite, pyrite, and gold. Sphalerite and galena also appear to be late; they show no correlation with the gold, silver, or chalcopyrite.

Carbonate and sodic alteration are the dominant alteration types. Carbonates are predominantly dolomitic or sideritic. Dolomite occurs as porphyroblasts in the less altered rocks and is interpreted to predate the mineralization. Siderite is closely associated with the mineralization. The sodic alteration is present only in the granite. Other alteration minerals in the area include sericite, silica, and chloritoid.

Fluid inclusion data indicate that gold deposition took place from a CO_2- rich medium during unmixing of the CO_2 phase over a temperature range of 250 - 330^{o}C and at pressures of approximately 1.5 kb.

The gold mineralization is related to the intrusion and subsequent alteration (deuteric?) of the granite of Hopewell Lake at about 1467 Ma. Initial $^{87}Sr/^{86}Sr$ ratios suggest

that the mineralizing fluids, and possibly the gold, were derived more-or-less directly from a depleted mantle source.

ACKNOWLEDGEMENT

This study was funded, in part, by the New Mexico Bureau of Mines and Mineral Resources, New Mexico Geological Society, Anaconda Minerals, and Sigma Xi. I am thankful to these institutions and also to members of my advisory committee and Mrs Lynn Brandvold who, together, arranged to obtain this support.

I gratefully acknowledge the considerable interest shown in this project by the co-chairmen of my advisory committee: Dr. David I. Norman and Dr. James M. Robertson, and also the various forms of support that I received from them. I extend sincere gratitude to Dr. Andrew Campbell, not only as a member of my advisory committee, but also for his invaluable input into the thesis, especially the section on fluid inclusion studies.

Mike Willams and Stewart Smith went out to the field with me a number of times; I learned a great deal about the regional geology of the Tusas Mountains from the many discussions I had with them. Joan Gableman helped in drafting the geologic map. I would like to thank Paul Bauer and Stewart Smith for their time and effort in grooming me for the thesis defense. Fellow graduate students in geoscience have been very supportive in diverse ways, and I would like to thank them all.

I am thankful to Dr. Nathanniel Richardson Jr. of Geoservices Inc., Liberia, and to Mr. Kenneth Ross of Bentley Int., without whose assistance I could not have come to the United States to further my education.

Finally, I wish to express my warmest appreciation and gratitude to my wife, Cynthia, who kept our "home" together all this while that I have been away.

TABLE OF CONTENTS

	Page
ABSTRACT	i
Acknowledgement	v
INTRODUCTION	1
Purpose	1
Regional Geology	2
Location	2
Precambrian Rocks	2
Structure and Metamorphism	6
Phanerozoic Rocks	8
Method of Investigation	8
PRECAMBRIAN GEOLOGY OF THE HOPEWELL AREA	10
LITHOLOGIES	10
Moppin Series	10
Quartz-chlorite-plagioclase schist	10
Quartz-chloritoid-sericite schist	12
Carbonate schist	13
Quartz-sericite schist	13
Burned Mountain meta-rhyolite	18
Metasediments	18
Metaconglomerates	20
Ortega quartzite	22
Plutonic Rocks	22

STRUCTURE 31
Folding 31
Foliation 33
Lineation 33
METAMORPHISM 38
GEOCHEMISTRY 41
Major and trace element chemistry 41
Rb-Sr systematics 47
GOLD MINERALIZATION 54
Gold analyses 54
Geology 57
Alluvial Prospects 57
Lode Mineralization 58
Supergene alteration 64
Hydrothermal alteration 66
Paragenesis 70
FLUID INCLUSION STUDIES 72
Analytical procedures 72
Inclusion petrography 73
Thermometric data and other experimental observations 78
Synthesis and interpretation of data 88
Estimation of pressure of entrapment 92
Pressure correction 95
DISCUSSION 96
Protoliths of major rock types and geologic setting 96
Timing of mineralization 97
Nature of mineralizing fluid and possible source 98
Migration of fluids 100

Source of metals 100

Controls of deposition 101

Genetic model 103

Type comparison 104

CONCLUSIONS 106

REFERENCES 108

APPENDIX A: 112

APPENDIX B: 116

APPENDIX C: 122

APPENDIX D: 123

LIST OF PLATES

1	Geologic map	in pocket
2	Cross Section	in pocket

LIST OF TABLES

1	Precambrian Rock Nomenclature, Northern Tusas Mountains	5
2	Modal Analyses of Samples of the Granite of Hopewell Lake	28
3	Chemical Analysis of Precambrian rocks from the Hopewell Area	42
4	Whole Rock Rb-Sr Isotopic Analyses	48
5	Pearson Correlation Coefficient Matrix	56
6	Paragenesis of the alteration and mineralization event in the Hopewell Mining Area	71

LIST OF FIGURES

1	Location map	3
2	Photomicrograph of carbonate schist	14
3	Rosettes of chloritoid in carbonate schist	15
4	Photomicrograph of quartz-sericite schist	17
5	Photomicrograph of the Burned Mountain metarhyolite	19
6	Photomicrograph of metaconglomerate	21
7	Photomicrograph of Ortega quartzite	23
8	Photograph of cross bedding in the vitreous Ortega quartzite	24
9	Photomicrograph of the granite of Hopewell Lake	27
10	Photograph of lenses of granite of Hopewell Lake in the mafic unit of the Moppin Metavolcanic Series	30
11	Classification of granite and allied rocks based upon modal composition in volume %	29
12	Photograph of minor fold in the Ortega quartzite	32

13	Photomicrograph of quartz-chlorite-plagioclase schist showing S_2 foliation crenulated by later domain cleavage	34
14	Stereographic projection of poles to the dominant foliation in the Hopewell area	35
15	Stereographic projection of extension lineations measured in the Moppin Metavolcanic Series	37
16	Photomicrograph of the Ortega quartzite	39
17	Normative plot of samples of the granite of Hopewell Lake on the An-Ab-Or ternary diagram of Barker	44
18	Zr/TiO_2 versus Nb/Y plot of samples of the metavolcanic rocks from the Hopewell area	45
19	Rb-Sr isochron diagram	50
20	Evolution diagram	51
21	Distribution of gold in rocks of the Hopewell area	55
22	Photograph of quartz-carbonate vein along S_2	58
23a	Photomicrograph of the ore showing gold grains in chalcopyrite	62
23b	Photomicrograph of ore showing gold grains mantled by specular hematite	63
24	Photograph of oxidation zone at the Croesus Mine showing supergene minerals coexisting with primary sulphide phases	64
25	Alteration types and their distribution	67
26	Photograph of fragmented siderite vein cemented by mineralized quartz vein	69
27	Photomicrograph of type 1, 2-phase aqueous inclusion	74
28	Photomicrograph of type 2, single-phase CO_2 liquid inclusion	76
29	Photomicrograph of type 3, 3-phase inclusion	76
30	Photomicrograph of type 3 inclusions showing CO_2-rich and aqueous-rich inclusions	77
31	Histogram of homogenization temperatures (i), and salinites (ii) of type 1 inclusions	80

32 Photomicrographs documenting phase changes in type 2 and 3 inclusions 81

33 Histograms of phase changes in type 2 and 3 inclusions 82

34 Homogenization temperature versus Density plot for the CO_2 system 84

35 Histogram of measured densities of type 2 and 3 inclusions 84

36 A quantatitive isothermal density - internal pressure diagram for coexisting CO_2 and H_2O fluids at +40°C 87

37 A polythermal $V_B - X_{H_2O}$ diagram with tie lines for coexisting CO_2 fluids and $2H_2O$-rich liquid 88

38 Empirical solvus plot for $CO_2 - H_2O$ inclusions with salinities ranging from 7.2 to 11.8 equi. wt. % NaCl (inset: solvus plot of Hendel and Hollister, 1981 for inclusions with 2.6 equi. wt. % NaCL in solution) 90

39 Histograms of salinities of type 3 inclusions 91

40 Solubility of CO_2 in a) 6 wt. % NaCl solution and, b) 20 wt. % NaCl solution at high temperatures and pressures 93

41 Histogram of estimated trapping pressures of inclusions in this study 94

INTRODUCTION

The discovery of several gold placers in the Hopewell district during the 1880's initiated lode gold exploration in the area. Rich pockets of oxidized ores were found but were rapidly mined out. Since the lower grade unoxidized ore could not be worked at the time, interest in the district ceased (Bingler, 1968). Although the mineralization is well-documented in the literature (Bingler, 1968; Graton, 1910; Gibson, 1981), there has been no detailed investigation.

Purpose

This study focuses on the gold mineralization in the Hopewell district. Its main objectives are to

1) Identify and describe the different rock types in the area of mineralization;

2) Determine the distribution of gold and associated elements in the district, and ascertain whether the unmineralized rocks were anomalously high in these elements;

3) Study the types of alteration and how they relate to mineralization;

4) Examine polished sections of the ore to determine the textural relationship between the ore mineral phases in order to establish the mineral paragenesis;

5) Study fluid inclusions from selected samples to determine the nature of the mineralizing fluids and, the temperature and pressure at which the mineralization formed;

6) Determine the age of mineralization;

7) Formulate a genetic model for the mineralization.

REGIONAL GEOLOGY

The Hopewell district is located in eastern Rio Arriba County, about 32 km west of Tres Piedras on US Highway 64 (Fig. 1). It covers a surface area of approximately 3.5 sq. km and lies within latitude 36^{o} 41' to 36^{o} 42.5' and longitude 106^{o} 13.5' to 106^{o} 15'. The district occurs in the northern Tusas Mountains area which is underlain by crystalline rocks of Precambrian age, volcanic and clastic rocks of Tertiary age, and Quaternary glacial and other unconsolidated deposits.

Precambrian rocks

The Precambrian rocks consist of a heterogeneous series of mafic to felsic volcanic and volcaniclastic rocks, immature and mature sediments, and granitic intrusions which

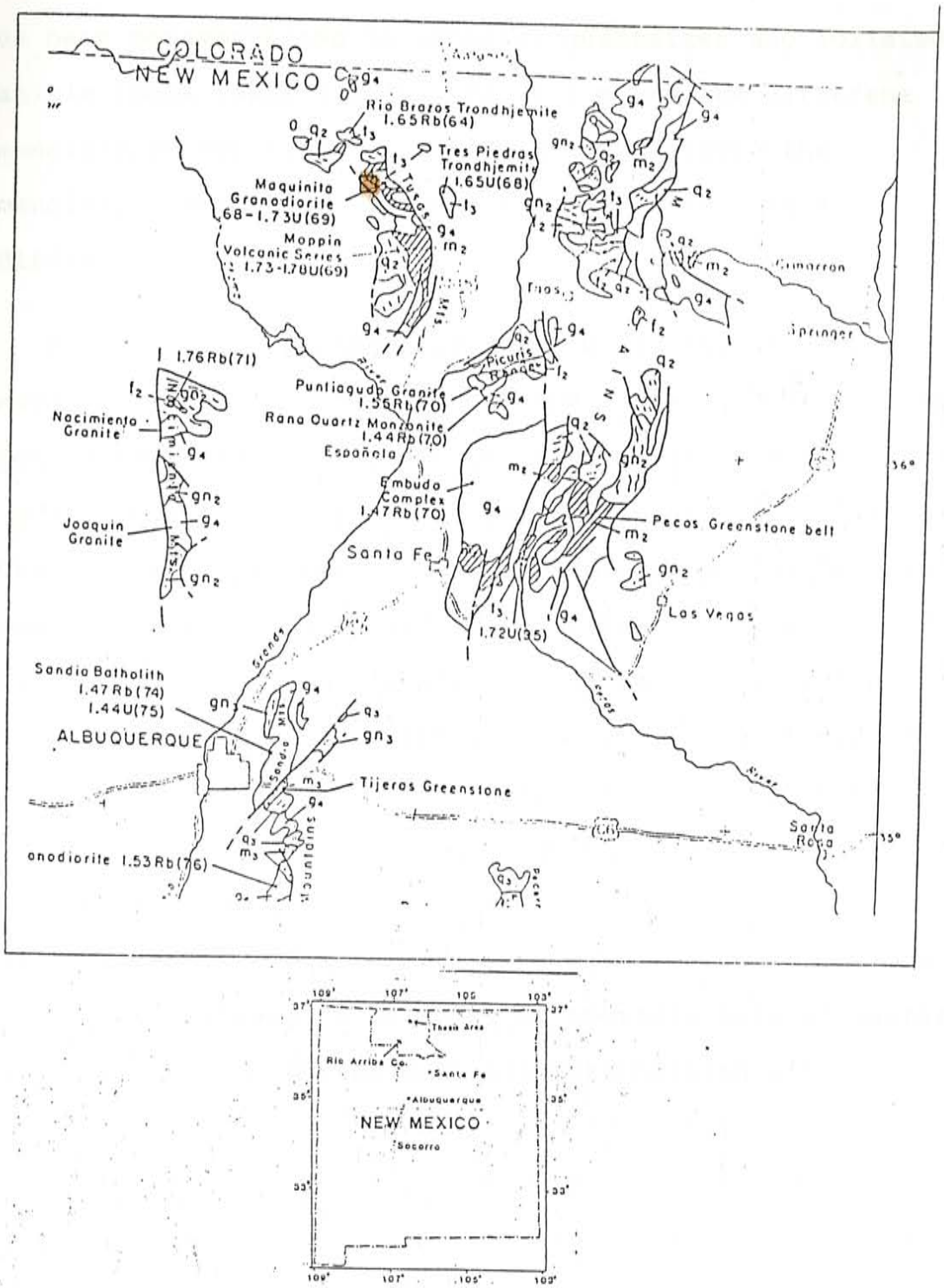

Fig. 1 Location map of study area. Taken from Condie, 1981, Precambrian rocks of southwestern United States and areas adjacent to New Mexico. (Study area in orange.)

have been metamorphosed to schists, quartzites and foliated granitic rocks respectively. Table 1 gives the different nomenclatures for rocks of the Tusas Mountains; the nomenclature used by Gibson was adopted, with slight modification.

Four distinct packages of rocks constitute the Precambrian supracrustals of northern Tusas Mountains. The Moppin metavolcanic and volcaniclastic series are postulated to pre-date all other rocks in the Tusas (Gibson, 1981). Rocks of the Moppin Series have variable compositions that range from mafic to felsic. Gibson (1981) suggests that mafic and intermediate members make up about 90% of the series; the felsic component comprises the remaining 10% and generally occurs in the stratigraphically uppermost portions of the series. Lying unconformably above the Moppin is the Burned Mountain metarhyolite, which is characterized by a pinkish green to tan colour and massive porphyritic texture. A sequence of immature metasedimentary rocks overlies the Burned Mountain metarhyolite and represents a transition zone between the metarhyolite and overlying mature quartzite. Rocks of the transition zone mature upwards through feldspathic and micaceous units into the youngest package, the vitreous and crossbedded Ortega quartzite.

Table 1.

Precambrian Rock Nomenclature
Northern Tusas Mountains

Just (1937)	Barker (1958)	Gibson (1981) and this study
Tusas Granite	Maquinita Granodiorite	Lineated Granodiorite
	Tres Piedras Granite	Granite of Hopewell Lake
Ortega Quartzite	Kiowa Mountain Formation	Feldspathic Metasediments
	Ortega Quartzite	Vitreous Quartzite
Vallecitos Rhyolite	Burned Mountain metarhyolite	Burned Mountain metarhyolite
Hopewell Series	Moppin Metavolcanic Series	Moppin Series

A number of plutonic rocks, of generally granitic composition, intrude the supracrustal succession of the Tusas Mountains. The plutonic rocks include the Maquinita granodiorite, a biotite-rich, lineated granodiorite; the granite of Hopewell lake, a leucocratic granite with distinctive quartz eyes (Gibson, 1981), the granodiorite of Spring Creek (Kent, 1980), the Tusas Mountain granite (Wobus, 1985) and the Tres Piedras granite (Gibson, 1981). Both the granite of Hopewell Lake and the Tusas Mountain granite were originally mapped as part of the Tres Piedras granite.

The emplacement age of the Maquinita granodiorite is 1755 Ma (Silver, in Robertson et al., in prep.). Since the Moppin series are intruded by the Maquinita granodiorite, the age of the latter constrains the minimum age of the Moppin Series. A U-Pb zircon age of 1700 Ma has been reported for the Burned Mountain metarhyolite (Silver, in Robertson et al., in prep.). The metasediments are postulated to have accumulated between 1650 and 1700 Ma (M. Williams, personal comm., 1985).

Structure and Metamorphism

The Precambrian rocks of the Tusas area have been affected by polyphase deformation and record at least three generations of deformation which has resulted in the super-position of folds (M. Williams, personal comm.,

1985). Three generations of folds (f_1, f_2, f_3) and their associated deformational events (D_1, D_2, and D_3) have been identified in the Precambrian rocks of northern Tusas Mountains. The first generation folds (f_1) are best developed in the Petaca schist, south of the Hopewell area, where they are characterized by extensional fabric with drawn-out pebbles lying parallel to fold axes (M. Williams, personal comm., 1985) Second generation (f_2) folds are steeply plunging and have axial planes which trend NW - SE with steep, near-vertical dips. The Hopewell anticline and Jawbone syncline are complimentary, large scale open folds whose axes trend roughly E - W and plunge shallowly to the west, and represent the third generation of folding (f_3). Other major structural elements are the regional northwest - southeast strike of planar structures within the rocks with steep northeast - southwest dips. Mineralogic and textural lineations are also represented in the rocks.

Precambrian rocks of the Tusas Mountain have been affected by a regional dynamothermal metamorphism which has transformed them into greenschists and amphibolites (Barker, 1958; Bingler, 1968; Kent, 1980; Gibson, 1981). Metamorphic grade increases from greenschist facies in the northwest to the amphibolite facies in the southeast. Peak metamorphism occurred during D_3 deformation and has been tentatively dated at 1450 Ma (Grambling and Ward, 1985). Grambling and Williams (1985) have estimated P - T of peak

metamorphism in the Hopewell area to be 3 kb and 425 +/- 25°C

Phanerozoic Rocks

The Tertiary and Quaternary rocks in the northern Tusas area are extensively described by Butler, 1946; Barker, 1958; Bingler, 1968; and Gibson, 1981. A basal Tertiary conglomerate, named the El Rito formation, rests with an angular unconformity on the Precambrian rocks of the study area. Porphyritic volcanic rocks of andesitic composition are intercalated with the conglomerate. Outcrops and float of the conglomerates and the volcanic rocks are abundant in the eastern portion of the Hopewell area, and also northwest of the spillway at Hopewell Lake. Basalts mapped as the Hinsdale formation by Wobus and Manley (1982) overlie the El Rito formation. A Quaternary glacial till (Ritito formation?) caps a number of ridges in the Tusas area. This unit is composed mainly of fragments of the Ortega quartzite and minor Burned Mountain metarhyolite cemented together by a poorly sorted matrix.

Method of investigation

The objectives of the study were accomplished by mapping the Hopewell Lake area at a scale of 1:3000. Thirty nine thin sections were examined. One hundred and eighteen

samples were analysed by fire assay and/or atomic absorption for Au, Ag, Cu, Pb, and Zn. Thirty samples, 11 of them obtained from outside of the study area were analysed for Au, As, and Sb by a combination of fire assay and neutron activation techniques. Major and trace element chemistry for 16 rock samples were obtained by X-ray fluorescence spectrometry. Fluid inclusions were studied in 8 doubly polished sections obtained from mineralized and unmineralized quartz veins. Five polished sections of the ore were studied in reflected light. Rb - Sr isotopic composition in 7 samples of the granite Hopewell Lake, and one sample of the altered metavolcanic rock were measured.

PRECAMBRIAN GEOLOGY OF THE HOPEWELL DISTRICT

LITHOLOGIES

Plates 1 and 2 are geologic map and cross section respectively of the study area and shows the distribution of the different rocks described below.

MOPPIN SERIES

Four rock types were identified in the Moppin Series based on mineral composition and textural differences. These are quartz-chlorite-plagioclase schist, quartz-chloritoid-sericite schist, carbonate schist, and quartz-sericite schist.

Quartz-chlorite-plagioclase schist

The quartz-chlorite-plagioclase schist occurs on an outcrop scale as inclusions and screens within the granite of Hopewell Lake. The inclusions represents deep exposures of the granite/schist contact, whereas the screens form when fingers and dike-like bodies of the granite extend upwards and outward into the schist. Fresh samples of the rock have a dark green lustrous sheen due to the moderate to high chlorite content of the rock. Samples of this rock type obtained from the Placer Creek commonly contain earthy brick red spots or euhedral cavities containing limonite after

ferroan carbonates and pyrite. In thin section, this rock shows a considerable variation in composition and texture. It is composed of a recrystallized, fine-grained quartz-chlorite matrix containing large, euhedral to subhedral crystals of plagioclase. Fine needles of plagioclase were observed in the matrix of some thin sections. The chlorite commonly occur as knots, some of which appear to be pseudomorphs of a precursor ferromagnesian mineral. Different degrees of alteration of plagioclase to epidote and sericite were observed in the thin sections of this rock. The quartz content of the rock varies from 5 to 40%. Plagioclase is of albite/oligoclase composition; the quartz-defficient variety of this unit contains up to 55% plagioclase and has a preserved porphyritic igneous texture. In some outcrops, the plagioclase phenocrysts are stretched out and form a textural lineation within the rock. The more clastic variety contains minor amounts of plagioclase fragments, often thoroughly sericitized. Both varieties contain between 10 and 40% carbonate, dolomite and/or siderite. Although it is not obvious that the carbonate replaces plagioclase, it is apparent that the carbonate is forming at the expense of the plagioclase; in areas of high carbonate content, the quartz-chlorite-plagioclase schist has a noticeably lower plagioclase content. This rock commonly contains 5 - 15% disseminated octahedral magnetite crystals.

The textures of the rock and its composition suggest that it is a meta-andesite.

Quartz-chloritoid-sericite schist

Quartz-chloritoid-sericite schist has a pronounced platy texture. In outcrop and in handspecimen, the rock is dark due to clots or rosettes of chloritoid which may constitute up to 30% of the rock. Rosettes grow across the rock fabric, suggesting that they may be late or post-kinematic. Along Placer Creek, this unit is interlayered with intensely altered quartz-chlorite-plagioclase schist, and the granite of Hopewell Lake.

The essential minerals observed in thin sections of this rock are: quartz (30 to 40%), sericite (20 to 30%), chloritoid (10 to 30%), and knots of chlorite which are commonly in minor amounts. The rock also contains varying degrees of carbonate alteration.

This rock is tentatively interpreted as representing altered intermediate volcanic and volcaniclastic rocks based on its composition and association with rocks which contain relict volcanic textures.

Carbonate schist

Carbonate schist commonly forms prominent bands flanked by less resistant rock types with which it is intercalated. The rock is poorly foliated, dense and composed, in order of abundance, of sericite, siderite, quartz, chloritoid, and minor chlorite.

The carbonate schist has a preserved porphyritic texture with plagioclase phenocrysts replaced in their entirety by sericite and carbonates (Fig. 2). Sericite and siderite together constitute between 60 and 70% of the rock. Chloritoid may be locally abundant and constitute up to 20% of the rock (Fig. 3). In thin section, rosettes of chloritoid and carbonate grains are intergrown but do not appear to be replacing each other. Accessory pyrite, magnetite and hematite are observed in thin section.

The protolith of this rock is difficult to determine due to the intense carbonate alteration, however, the texture suggests that the protolith was a hypabyssal rock.

Quartz-sericite schist

On an outcrop scale, quartz-sericite schist is intercalated with lenses of medium to coarse-grained fragmented rock which appears, based on its composition, to be a brittlely deformed granitoid. The quartz sericite schist has a cream to pinkish green colour, and a pronounced

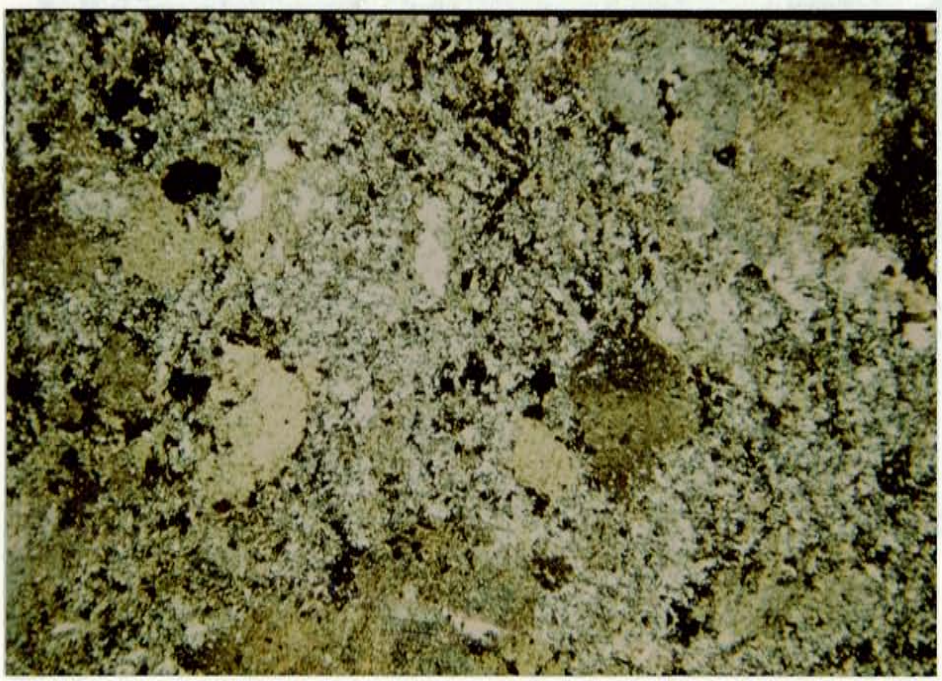

Fig. 2 Photomicrograph of carbonate schist with plagioclase phenocrysts replaced by sericite and siderite (field of view is 4 mm across; polars crossed).

Fig. 3 Rosettes of chloritoid in carbonate schist (field of view is 4 mm across; polars crossed).

platy texture which is due mainly to the fine muscovite content.

The mineralogy of the rock is simple; it consists of quartz and sericite in roughly equal amounts and minor amounts of chlorite, and accessory hematite and tourmaline. The quartz occurs in the matrix with sericite, and also as larger crystals set in the matrix. The non-undulose extinction of the quartz crystals and their near perfect crystal shapes suggest they may be of igneous origin, perhaps phenocrysts in a primary volcanic rock. Schistosity is marked by preferred orientation of sericite (Fig. 4). In a few sections of the quartz-sericite schist, the sericite flakes are rather randomly distributed resulting in a more homogeneous and tough texture.

The felsic nature of this rock and the presence of quartz with almost perfect crystal shapes indicate that it is a felsic extrusive rock.

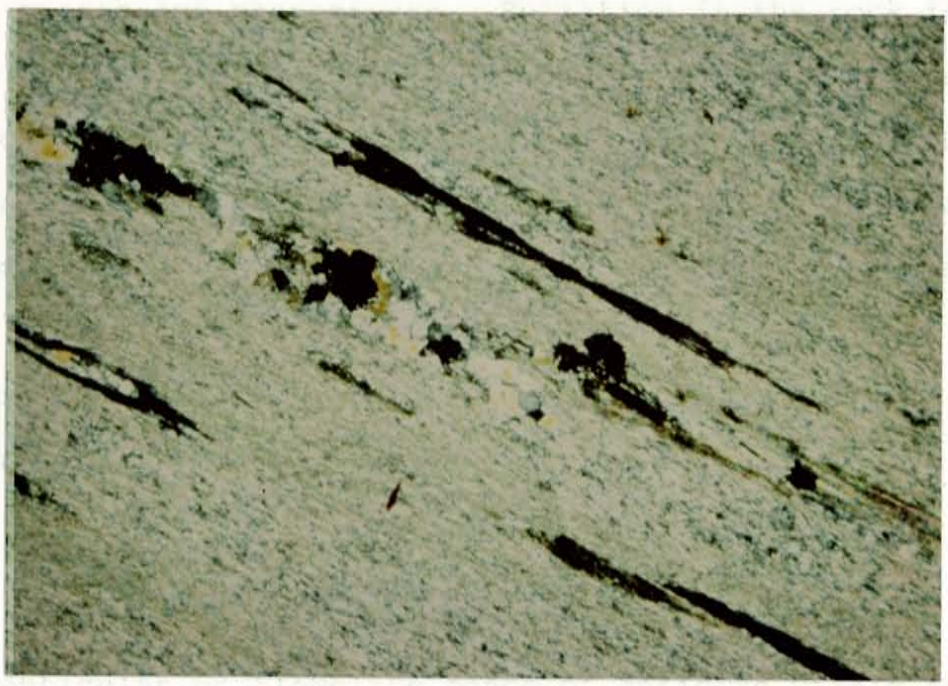

Fig. 4 Photomicrograph of quartz-sericite schist. Drawn out quartz, and knots of chlorite mark extension lineation in the rock (field of view is 4 mm across; polars crossed).

BURNED MOUNTAIN METARHYOLITE

A diagnostic feature of the Burned Mountain metarhyolite is its dense, almost vitreous texture and bluish quartz-eye phenocrysts. Foliation in the rock is weakly developed and is marked by alignment of lenticular, cream coloured fragments in a pinkish groundmass. In thin section, the quartz phenocrysts are euhedral to subhedral, only moderately strained and constitute about 15% of the rock. The rock also contains about 5% microcline phenocrysts. The quartz-microcline phenocrysts are set in an aphanitic matrix composed mainly of quartz and minor sericite. Accessory hematite and zircon have been identified in thin section.

Lenticular or flamelike bands of sericite within the quartz-rich matrix, forming up to 30% of the rock, and broken quartz phenocrysts in the only thin section of this rock examined, together suggest relict eutaxitic textures characteristic of welded rhyolite tuffs (Fig. 5).

METASEDIMENTS

Metaconglomerate and Ortega quartzite are the two mappable units in this package of rocks that are exposed along the Placer Creek.

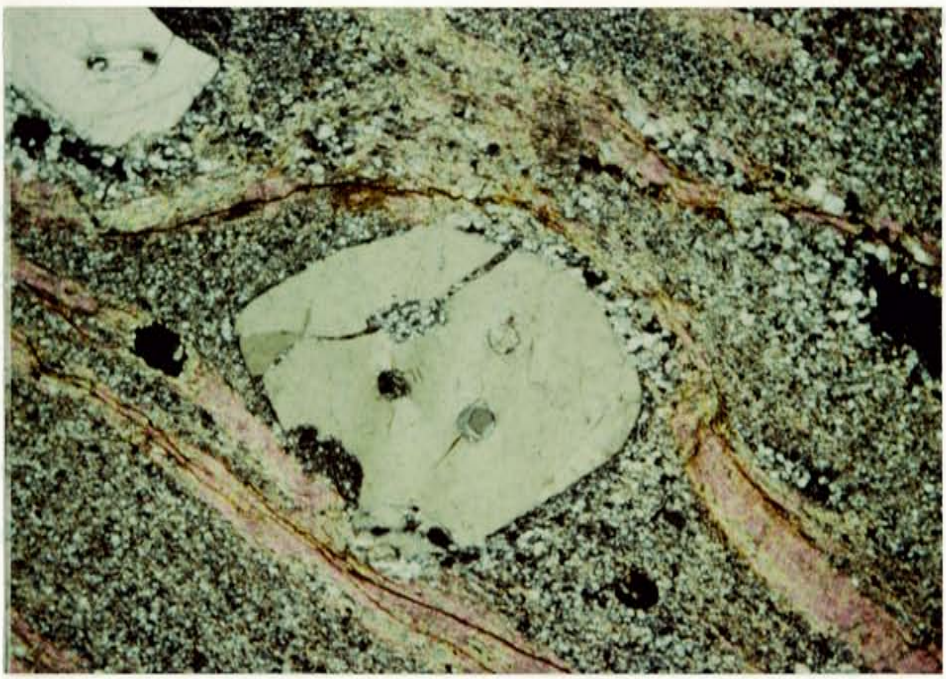

Fig. 5 Photomicrograph of the Burned Mountain metarhyolite. The lenticular bands of sericite and broken quartz phenocrysts are interpreted as relict eutaxitic textures diagnostic of welded ash flow tuffs (field of view is 4 mm across; polars crossed).

Meta-conglomerate

Metaconglomerate is the basal portion of the metasedimentary succession and directly overlies the Burned Mountain metarhyolite with which it is locally interbeded. The unit is correlative with the micaceous metasediment of Smith (1986). It is matrix supported and composed of about 20% pebbly vein quartz and lithic fragments of the underlying felsic Moppin and Burned Mountain metarhyolite set in a poorly sorted matrix of sericite and quartz (Fig. 6). Also present in the matrix are flamelike bands of sericite similar to that described in the quartz-sericite schist and the metarhyolite. Hematite, forming 3 to 4% of the rock, is dispersed in the matrix. Preferred orientation of fine sericite and stretched pebbles define a non penetrative foliation in this rock. Lenses of this unit intercalated with the underlying metarhyolite have a less mature matrix. It has thus been inferred that the unit matures upward into the clean vitreous quartzite above, even though this gradual transition is not exposed in the area of this study. No feldspars were observed in thin sections of the this rock; the abundance of sericite in the matrix however suggests that the rock initially contained a significant amount of potash feldspar which has been converted to sericite during metamorphism.

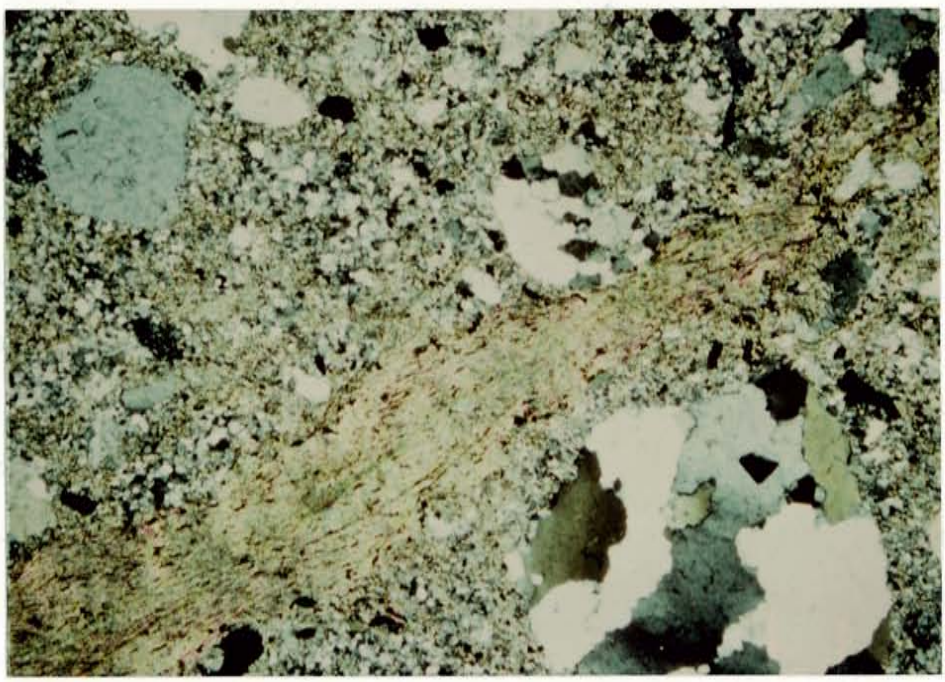

Fig. 6 Photomicrograph of matrix supported metaconglomerate (field of view is 4 mm across; polars crossed).

The presence of fragments of the felsic Moppin and Burned Mountain metarhyolite indicates that the metaconglomerate has been derived from these units.

Ortega Quartzite

The Ortega quartzite is even-grained and composed of about 90% quartz and accessory kyanite, viridine, specular hematite and muscovite. The accessory minerals are concentrated along crossbeds and bedding planes in the quartzite (Fig. 7). The rock is massive and forms prominent ridges wherever it crops out. The younging direction determined from cross bedding and graded bedding indicates that the quartzite youngs southward in the Hopewell area. Well-preserved cross-bedding commonly marked by high concentrations of specular hematite, kyanite, and in the lowermost 50-100m of the section , viridine, occurs in the quartzite (see Fig. 8). In the lower portion of the of the metaconglomerate, graded bedding is also well-preserved and it too consistently faces to the south.

PLUTONIC ROCKS

The granite of Hopewell Lake, described and informally named by Gibson (1981), is the only intrusive rock in the study area. The rock is coarse-grained, pinkish, and commonly contains megacrysts of quartz which stand out

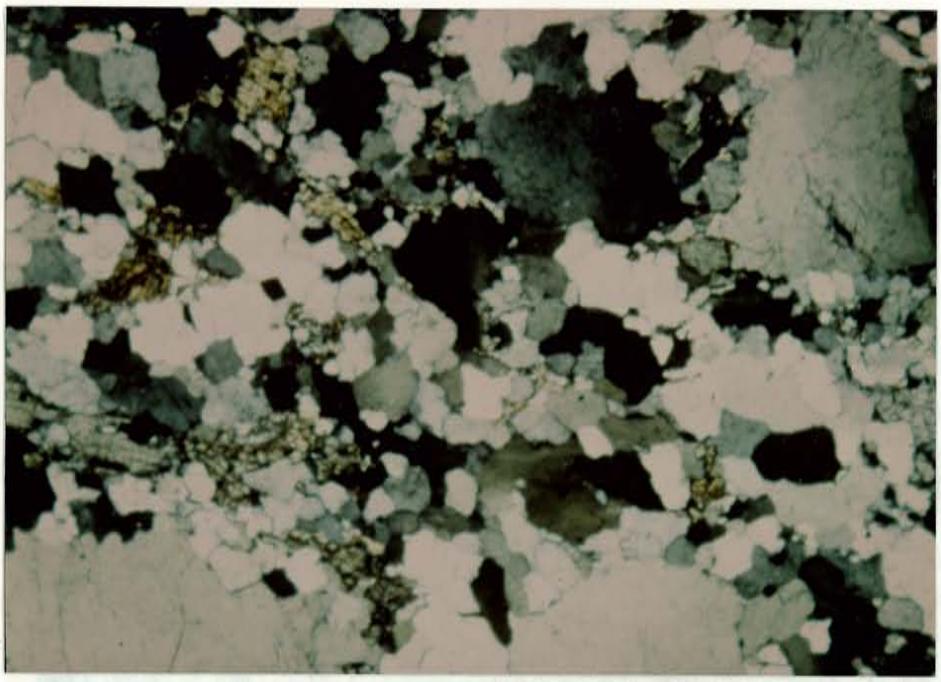

Fig. 7 Photomicrograph of Ortega quartzite. Minor amounts of kyanite can be seen in the rock (field of view is 4 mm across; polars crossed).

Fig. 8 Photograph of cross bedding in the vitreous Ortega quartzite.

prominently on weathered surfaces. Inclusions and screens of the chlorite-rich Moppin Series occur within the granite. Near the contacts of the two rocks, the granite is greenish, apparently resulting from assimilation of mafic components from the Moppin. Plagioclase phenocrysts in the latter are pinkish. In most outcrops, the granite is brittlely deformed; the quartz megacrysts are stretched and fracture cleavages are coated with fine sericite.

Quartz megacrysts constitute 0-25% of the rock. In the more intensely deformed varieties, the feldspars are ground up into a fine matrix (Fig. 9). A classification scheme based on modal estimates (Table 2) of quartz and feldspars in thin sections indicates that samples collected from the granite of Hopewell Lake have the apparent mineralogy of a granite, containing 25 - 30% quartz; 25 - 35% plagioclase of albite to oligoclase range; and 20 - 35% microcline and untwinned potash feldspars (Fig. 11).

Minor granodiorite and quartz-monzonite phases occur as lenses within the mafic unit of the Moppin (Fig. 10). The sheared granitoid which is interbeded with the quartz-sericite schist of the Moppin Series is interpreted as representing the margin of the granitic body.

Alteration of feldspars to sericite and carbonate is quite common in the rock. In outcrop, carbonate alteration in the granite is noticeable on weathered surfaces by

reddish-brown spots of limonite after siderite. The degree of feldspar alteration varies considerably from fine flakes to a complete replacement of the primary plagioclase or microcline crystals.

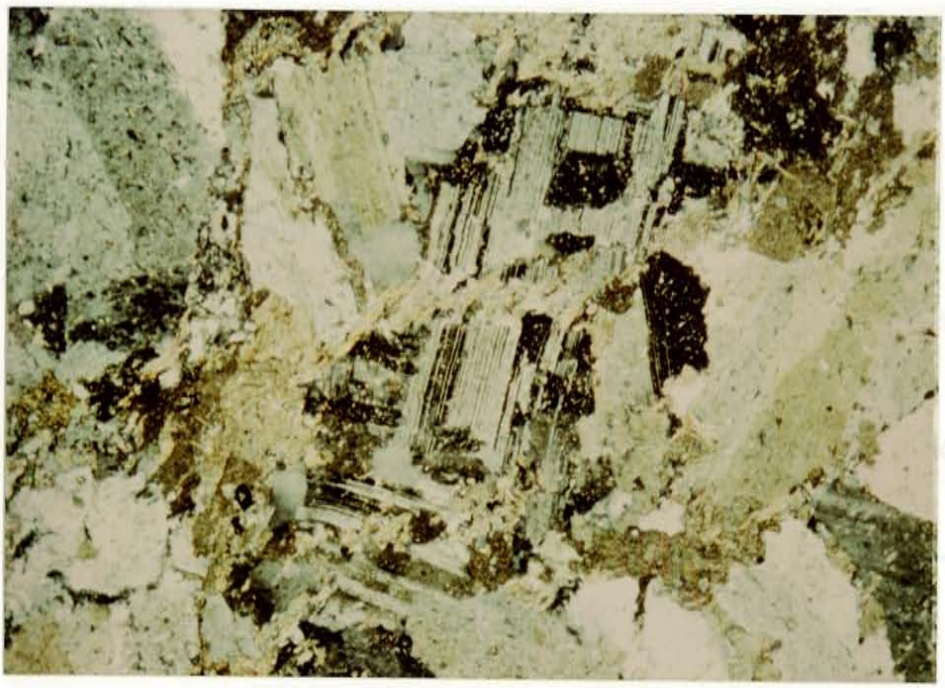

Fig. 9 Photomicrograph of the granite of Hopewell Lake showing brittle deformation, and carbonate and sericite alteration. The alteration can be seen, in the photo, to be spatially associated with the deformation fabric (field of view is 4 mm across; polars crossed).

Table 2.

MODAL ANALYSIS OF SAMPLES OF GRANITE OF HOPEWELL LAKE

Sample #	Absolute Vol. % Q	AK	PLG	Normalized Vol. % Q	AK	PLG	Name
14B	30	15	45	33.3	16.7	50	Granodiorite
136	35	20	35	38.9	22.2	38.9	Granite
133	25	35	30	27.8	38.9	33.3	Granite
1A	30	30	35	31.6	31.6	36.8	Granite
116	20	15	55	22.2	16.7	61.1	Granodiorite
129A	20	35	35	22.2	38.9	38.9	Granite
47B	15	20	55	16.7	22.2	61.1	Quartz Monzonite
125	20	45	25	22.2	50	27.8	Granite

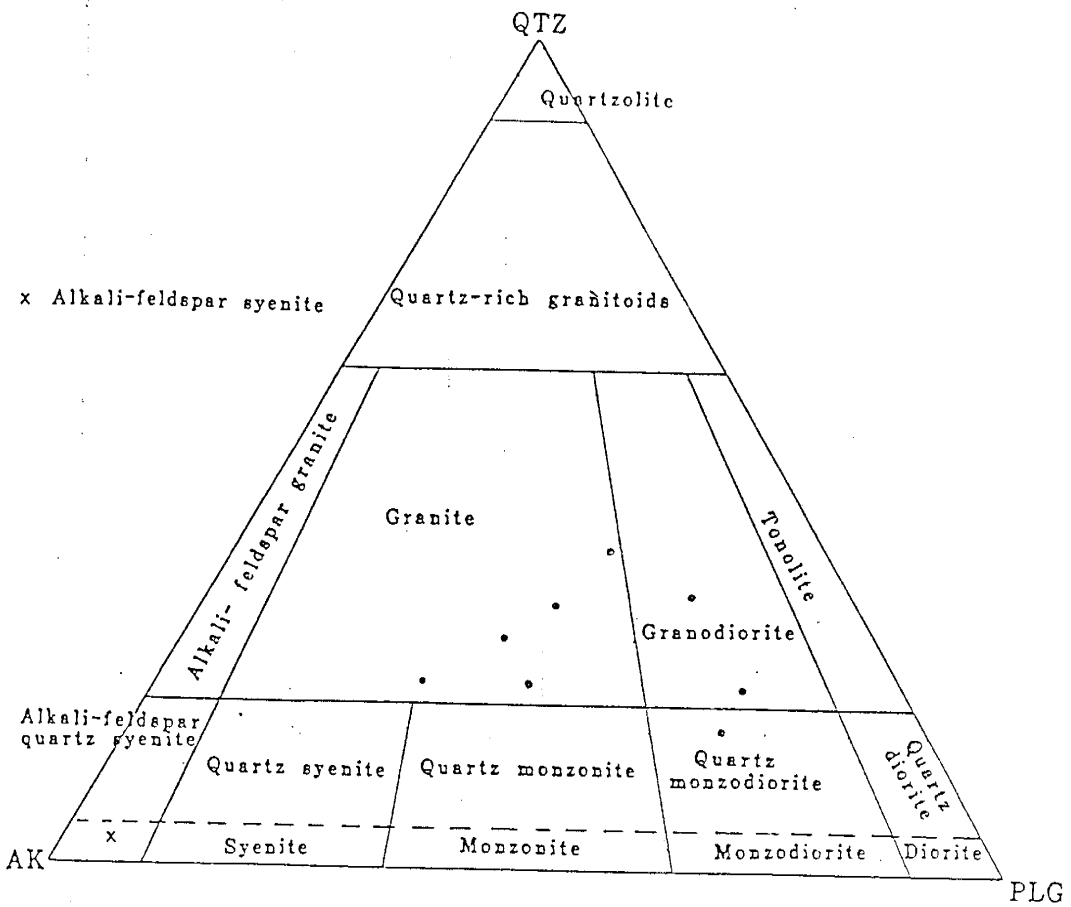

Fig. 11 Classification of granite and allied rocks based upon modal comp. in vol. % (normalized). After A. L. Streckeisen, 1976. Samples of the granite of Hopewell Lake shown by "o."

Fig. 10 Photograph of lenses of granite of Hopewell Lake in the mafic unit of the Moppin Metavolcanic Series.

STRUCTURE

Structural features in the Hopewell area include folding, foliations, and lineations associated with deformation events, and relict sedimentary structures in the metasedimentary package.

Folding

Three generations of folds were produced by the three deformational events that have affected rocks in the northern Tusas Mountains. The f_1 folds are poorly expressed. Textural lineations in the supracrustals which parallel the axes of f_1 folds in the nearby Petaca schist, have been interpreted as a subtle manifestation of f_1 in the Hopewell area.

The f_2 folds are well developed in the Moppin Series. They are tight folds and plunge between 50 - 80°E to the SE. Axial planes of these folds trend NW - SE and have steep, near-vertical dips. The major foliation in the Moppin Series is interpreted as the axial plane foliation related to the second folding event. Steeply plunging f_2 folds are apparently not present in the Burned Mountain metarhyolite and the overlying quartzite. The Moppin Metavolcanic Series probably recorded the different deformation events better due to the relatively less competent nature, resulting from

Fig. 12 Photograph of minor fold, associated with f_3, in the Ortega quartzite.

the high phyllosilicate content, of members of the series.

The f_3 folds generally have large wavelengths and are best represented in the Ortega quartzite (Fig. 12). The axes of the f_3 folds trend N75^{o}W and have a gentle plunge of about 30^{o} to the NW

Foliation:

All of the Precambrian rocks in the Hopewell area are foliated and contain either a penetrative fabric, or a non-penetrative fracture cleavage. In many of the rocks, especially those with penetrative foliation, the dominant foliation is crenulated by a later domain cleavage (Fig. 13). A foliation plane preceding the dominant foliation is almost completely obliterated; intersection lineations in the plane of the dominant foliation are the only clues of this earlier foliation. The average strike of the major foliation is N60^{o}W; dip values are between 60^{o} and vertical to the NE or SW (Fig. 14).

Lineation:

Mineralogic and textural lineations are observed in all of the Precambrian rocks in the study area. In the Moppin Series, rosettes of chloritoid mark the intersection of S_1 and S_2, the foliation planes associated with first and second deformation events respectively. In the quartzite,

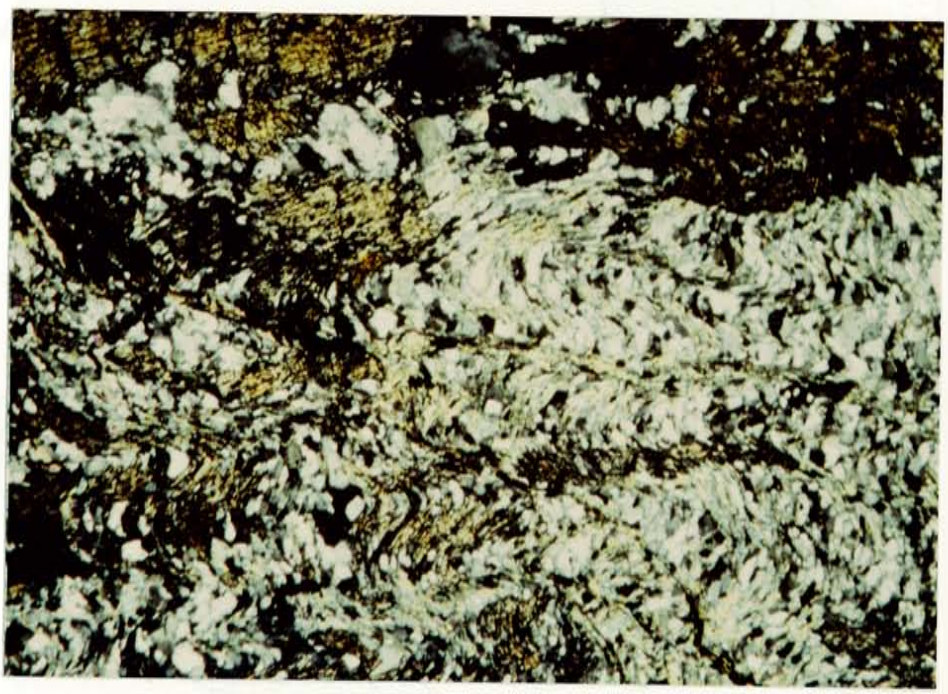

Fig. 13 Photomicrograph of quartz-chlorite-plagioclase schist showing S_2 foliation crenulated by later domain cleavage, S_3 (field of view is 1 mm across; polars crossed).

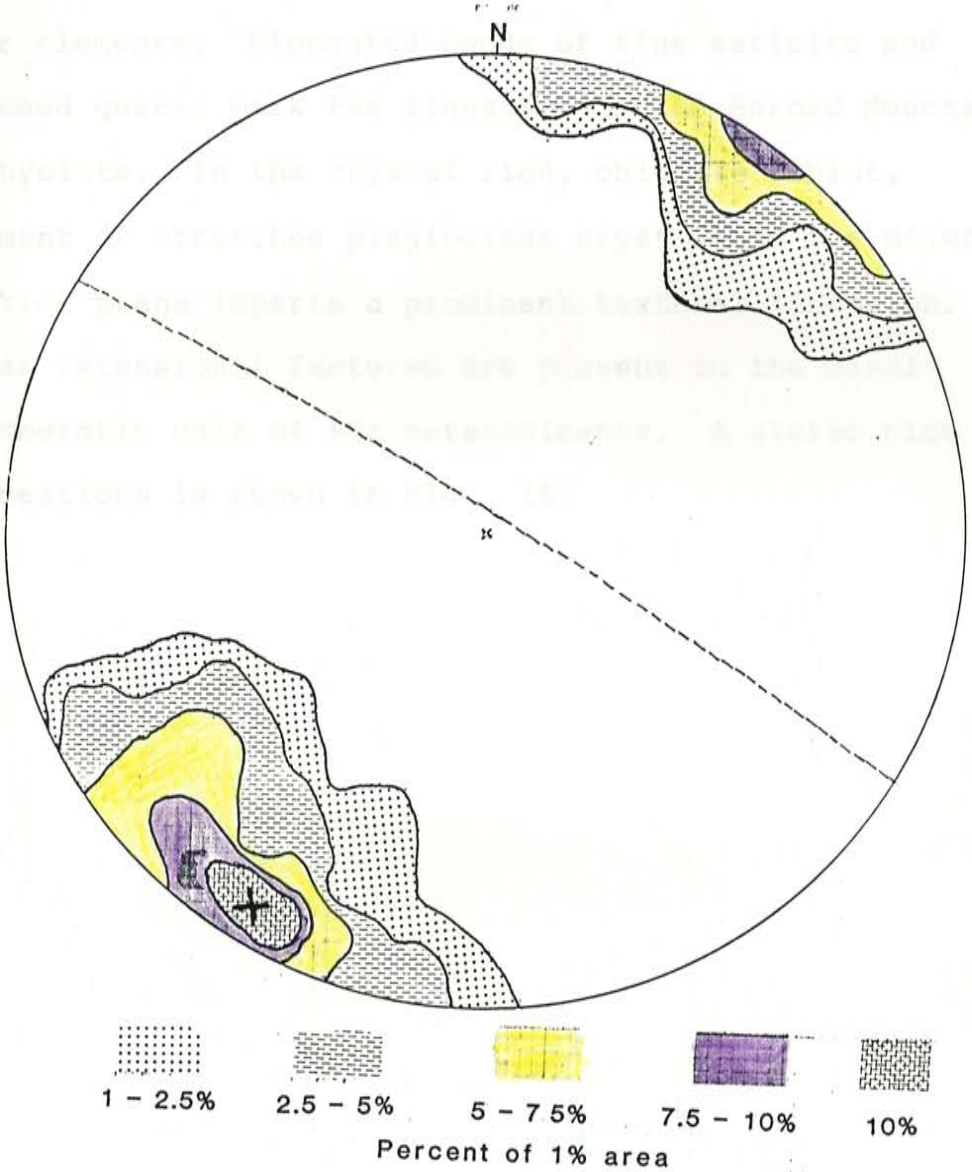

Fig. 14 Contoured lower hemisphere stereographic projection of poles to the dominant foliation (S_2) from all units in the Hopewell area. Statistical S_2 plane maximum at N60°W, 84°SW. X is pole maximum, n is number of data points.

oriented blades of kyanite and specular hematite are the linear elements. Elongated bands of fine sericite and stretched quartz mark the lineation in the Burned Mountain metarhyolite. In the crystal rich, chlorite schist, alignment of stretched plagioclase crystals in the major foliation plane imparts a prominent textural lineation. Similar extensional features are present in the basal conglomeratic unit of the metasediments. A stereo plot of 78 lineations is shown in Fig. 15.

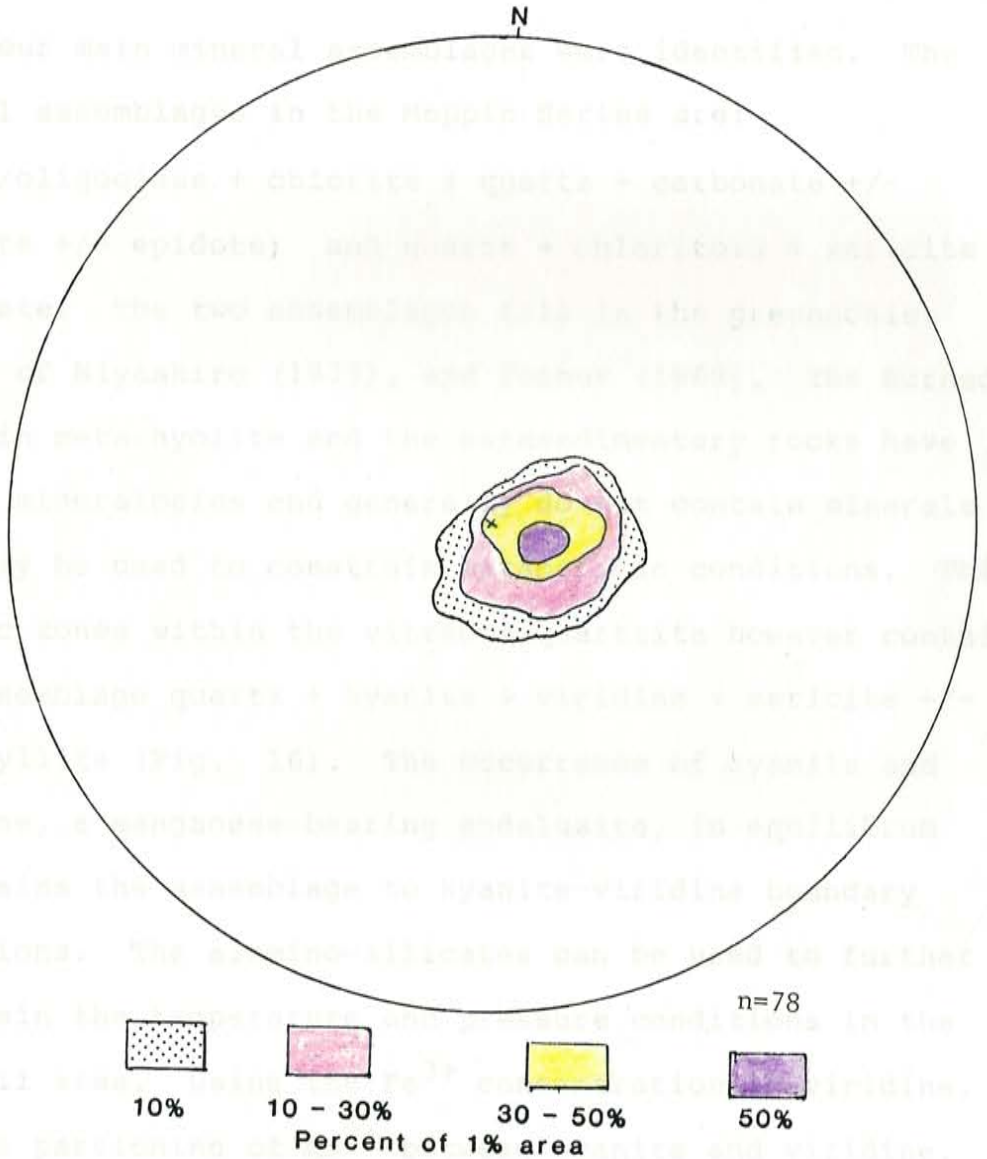

Fig. 15 Contoured lower hemisphere stereographic projection of extension lineations measured in the Moppin Metavolcanic Series (n is number of data points).

METAMORPHISM

Four main mineral assemblages were identified. The typical assemblages in the Moppin Series are: albite/oligoclase + chlorite + quartz + carbonate +/- sericite +/- epidote; and quartz + chloritoid + sericite + carbonate. The two assemblages fall in the greenschist facies of Miyashiro (1973), and Turner (1968). The Burned Mountain metarhyolite and the metasedimentary rocks have simple mineralogies and generally do not contain minerals that may be used to constrain metamorphic conditions. Thin pelitic zones within the vitreous quartzite however contain the assemblage quartz + kyanite + viridine + sericite +/- pyrophyllite (Fig. 16). The occurrence of kyanite and viridine, a manganese-bearing andalusite, in equilibrum constrains the assemblage to kyanite-viridine boundary conditions. The alumino-silicates can be used to further constrain the temperature and pressure conditions in the Hopewell area. Using the Fe^{3+} concentration in viridine, and the partioning of Mn^{3+} between kyanite and viridine, Grambling and Williams (1985) have estimated the peak metamorphic conditions in the Ortega quartzite within the area studied to be 425-450^{o}C and 3 kb. A fourth assemblage typical of the intrusive rocks is quartz + albite/oligoclase + microcline + sericite +/- carbonate +/- epidote. This assemblage, like all others in the area, fits the

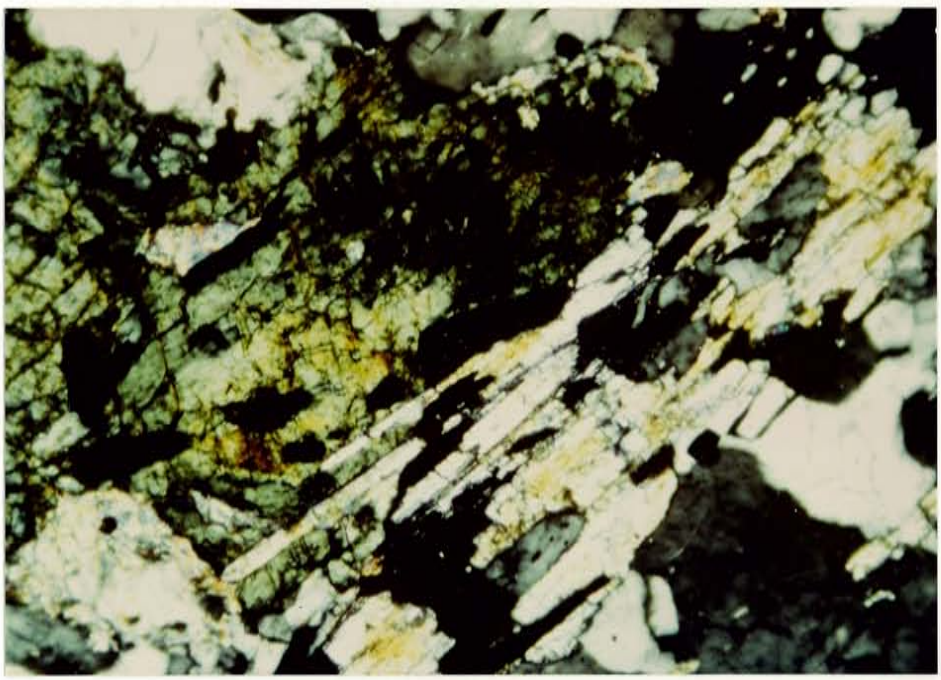

Fig. 16 Photomicrograph of the Ortega quartzite with kyanite (lower right) and viridine (upper left) coexisting (field of view is 4 mm across; polars crossed).

greenschist facies assemblage of Miyashiro (1973), and Turner (1968).

Thus the mineral assemblages in the different rocks from the Hopewell area suggest that metamorphic conditions did not exceed the greenschist facies.

GEOCHEMISTRY

Major and Trace Element Chemistry

The results of major and trace element analyses of 16 plutonic and metavolcanic samples from the Hopewell area are shown in Table 3, along with CIPW norms.

A normative Ab-An-Or plot of all samples from the granite of Hopewell Lake for which geochemical data were obtained indicate that they are trondhjemites (Fig. 17), in contrast to the modal plot (Fig. 11) which suggests that they are granites.

Trace element analyses of 10 samples from the Moppin Metavolcanic Series and a single sample from the Burned Mountain metarhyolite have been plotted on a Zr/TiO_2 versus Nb/Y variation diagram (Fig. 18) to determine their protoliths. All the elements used in this plot are relatively immobile and have been demonstrated by Floyd and Winchester (1978) to be quite reliable in identifying rocks suspected to have been affected by later alteration processes. The Burned Mountain metarhyolite plots in the rhyolite field on the diagram. The Moppin Series rocks plot over a range of compositions from dacite to alkaline basalt. Samples obtained from the chlorite-rich Moppin unit plot as alkaline basalt, subalkaline basalt, and andesite. The carbonate schist plots in the andesite field; the

Table 3.

CHEMICAL ANALYSIS OF PRECAMBRIAN ROCKS FROM THE HOPEWELL AREA

%	1ZK-2A*	-14A*	-89C*	12K-5*	-126B*	-82*	ADIT #3*	-5G-1*	-129B*
SiO_2	51.19	44.04	71.08	72.57	61.56	71.53	74.62	67.23	48.78
TiO_2	0.58	0.81	0.38	0.32	0.52	0.32	0.34	0.37	1.01
Al_2O_3	14.56	13.32	16.02	17.15	16.15	14.23	10.84	13.13	15.19
Fe_2O_{3T}	10.87	9.59	5.55	1.27	6.78	6.70	7.19	8.11	10.69
MgO	5.14	7.36	0.39	0.03	1.79	0.27	0.45	0.71	5.27
CaO	6.41	8.16	0.20	0.13	3.47	0.16	0.08	2.06	6.61
Na_2O	1.85	2.64	1.10	1.19	3.31	0.89	0.80	0.57	3.00
K_2O	1.28	0.33	3.20	3.32	1.94	3.08	2.09	2.31	0.27
MnO	0.22	0.18	0.01	0.001	0.14	0.02	0.06	0.21	0.17
P_2O_5	0.13	0.30	0.16	0.10	0.18	0.09	0.05	0.13	0.19
LOI	8.65	13.94	2.47	2.35	2.28	2.15	2.39	3.92	7.63
Total	100.88	100.68	100.56	98.42	98.11	99.43	98.90	98.74	98.80
(ppm)									
Ni	35	170	8	5	8	5	13	9	44
Cu			2	2	20	2	10508	5	33
Pb	12	15	30	51	66	12	28	56	12
Zn	158	130	124	22	368	30	92	672	116
Rb	28	6	73	97	46	70	58	69	4
Sr	221	650	168	633	494	180	146	179	630
Y	19	14	22	7	34	5	9	12	26
Zr	66	58	136	145	133	99	86	86	103
Nb	4	5	8	7	7	7	3	6	8
Ga	14	13	16	21	18	15	13	16	17
Th	1.39		3	5	5	3	388	3	
Zr/TiO_2	0.011	0.007	0.036	0.045	0.026	0.031	0.025	0.023	0.01
Nb/Yi	0.239	0.342	0.357	0.910	0.123	1.418	0.3	0.542	0.314
			CIPW MINERAL NORMS (WT %)						
Q	8.82	0.00	48.80	52.61	21.56	50.23	57.09	41.14	3.98
C	0.00	0.00	10.79	11.65	2.75	9.37	7.26	6.28	0.00
Or	7.56	1.95	18.91	19.62	11.46	18.20	12.35	13.65	1.60
Ab	15.49	22.29	9.18	9.60	27.64	7.40	0.66	4.69	24.92
An	27.73	23.55	0.00	0.12	16.16	0.23	0.07	9.38	27.43
Hyp	25.66	15.51	7.89	1.27	13.07	9.23	10.43	12.56	24.52
Ap	0.30	0.70	0.37	0.23	0.42	0.21	0.12	0.30	0.44
Mt	1.87	1.65	0.96	0.22	1.17	1.16	1.24	1.40	1.84
Il	1.10	1.54	0.72	0.61	0.99	0.61	0.65	0.70	1.92

Table 3. (continued)

CHEMICAL ANALYSIS OF PRECAMBRIAN ROCKS FROM THE HOPEWELL AREA

%	1ZK-47A*	-31B**	-14B+	-136+	-133+	-127B+	-4A+
SiO_2	40.73	79.54	55.78	68.95	63.42	62.84	68.57
TiO_2	0.44	0.17	0.28	0.21	0.39	0.41	0.33
Al_2O_3	9.16	10.35	12.68	17.03	16.83	17.08	15.88
Fe_2O_{3T}	8.51	2.20	3.80	2.18	3.76	3.57	3.46
MgO	10.17	0.40	2.60	0.99	1.56	1.73	1.17
CaO	10.65	0.42	6.36	0.99	1.58	2.66	0.47
Na_2O	0.69	0.99	5.26	5.19	5.95	5.86	6.21
K_2O	0.23	3.13	0.41	2.53	1.77	1.70	0.93
MnO	0.23	0.07	0.12	0.03	0.04	0.07	0.06
P_2O_5	0.39	0.02	0.13	0.08	0.17	0.18	0.14
LOI	18.68	1.79	10.01	2.12	2.62	3.26	1.48
Total	99.86	99.07	97.43	100.29	98.09	99.36	98.69
(ppm)							
Ni	305	7	14	9			
Cu		8					
Pb	12	15	14	12	8	6	
Zn	285	130	53	27			
Rb	2	87	8	59	37	33	
Sr	779	91	508	384	842	573	
Y	16	66	6	6	10	11	
Zr	83	255	91	86	124	122	
Nb	17	31	7	6	9	10	
Ga	11	18	11	16			
Th	3	14		1		3	
Zr/TiO_2	0.019	0.150	0.033	0.041	0.032	0.030	
Nb/Yi	1.031	0.471	1.132	0.906	0.926	0.885	
			CIPW MINERAL NORMS (WT %)				
Q	0.38	59.12	8.93	24.65	15.06	12.73	24.59
C	0.00	4.64	0.00	4.17	2.69	1.22	4.14
Or	1.36	18.50	2.42	14.95	10.46	10.05	5.50
Ab	5.26	8.31	44.13	43.63	49.73	49.16	52.55
An	21.52	1.92	9.98	4.68	6.97	12.18	1.42
Hyp	25.29	3.83	2.99	5.14	8.42	8.61	7.18
Ap	0.90	0.05	0.30	0.19	0.39	0.42	0.32
Mt	1.47	0.38	0.66	0.38	0.65	0.62	0.60
Il	0.84	0.32	0.53	0.40	0.74	0.78	0.63

* Moppin metavolcanic rock

** Burned Mountain metarhyolite

\+ Granite of Hopewell Lake

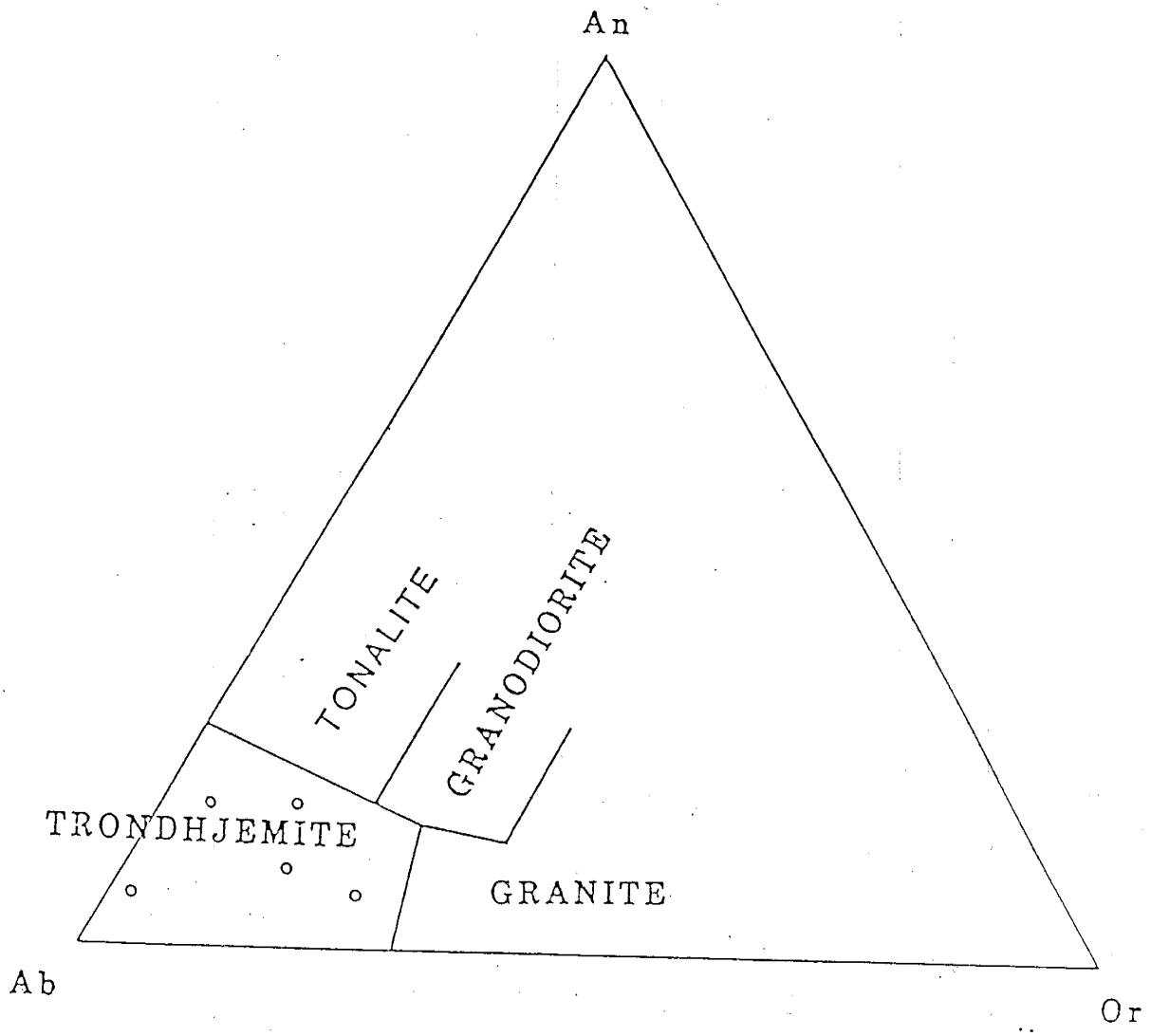

Fig. 17 Normative plot of 5 samples of the granite of Hopewell Lake (shown by "o") on the An-Ab-Or ternary diagram of Barker (1979).

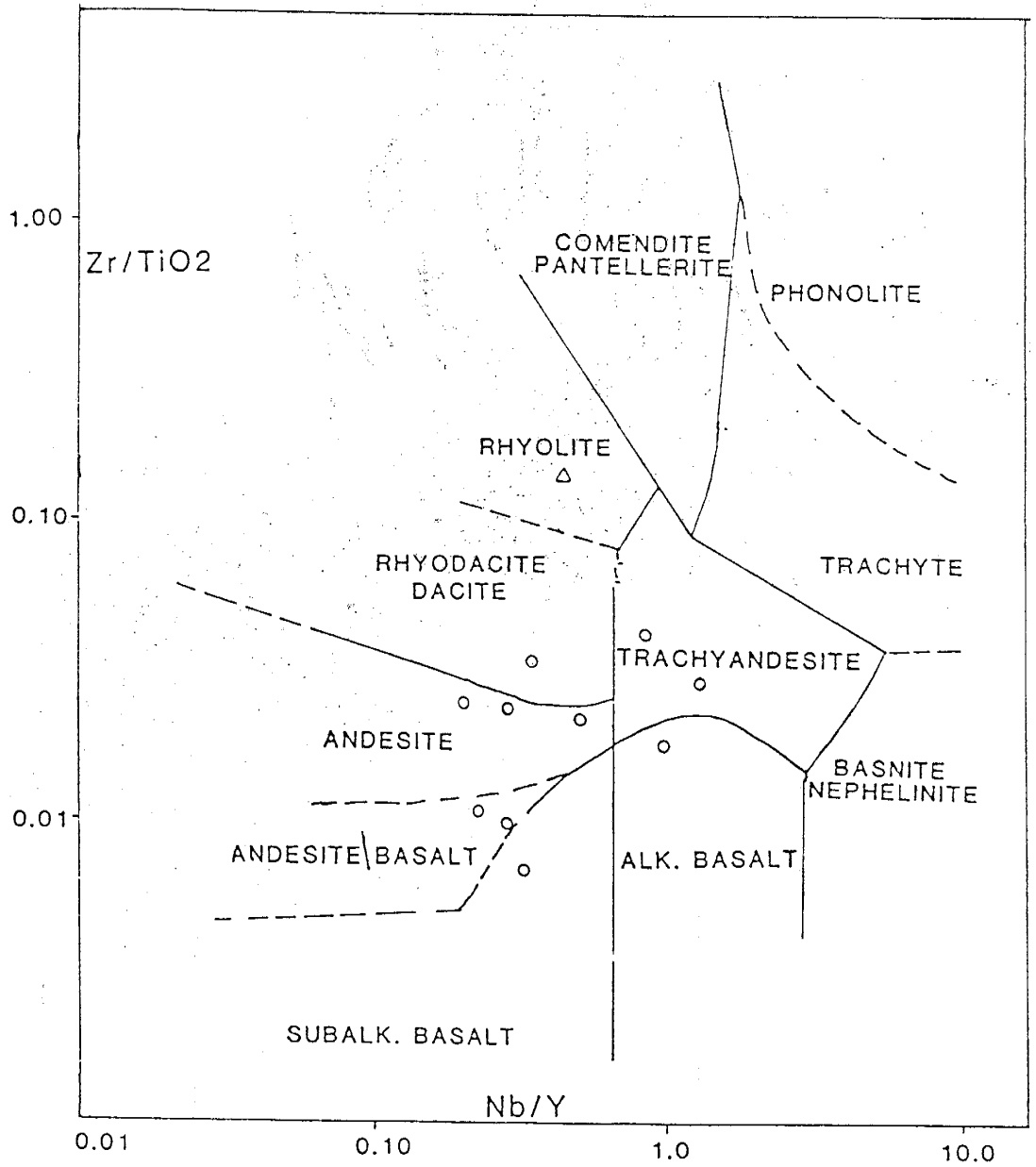

Fig. 18 Zr/TiO_2 versus Nb/Y plot of samples of the metavolcanic rocks from the Hopewell area on a variation diagram to determine their protoliths (after Winchester and Floyd, 1977).

quartz-sericite schist, and quartz-chloritoid-sericite schist all plot as dacite, trachyandesite, or andesite. The chemistry of the rocks generally conform with the contrasting protoliths assigned to members of the series based on petrographic data, although in the more altered areas, the original composition of the rocks is obscured by massive additions of silica, carbonate and sodium.

The Burned Mountain metarhyolite has the chemical signature of a rhyolite on both Fig. 17 and on plots using major element chemistry (see Gibson, 1981; Kent, 1980). Rocks of the Moppin Series form a compositional continuum of subalkaline (both tholeiitic and calcalkaline) and mildly alkaline volcanics, with the subalkaline members dominating. The series may be compared with successions in the Snow Lake-Flin Flon area of north central Canada, and the Birimian of West Africa (Condie, 1982a), both of which are characterized by compositionally continuous subalkaline volcanic suites.

Rocks of the Moppin Series are enriched in K and Si, and depleted in Na, Ca, and Mg when compared with average rock types of comparable compositions (see Condie, 1982b; and Best, 1982). The Burned Mountain metarhyolite shows a mild depletion in all three alkalis. The intrusives must be variably depleted in K and enriched in Na, in order to explain the observation that samples of the granite plot as

trondhjemites on the normative Ab-An-Or diagram.

Field and petrographic studies indicate that the Precambrian rocks in the study area have been affected by later alteration events. The net effect of contact metasomatism associated with the intrusion of the granite of Hopewell Lake, regional metamorphism, and later hydrothermal alteration is capable of obscuring the primary composition of the rocks. For example, thin sections of the granite of Hopewell Lake examined contain between 20 to 35% potash feldspar with diagnostic cross-hatched microcline twinning. Large amounts of Na must have been added to the rock to change its chemistry to that of trondhjemite without altering the gross crystal structure of the feldspar. The use of the present chemistry of rocks in the study area, especially major-element chemistry, to determine their protoliths therefore has considerable limitations and must be viewed with some caution.

Rubidium - Strontium systematics

Rb - Sr isotopic analyses on 8 whole rock samples are shown in Table 4. Six of the samples were obtained from an outcrop of the granite of Hopewell Lake at the spillway. One other granite sample was collected from the main area of mineralization, approximately 0.5 km southwest of the spillway. The eighth sample is a mineralized metavolcanic

Table 4.
Whole rock Rb-Sr analyses

Sample #	Rb ppm	Sr ppm	$^{87}Rb/^{86}Sr$	$^{87}Sr/^{86}Sr$
ghl-1	47.2	403	.33920 ± .00169	.70997 ± .00001
ghl-2	41.8	492	.24610 ± .00123	.70788 ± .00001
ghl-3	42.6	888	.13880 ± .00069	.70545 ± .00001
ghl-4	43.1	724.6	.17220 ± .0008	.70601 ± .00001
ghl-5	38.0	857	.12830 ± .00064	.70532 ± .00001
ghl-6	48.9	403.98	.35030 ± .0017	.709818 ± .000006
IZK-68B	47.8	209.9	.65940 ± .0033	.716149 ± .00001
ADIT #2*	37.3	178.1	.6066 ± .003	.718667 ± .000006

* altered metavolcanic rock

rock adjacent to this last granitic sample. The samples were all altered; the granite contained both sodic and carbonate alteration and the metavolcanic rock had carbonate alteration only.

The data is plotted on an isochron diagram in Fig. 19. The 7 granite samples define an isochron with a date of 1467 +/- 43 Ma and an initial $^{87}Sr/^{86}Sr$ ratio of 0.70256 +- 0.00029 at 2σ error. Fig. 20 is an evolutionary diagram constructed using the data from all the 8 whole rock samples.

It can be seen that the Rb - Sr isotopic compositions of samples from the granite of Hopewell Lake (including the one sample from the mineralized area) were reset between 1400 and 1560 Ma (Fig. 20). The metavolcanic rock does not appear to have been affected. $T_{depleted\ mantle}$ for all the samples range between 1560 and 2600 Ma. $T_{bulk\ earth}$ values for the samples range from 1000 to 1860 Ma. Model age ($T_{bulk\text{-}earth}$) of single Moppin rock is 1860 Ma. All the granite samples have negative $\varepsilon_{Sr}(1460)$ indicating that they were depleted relative to bulk earth.

The low initial $^{87}Sr/^{86}Sr$ ratio of the granite samples indicates that the granite was: 1) derived from a depleted mantle source, 2) formed by partial melting of a pre-existing rock derived from a depleted mantle, or 3) that the Rb - Sr systematics of the granite have been profoundly

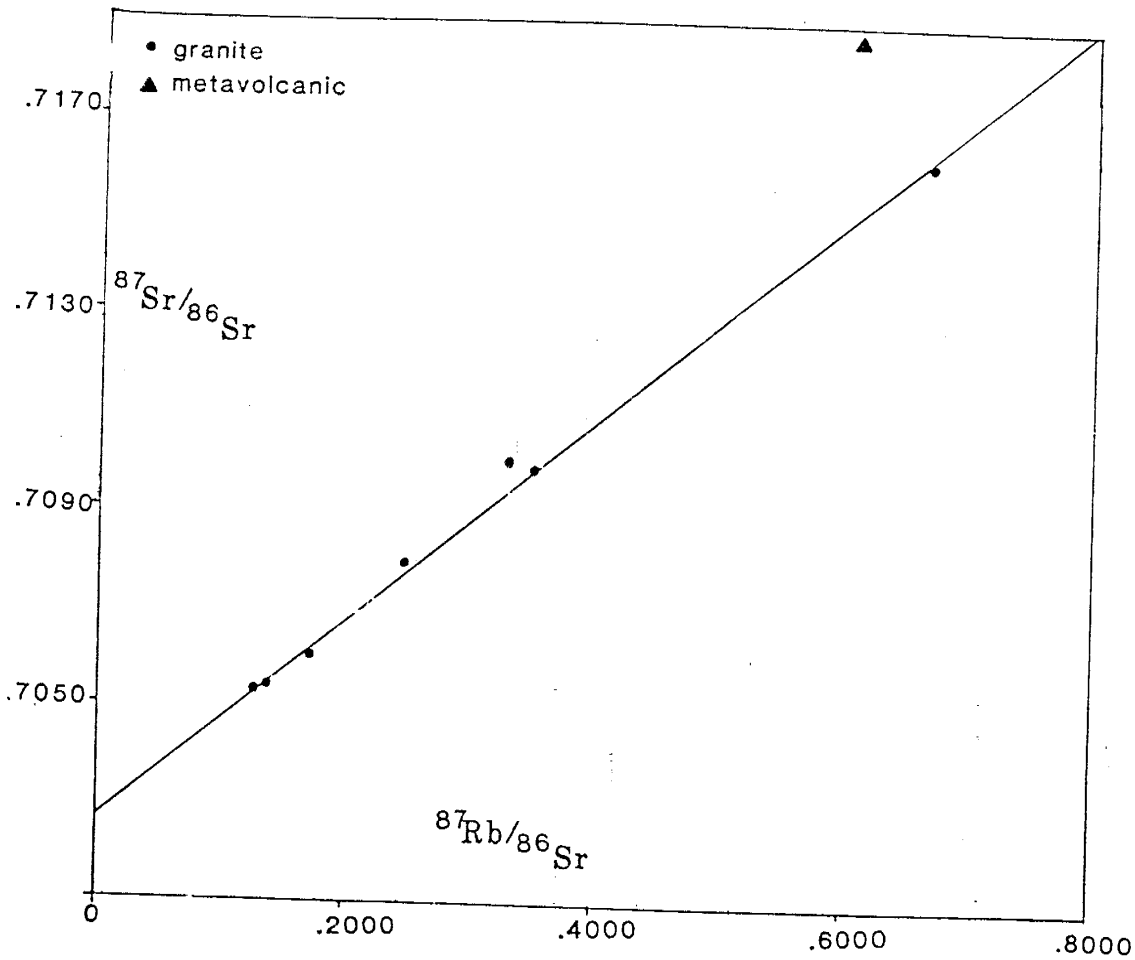

Fig. 19a Whole rock Rb-Sr isochron diagram

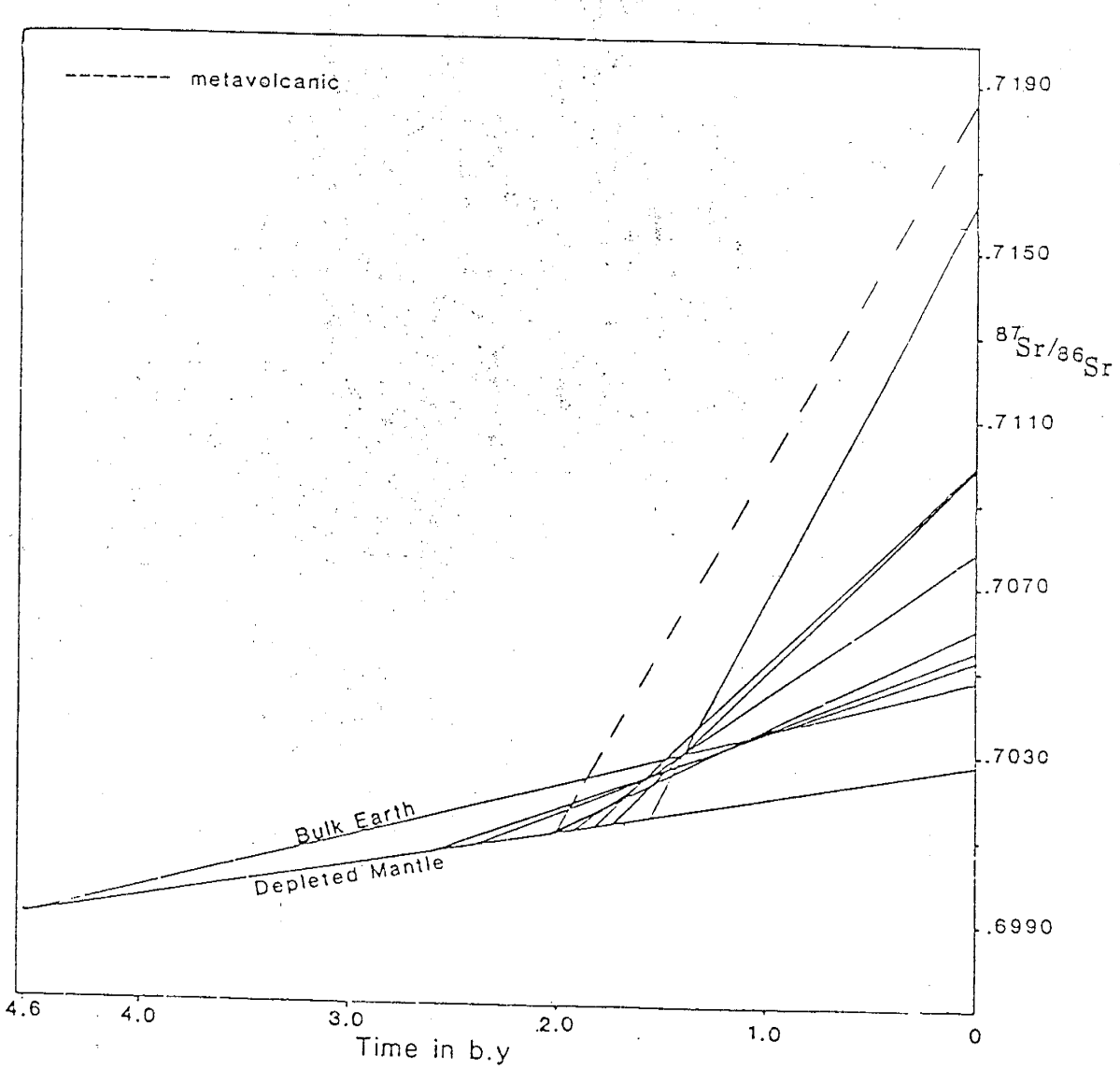

Fig. 20 Evolution diagram

affected by later fluids which were derived from a depleted mantle source.

The metavolcanic sample is shown on Fig. 19 and plots off the isochron. This suggests that the metavolcanic series are older and genetically unrelated to the granite of Hopewell Lake.

The low initial ratio indicates that the granite has not interacted to any measureable extent with crustally derived fluids, since the Sr isotopic composition of the granite would have increased significantly in any such interaction. The ubiquitous carbonate (and sodic ?) alteration present in the granite is therefore interpreted to be the result of hydrothermal alteration in which the fluids involved were magmatic. The whole rock isochron date, then, represents either the emplacement age of the granite, or that of the hydrothermal event.

If the date is the emplacement age of the granite, then we must explain: a) the abnormal Sr enrichment of the granite, b) the well developed megascopic metamorphic fabric of the granite, c) the folded granite - Moppin contact, d) the widespread sodium enrichment, and e)the carbonate +/- gold mineralization, all of which are absent from all other well dated (U - Pb) 1400 - 1500 Ma granites in New Mexico. These other granites, however, are intruded into rocks that are much younger than the Moppin Series that the granite of

Hopewell Lake intrudes (Robertson et al., in prep.). The granite of Hopewell Lake may thus be a much deeper equivalent of the 1400 - 1500 Ma granites, hence its uniqueness may be partly explained.

A Sr-bearing CO_2- rich fluid with such low initial ratio must have originated from a depleted mantle source; the fluid was most likely extracted from the mantle as part of a magma, and subsequently exsolved to form a separate phase only at relatively lower (mid. to shallow crustal) pressures. It is not likely that a mantle derived fluid could travel, independently, from source to the upper crust with its low initial ratio unmodified. There is no convincing evidence of any later magmatism in the immediate vicinity that might have provided an alternate "vechile" for transporting the fluid. Therefore the preferred explanation calls for a close genetic and chronologic relationship between the fluid and the associated granite of Hopewell Lake, and a single age for both.

GOLD MINERALIZATION

Gold analysis

Results of Au analyses are presented along with those of Ag, Cu, Pb and Zn in Appendix B; on Fig. 21, the gold values are plotted to show their distribution in the different lithologic units. A correlation coefficient matrix of all the elements analysed is given in table 5.

A detailed description of the procedure for gold analysis is given in Appendix A. Analytical methods for determining concentrations of Ag, Cu, Pb, Zn, and several other elements are contained in Brandvold (1974). Thirty samples were analysed for As, Sb, and very low concentration of gold by neutron activation analysis. Eleven of the latter set of samples were obtained from adjoining areas to the present study area; these were to provide background values and also ascertain which of the felsic intrusives outside of the study area might be a metal source.

A high positive correlation exists among the elements Au, Ag, and Cu. From a rather limited data base, there appear to be a significant correlation of As and Sb with Au. Pb and Zn do not show any correlation with Au, Ag, or Cu.

Gold values in the Moppin Series rocks range from 0.1 ppb to 1160 ppm. Typical values for Au in the mineralized areas range from 1 to 10 ppm. The relatively higher Au

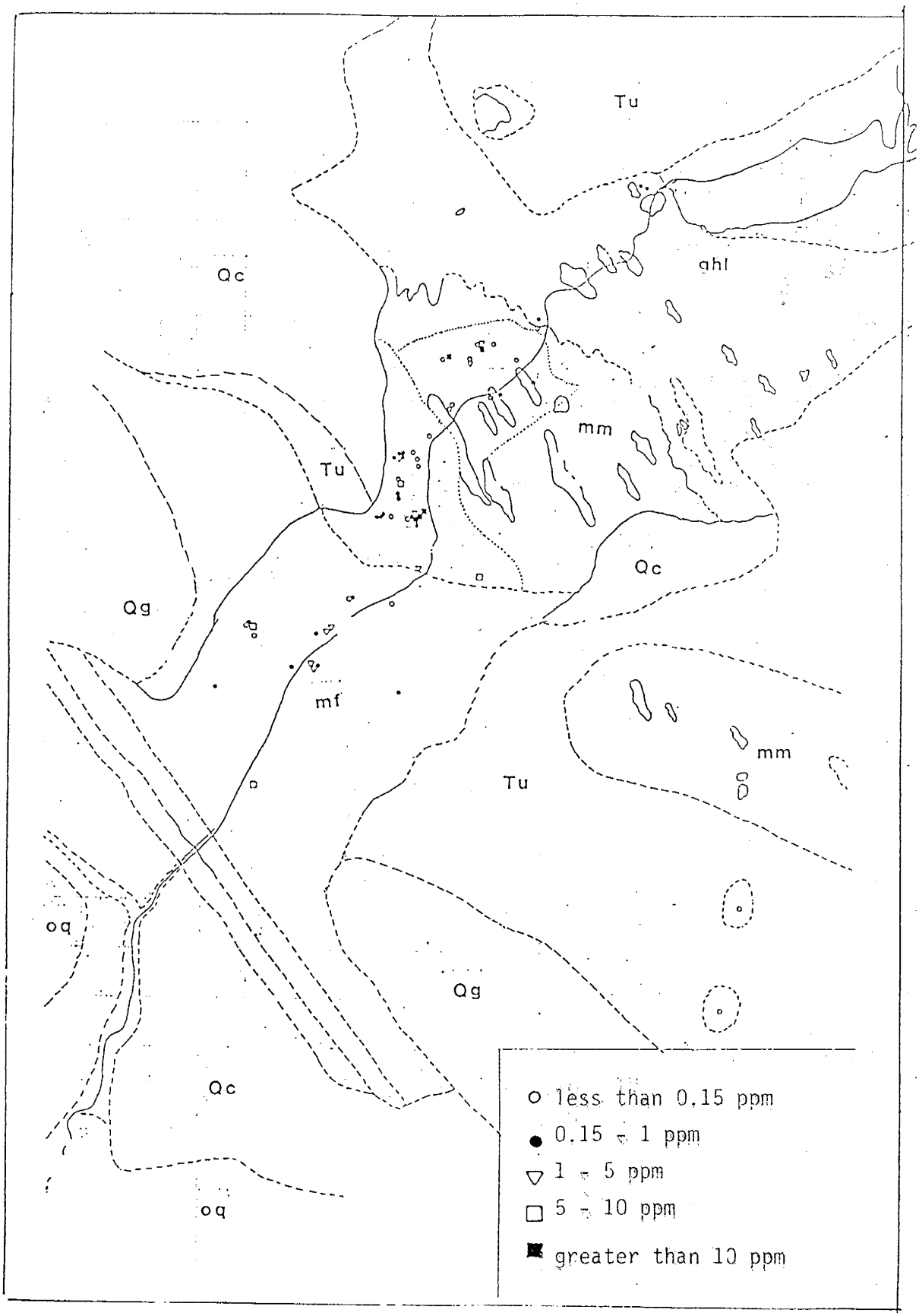

Fig. 21 Distribution of gold in rocks of the Hopewell area.

Table 5.

PEARSON CORRELATION COEFFICIENT MATRIX

	Au	Ag	Cu	Pb	Zn	As	Sb
Au	1.000	0.8855	0.9451	-0.0389	-0.0096	0.9974	0.6610
	(61)	(48)	(54)	(29)	(30)	(8)	(8)
	P=*****	P=0.000	P=0.0000	P= .841	P= .960	P=0.000	P= .074
Ag	0.8855	1.0000	0.8679	0.2337	0.2238	0.0000	0.4872
	(48)	(48)	(46)	(25)	(26)	(4)	(4)
	P=0.000	P=*****	P=0.000	P= .261	P= .272	P=1.000	P= .513
Cu	0.9451	0.8679	1.0000	-0.0300	-0.0277	0.0000	0.4872
	(54)	(46)	(54)	(29)	(30)	(4)	(4)
	P=0.000	P=0.000	P=*****	P= .877	P= .884	P=1.000	P= .513
Pb	-0.0389	0.2337	-0.0300	1.0000	0.7154	-0.5000	0.9907
	(29)	(25)	(29)	(29)	(29)	(3)	(3)
	P= .841	P. 261	P= .877	P=*****	P=0.000	P= .667	P= .087
Zn	-0.0096	0.2238	-0.0277	0.7154	1.0000	-0.4647	0.9954
	(30)	(26)	(30)	(29)	(30)	(3)	(3)
	P= .960	P= .272	P= .884	P=0.000	P=*****	P= .692	P= .061
As	0.9974	0.0000	0.0000	-0.5000	-0.4647	1.0000	0.6595
	(8)	(4)	(4)	(3)	(3)	(8)	(8)
	P=0.000	P=1.000	P=1.000	P= .667	P= .692	P=*****	P= .075
Sb	0.6610	0.4872	0.4872	0.9907	0.9954	0.6595	1.0000
	(8)	(4)	(4)	(3)	(3)	(8)	(8)
	P= .074	P= .513	P= .513	P= .087	P= .061	P= .075	P=*****

Coefficient / # of Cases / Significance

values consistently occur in the more altered rocks, or are associated with quartz veins.

Values of gold less than 1 ppb in samples of unaltered rock of all types and the observation that mineralization is not restricted to any particular rock type is interpreted to indicate that none of the exposed unmineralized rocks in the study area contained annomalous concentrations of Au prior to the alteration - mineralization event. The gold and most of the associated elements must have been derived from a source external to their immediate environment of deposition.

Geology

Alluvial Prospects

Both alluvial and lode gold mineralization are present in the district. A large proportion of gold mined from the district was reportedly won from the alluvial prospects located along the Placer Creek. This is rather suprising because the physiography of the district would make the alluvial prospects least attractive. There are virtually no alluvial flats along the Placer Creek, the only major drainage in the area. Furthermore, the sites where the alluvial materials were reportedly mined are located upstream of all the known lode deposits, perhaps indicating more lode gold mineralization within the catchment of the

Placer Creek. The occurrence of alluvial deposits may be conceivable within the flats of the Rio Vallecito; this drainage, to my knowledge, has not been tested. A few specks and small nuggets of native gold were observed in the stream bed of the Placer Creek. The limited amounts of alluvial prospects along the Placer Creek are unlikely to contain any significant total amounts of gold to sustain a commercial operation.

Lode Mineralization

Lode Gold mineralization occurs principally in rocks of the Moppin Series (Fig. 21). Gold values greater than 20 ppb have been found in the granite of Hopewell lake within and outside of the study area. Only one of 5 Burned Mountain metarhyolite samples analysed contained Au at a level greater than 1 ppb. All 4 samples of the metasediments overlying the metarhyolite also contained less than 1 ppb of Au. Within the Moppin Series, mineralization is not associated with any particular lithology. Although the greatest number of Au values greater than 5 ppm were found in the carbonate schist, at least one value of Au greater than 5 ppm was found in other members of the series.

The lode gold mineralization occurs in two distinct forms: quartz and quartz-carbonate veins and veinlets, and massive, replacement sulphide veins and disseminations.

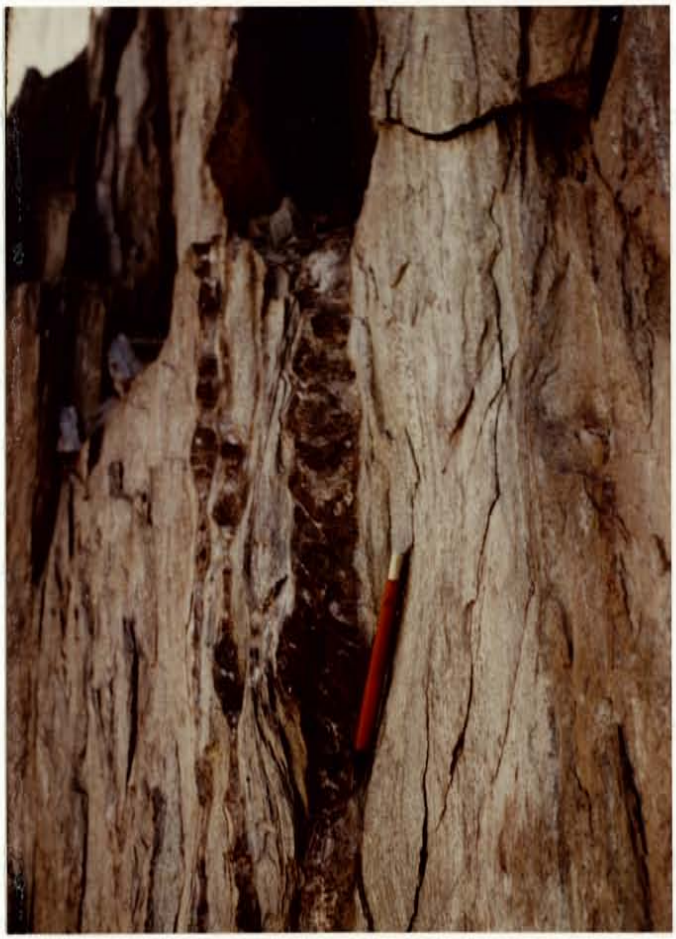

Fig. 22 Photograph of quartz-carbonate vein along S_2 in the felsic unit of the Moppin Series.

The quartz and quartz-carbonate veins commonly occur in brittlely deformed rocks which are the felsic members of the Moppin. These show localized carbonate alteration extending no more than about 15 cm from the veins. The replacement sulphide veins principally occur in rocks with ductile deformation fabric and generally mafic in composition. Sulphides are generally a minor component in the quartz and quartz-carbonate veins whereas they may constitute more than 75% of the sulphide viens. Although the mineralization is limited to the Moppin Series rocks, mineralized veins follow structural discontinuities which are also present in the other Precambrian successions.

The quartz and quartz-carbonate veins are commonly discontinuous along strike and occur as discrete lenses or pervasive stringers which pinch and swell in an irregular fashion. A few are continuous on an outcrop scale. Although the quartz veins occur along all the different deformation fabrics, a majority of them follow S_2, the major foliation in the Moppin series (FIG. 22). The veins commonly range from a few centimeters up to 30cm in width. The replacement sulphide veins are tabular and consist of chalcopyrite- and pyrite-rich vein and adjacent schist with impregnations of these sulphides. The veins may range from less than 1 cm up to about 30 cm in width. Pyritic haloes which extend several metres from the veins may contain more than 10 ppm of Au; the Au values, however drop sharply with

distance from the vein. At the Croesus mine, 2 samples from a sulphide vein, about 15 cm in width, assayed 1160 and 52.6 ppm of Au respectively; a sample obtained about 2m from the sulphide vein had 12 ppm, and 4 samples from 2 to 5m away from the vein averaged about 1 ppm Au. Two samples from greater than 5m from the vein contained less than 0.15 ppm Au. The gold content of rocks enclosing the quartz and quartz-carbonate veins drop to values below 0.15 ppm over distances not exceeding 30 cm away from the veins.

Pyrite, chalcopyrite, galena, sphalerite, arsenopyrite and specular hematite are the common ore minerals. All these minerals do not always occur together. The specular hematite is commonly associated with the quartz and quartz-carbonate veins. The ore minerals occur in a quartz matrix which may rarely contain disseminations of native gold. Observations from 5 polished sections indicate that a large proportion of the gold occurs, together with grains of pyrite and chalcopyrite, in specular hematite which is a late hypogene phase replacing the chalcopyrite, pyrite and arsenopyrite (Fig. 23 a and b). Disseminations and microveins of native gold have been observed within unaltered pyrite and chalcopyrite. Residual scales and veinlets of gold are visible in relief on a weathered chalcopyrite crystal.

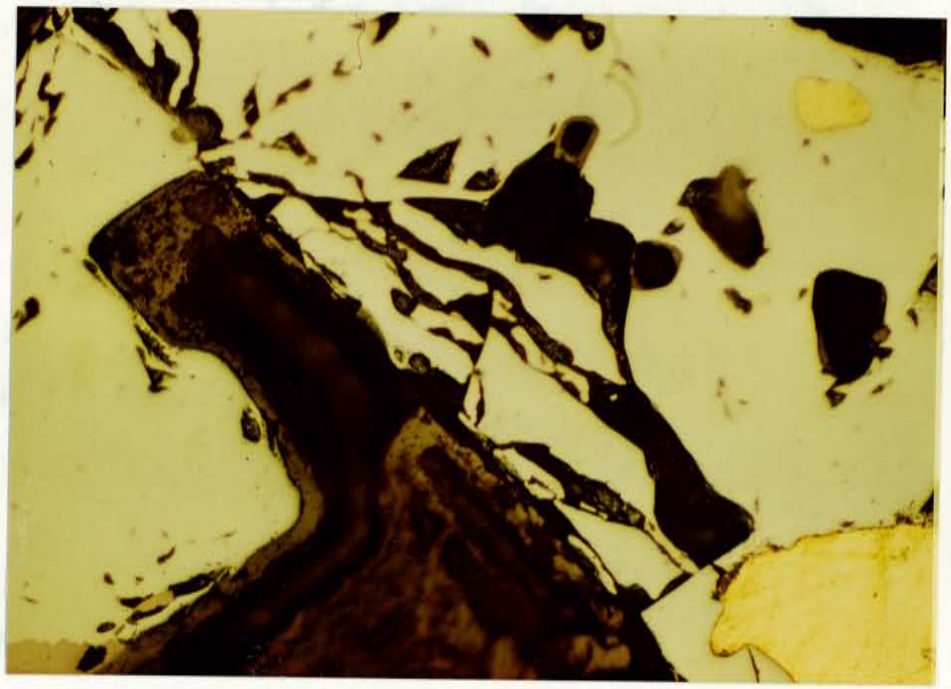

Fig. 23a Photomicrograph of the ore showing gold grains (golden) in chalcopyrite (field of view is 0.25 mm).

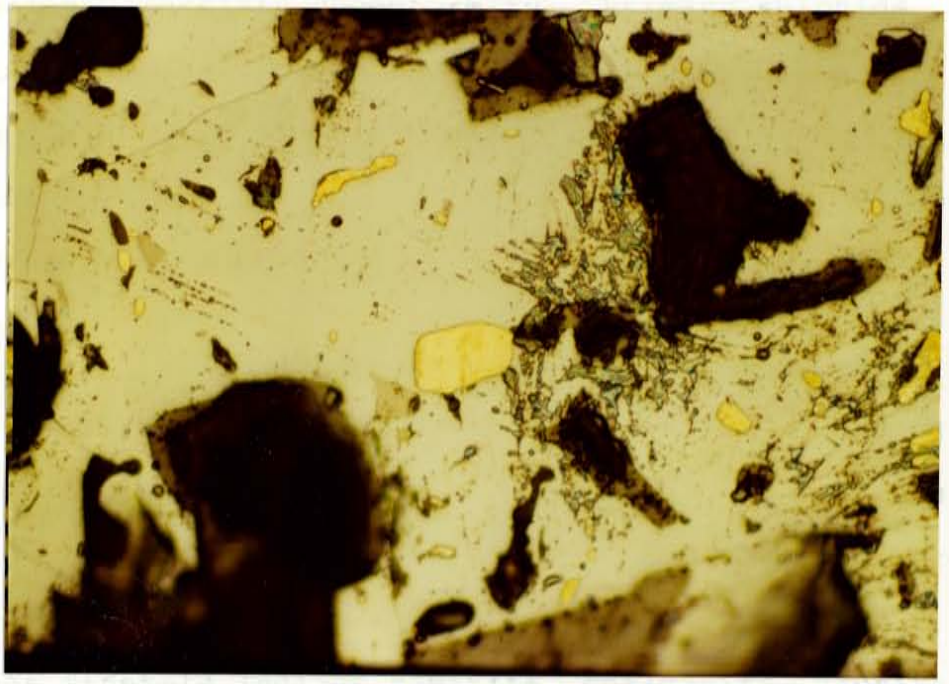

Fig. 23b Photomicrograph of ore showing gold grains mantled by specular hematite (field of view is 0.5 mm).

Supergene enrichment

Hypogene mineralization has been enriched by supergene processes within the extensive oxidation mantle below the Precambrian - Tertiary unconformity. Primary sulphide minerals have been leached from, or oxidized in the supergene zone leaving residual pockets of gold in limonite. The oxidation is thorough in some places reducing all the primary sulphides to earthy limonite; in other places primary sulphides co-exist with the limonite.

The oxidation mantle occurs over a large area along the Placer gorge and is characterized by reddish brown spots of limonite after ferromagnesian minerals, ferroan carbonates, chloritoids, and sulphide phases. At the Croesus mine, supergene minerals include hematite, chalcocite, azurite and malachite, in addition to the pervasive limonite (Fig. 24). The oxidation mantle may have a very irregular configuration: along the Placer gorge, both oxidised and unoxidised ores are exposed by erosion. Bingler (1968) has suggested that the oxidation may be related to exposure of the Precambrian rocks prior to the deposition of the Tertiary units.

Fig. 24 Photograph of oxidation zone at the Croesus Mine showing supergene minerals coexisting with primary sulphide phases.

Hydrothermal Alteration

The different types of alteration present in the rocks are carbonatization, sodic alteration, silicification and sericitation (Fig. 25). The carbonates are dolomite and siderite. Dolomite occurs as porphyroblasts in the chlorite-rich rocks. The dolomite crystals were observed, in thin section, to have deformed twin lamellae which suggests that they were affected by at least one of the deformation events and therefore preceded the mineralization. Siderite is present in the more altered rocks where it is found to be closely associated with the mineralized veins, and also in the granite of Hopewell Lake. More intense carbonate alteration are found in the mafic unit of the Moppin whose composition and well developed structural fabric made it more suceptible to alteration. The observation that some siderite veins in the mineralized area are brecciated and cemented by mineralized quartz veins (Fig. 26) suggests that some carbonatization preceded the mineralization and provided conduits, upon subsequent deformation.

Sodic alteration is observed only in the granite of Hopewell Lake within which the alteration appears to be extensive. Chemical data on 5 samples of the granite collected from different areas are all affected by this alteration.

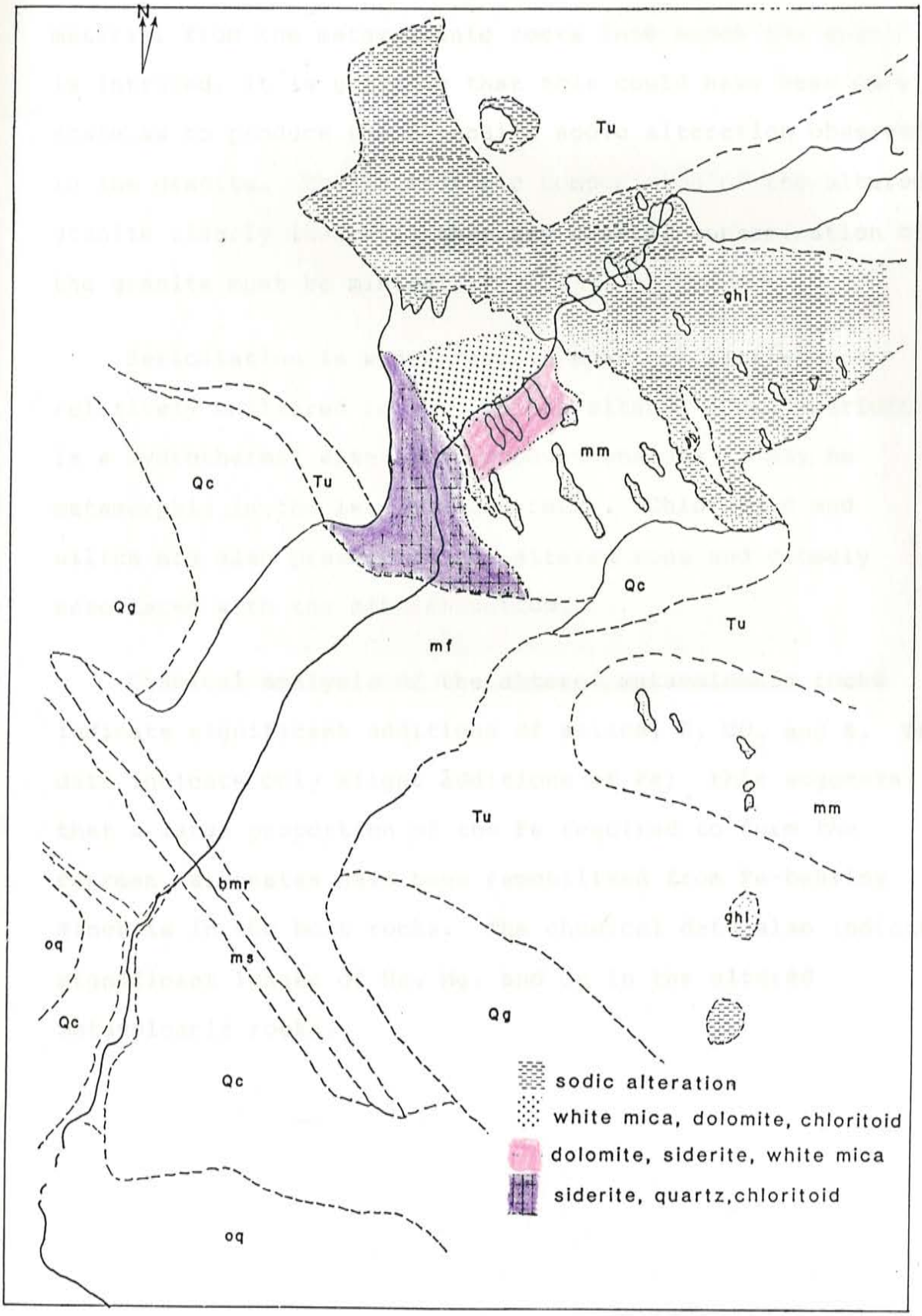

Fig. 25 Alteration types and their distribution

Although there could have been some assimilation of Na-rich material from the metavolcanic rocks into which the granite is intruded, it is unlikely that this could have been on a scale as to produce the extensive sodic alteration observed in the granite. The Sr isotopic composition of the altered granite clearly indicates that any crustal contamination of the granite must be minimal.

Sericitation is widespread in both the altered and relatively unaltered rocks. In the altered rocks, sericite is a hydrothermal alteration product whereas it may be metamorphic in the less altered rocks. Chloritoid and silica are also present in the altered zone and closely associated with the mineralization.

Chemical analysis of the altered metavolcanic rocks indicate significant additions of silica, K, CO_2 and S. The data indicate only slight additions of Fe; this suggests that a large proportion of the Fe required to form the ferroan carbonates have been remobilized from Fe-bearing minerals in the host rocks. The chemical data also indicate significant losses of Na, Mg, and Ca in the altered metavolcanic rocks.

Fig. 26 Photogroph of fragmented siderite vein cemented by mineralized quartz vein.

Paragenesis

An overall paragenetic sequence of the mineralization and associated alteration based on the petrographic and field relationship discussed in the above sections, is presented in Table 6. Dolomite and sericite are the principal premineralization minerals. Siderite, quartz, chloritoid, tourmaline, pyrite and the ore minerals characterize the mineralization. Supergene minerals: chalcocite, limonite, azurite, and malachite post date the mineralization.

Table 6 Paragenesis of alteration and mineralization event in the Hopewell mining area.

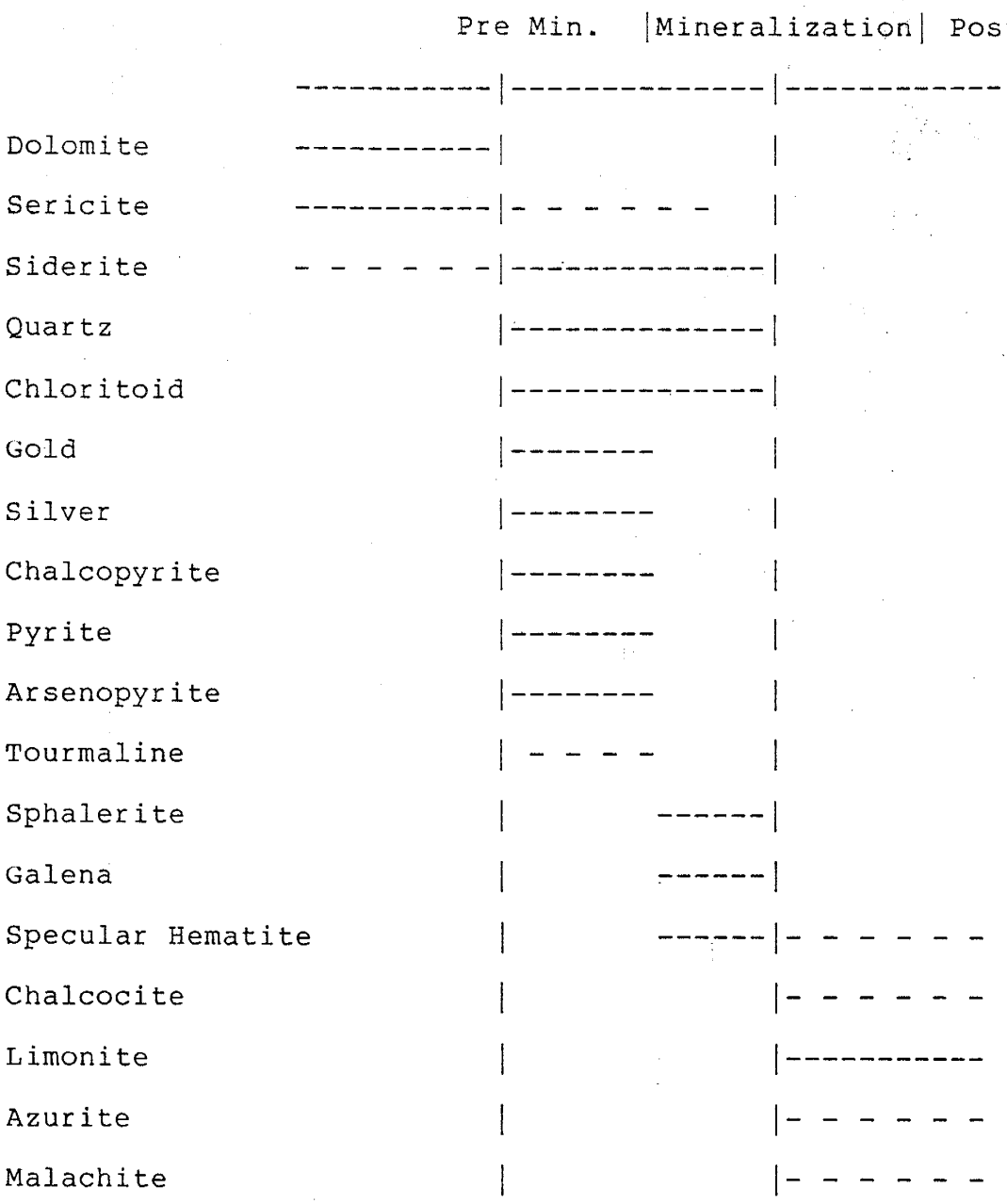

--------- common mineral

- - - - - less common mineral

FLUID INCLUSION STUDIES

Inclusions examined in this study were all hosted by quartz veins obtained from the altered Moppin Series, the quartzite, and the granite of Hopewell Lake. Quartz veins from the different host rocks all contained inclusions that are similar in morphology, chemistry and were trapped under similar P-T conditions.

Analytical Procedure

The stage was calibrated using de-ionized water, organic compounds, and sodium nitrate over the temperature range -63.5^{o}C to +306.8^{o}C. Recommendations contained in Roedder(1984, pg 206-211) were followed in the selection of standards for calibration. Heating and freezing rates for the various runs started between 5 and 20^{o}C/min and were reduced to 0.1-0.3^{o}C/min. near phase transitions. Measurements on phase transitions taken at temperatures below 31.1^{o}C were reproducible to +/-0.3^{o}C or better. Similar precisions were obtained for aqueous inclusions homogenizing at temperatures between 100 and 160^{o}C. The reproducibility of CO_2 / H_2O inclusions homogenizing at temperatures greater than 200^{o}C was about +/- 5^{o}C due to the inability to tell exactly when homogenization occurred.

Inclusion Petrography

Classification of the inclusions was based on inclusion morphology and phase relations at room temperature. All of the inclusions examined in the study may be grouped into three categories:

Type 1 inclusions were observed in all sections studied. They are two-phase aqueous inclusions, fairly uniform in size (<2um to ~10um), and of spherical to slightly elongate shapes. This type of inclusion is often closely spaced and may form either trails of inclusions or have a rather random-planar distribution. They do not have a three dimensional distribution and appear to delineate fractures nearly parallel to the polished sections (Fig. 27). They are interpreted as secondary inclusions based on their distribution and apparent association with fractures.

Inclusion types 2 and 3 are distributed randomly throughout many of the sections. They generally occur as isolated inclusions and are not co-planar. The sizes of these inclusion range from <5um to ~40um, with highly variable shapes. Also, unlike type 1 inclusions, types 2 and 3 inclusions exhibit variable phase ratios (see Fig. 28 and 29). Type 2 inclusions are single phase, high-density liquid-CO_2 inclusions. At room temperature they appear dark and may be mistaken for decrepitated inclusions. On cooling to between 10 and -10^{o}C they nucleate a vapour bubble to

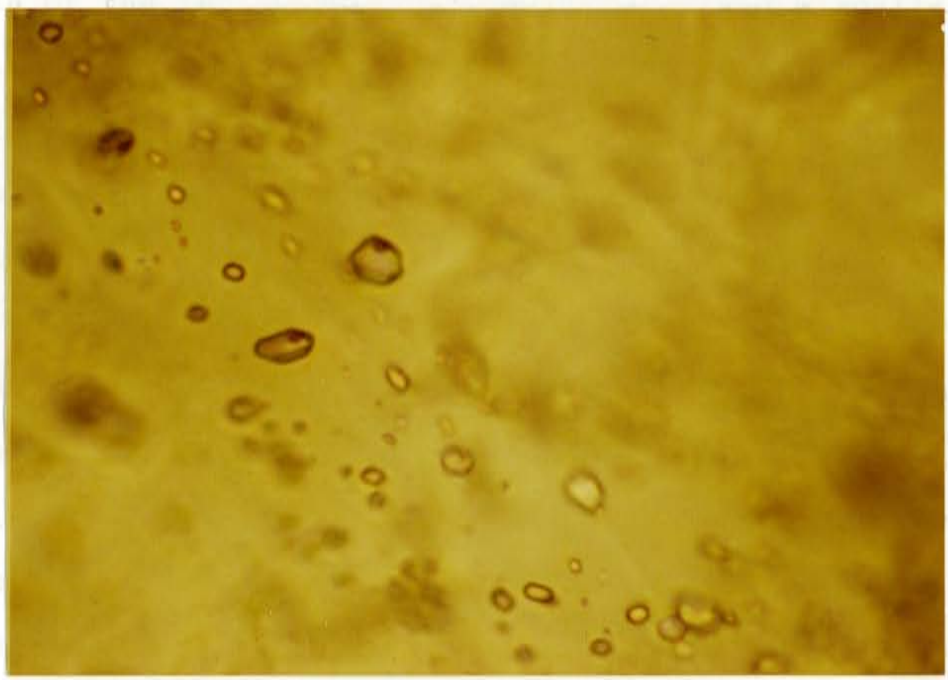

Fig. 27 Photomicrograph of type 1, 2-phase aqueous inclusion (field of view is about 200 μ).

form 2-phase inclusions (Fig. 28). The inclusions freeze when supercooled to between -90 and -110°C and melt upon warming at or near -56.6°C, which is the triple point of CO_2. They are therefore interpreted as liquid-CO_2 inclusions. Type 3 inclusions furnished most of the quantitative data used in this study. They are 3-phase inclusions consisting of an aqueous component which wets the walls of the inclusions; a liquid CO_2; and a smaller CO_2-rich vapour bubble within the liquid CO_2. A striking feature of these inclusions is the vigorous motion of their vapour bubbles. At room temperature, several of this type of inclusion contained only two phases: CO_2 fluid phase, and an aqueous phase. Upon slight cooling however, a liquid phase and a vapour phase were observed in place of the CO_2 phase. The volume % of the CO_2 phase in these inclusions varied from ~5% to ~90% (Fig. 30). About a dozen of the type 3 inclusions contained solid particles which do not dissolve when the inclusions are heated to homogenization. These particles are interpreted as pseudo-daughter minerals. Type 2 and 3 inclusions are interpreted as primary inclusion based on their distribution in the sections and lack of association with planar structures.

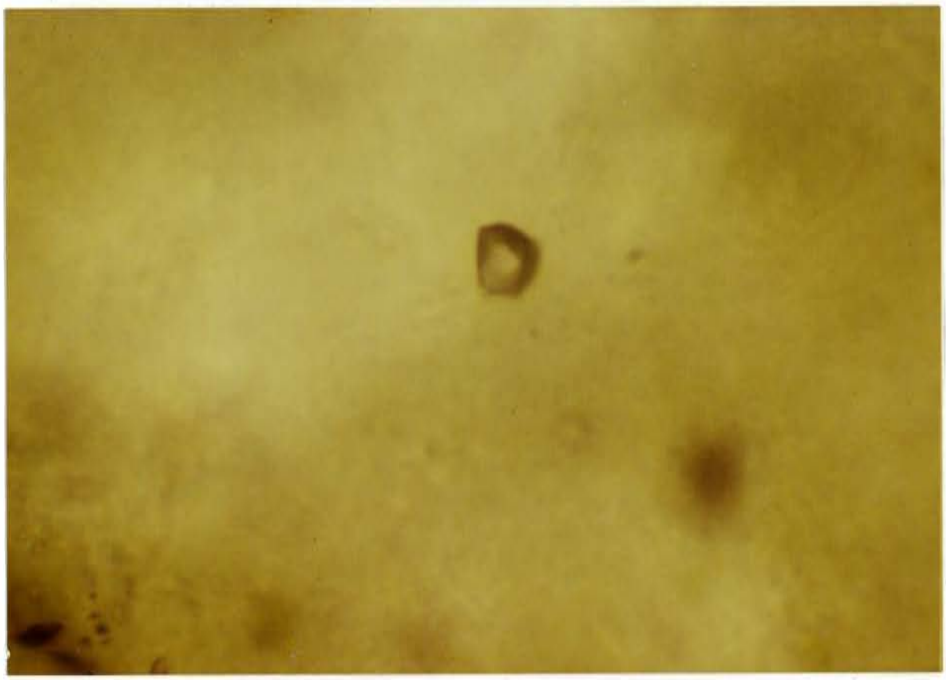

Fig. 28 Photomicrograph of type 2, single-phase CO_2 liquid inclusion (field of view is about 250 μ).

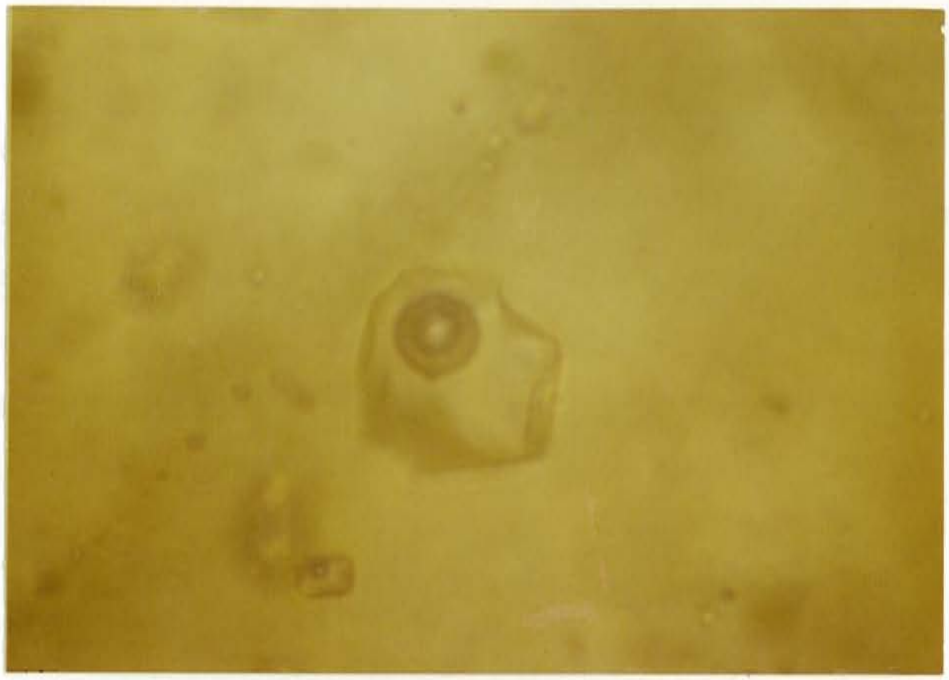

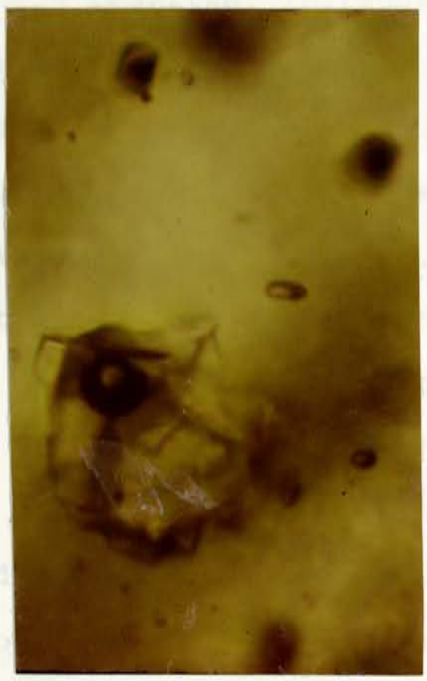

Fig. 29 Photomicrograph of type 3, 3-phase inclusion consisting, at room temperature, of CO_2 liquid, CO_2-rich vapour, and an aqueous phase. Fig. 30 Photomicrograph of type 3 inclusions showing CO_2-rich and aqueous-rich inclusions. (field of view is 200 μ across)

Thermometric Data and other Experimental Observations

Type 1

Histogram of Th, and salinities obtained from the freezing point depression of ice in the type 1 inclusions are shown on Fig. 31. The low Th. values (90 - 180^{o}C) support the secondary nature of these inclusions. The few high Th values may be of primary inclusions that were misclassified.

Type 2

When type 2 inclusions were cooled down to between -90 and -110^{o}C the liquid froze with a resultant increase in the size of the vapour bubble. The solid melted between -56 and -60^{o}C on the warming cycle; most melting at -56.5+0.2^{o}C. The co-existence of solid, liquid and its vapour phase marks a triple point. The triple point of pure CO_2 is -56.6^{o}C therefore strongly indicating the presence of CO_2. Melting temperatures down to -60^{o}C may be attributed to the presence of other gases (Collins, 1979; Burruss, 1981). Within individual inclusions, melting of the solid phase was instantaneous and also occurred at the same temperature for all of the CO_2-bearing inclusions in the field of view.

Type 3

The phase changes observed in the type 3 inclusions during the heating and freezing cycles are shown in Fig. 32 and 33. The data in Fig. 33 are numbered 1 to 8 to reflect the order in which they were obtained.

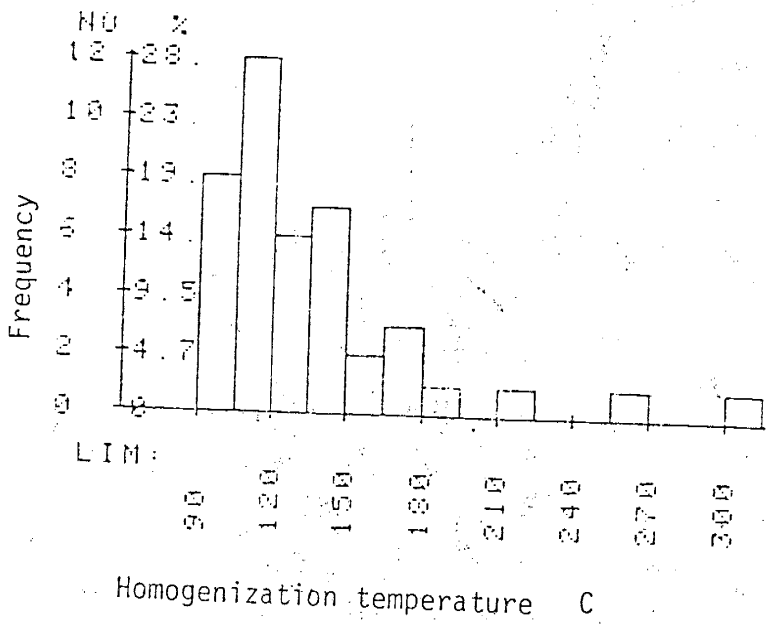

(i)

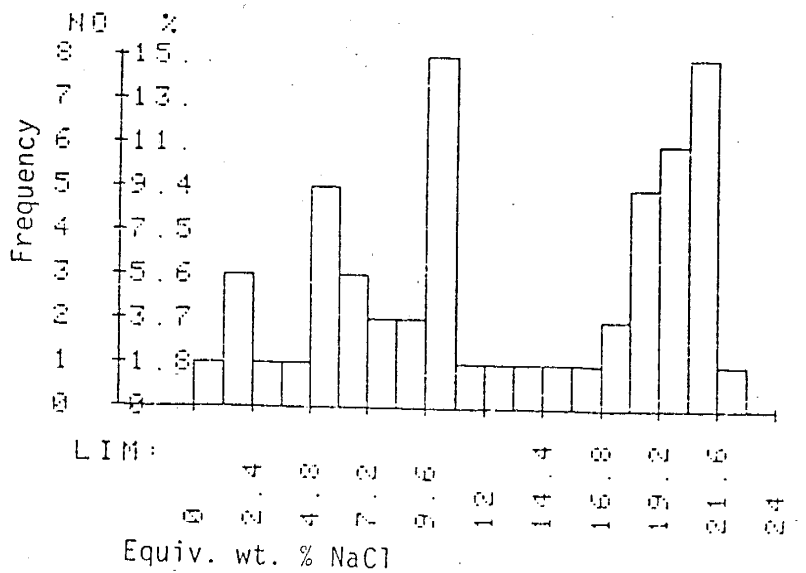

(ii)

Fig. 31 Histogram of homogenization temperatures (i), and salinities (ii) of type 1 inclusions.

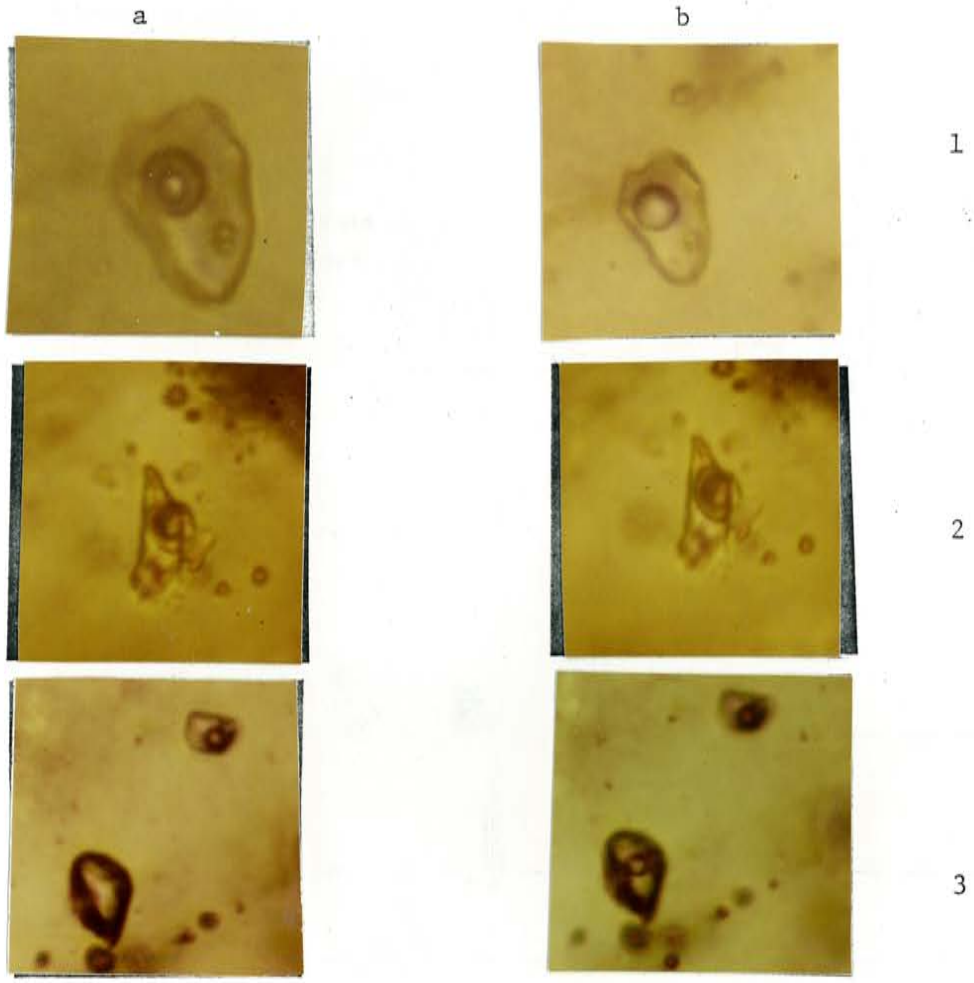

1 Liquid to vapor homogenization in Type 3 inclusion
2 Clathration in Type 3 inclusion. Distorted liquid CO_2 "bubble" indicates presence of clathrate (b) clath rate has melted and liquid CO_2 phase is spherical.
3 Type 2, single phase liquid CO_2 inclusion nucleates a vapor bubble on cooling.

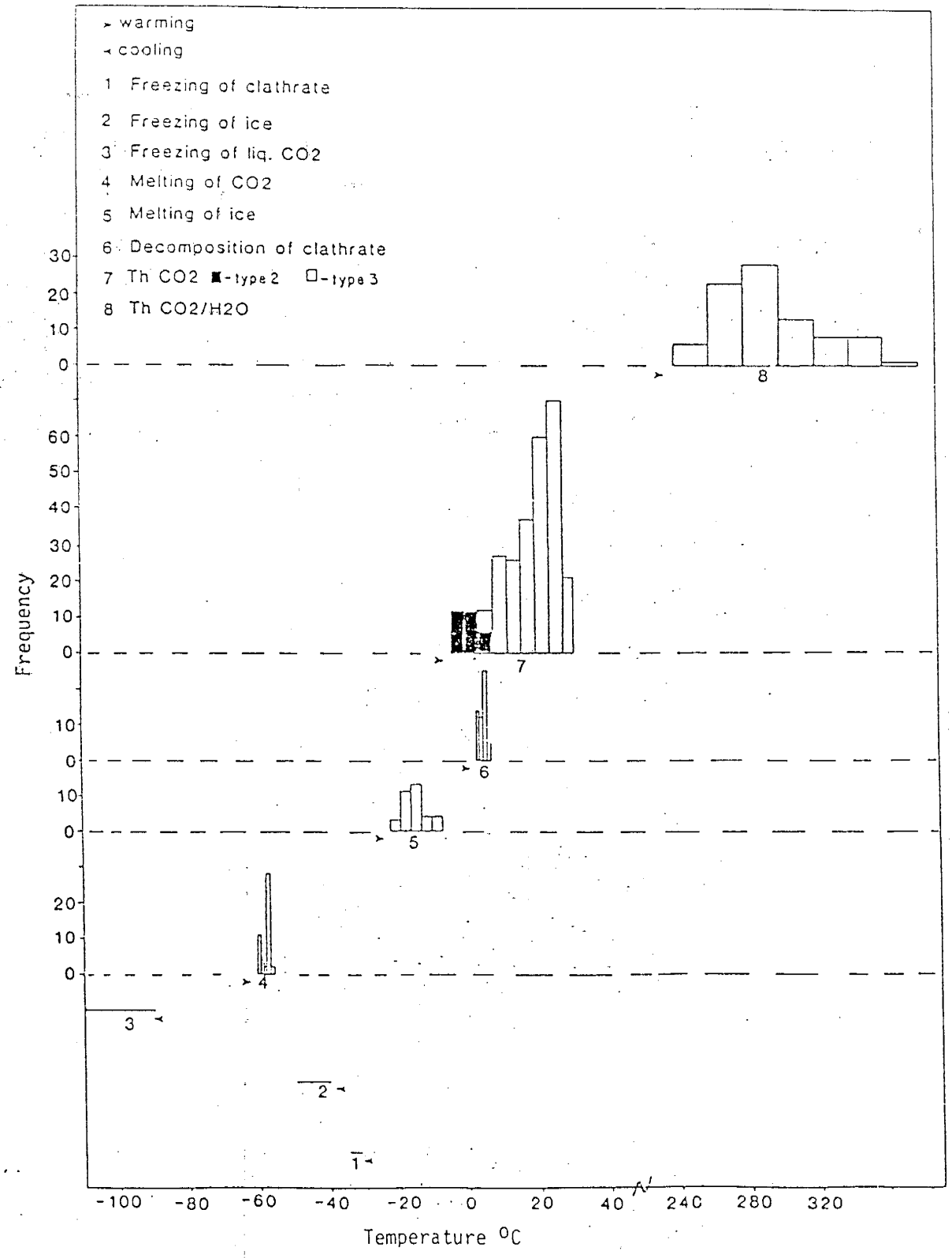

Fig. 33 Histograms of phase changes in type 2 and 3 inclusions

The volume % of the CO_2 phase in the type 3 inclusions was visually estimated at 40°C (appendix D). Roedder's chart for estimating the volume % of phases in spherical inclusions (Roedder, 1984) was modified and used in this study. It must be mentioned here that the volume measurement constitutes the single most significant source of error in the study. The error is estimated at +/- 10%. Homogenization temperatures ($Th/CO_2:H_2O$) were obtained with much difficulty; due to the high internal pressure of the CO_2 phase in these inclusions, a large proportion of them decrepitated before homogenization. The optical resolution on inclusions that did not decrepitate was rather poor and significantly affected the accuracy of measurements made on them. The CO_2-rich (>75 volume % CO_2 phase) and the aqueous-rich (>75 volume % aqueous phase) inclusions homogenized to vapour and liquid phases respectively between temperatures of 250 to 330°C. Inclusions with intermediate amounts of CO_2 and H_2O commonly decrepitated or homogenized at higher temperatures.

Synthesis and interpretation of data

The density of the CO_2-phase in the type 2 and 3 inclusions were determined using a Th-density plot (Fig. 34). Density values are shown in Appendix D and also in fig. 35.

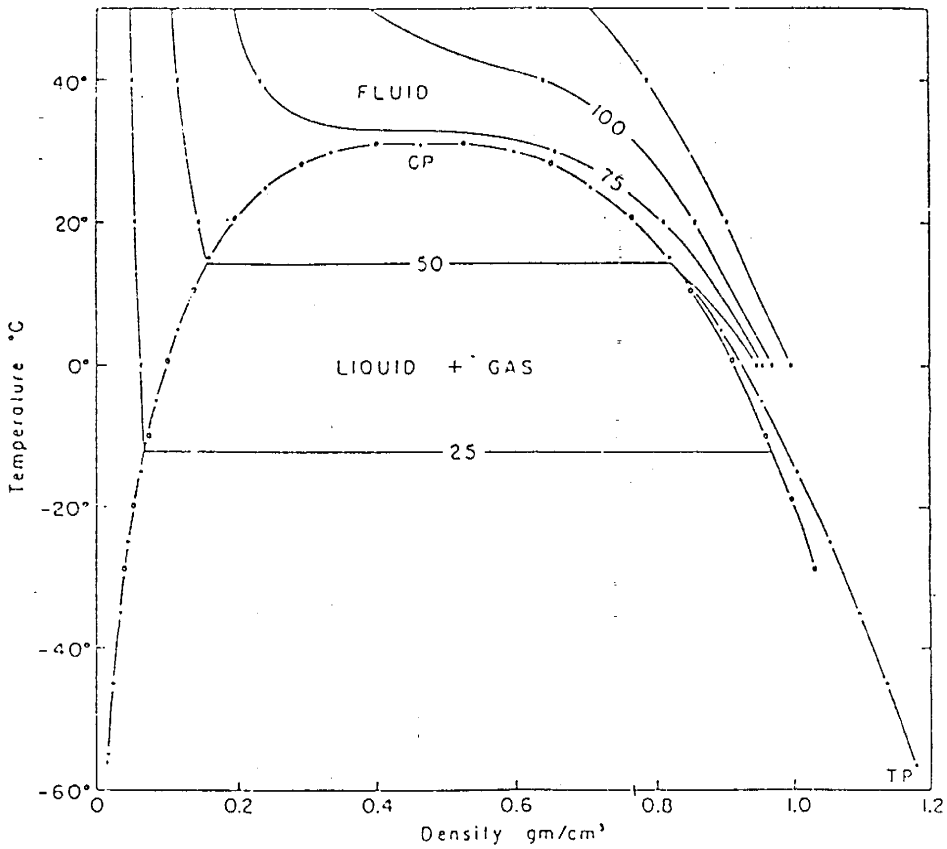

Fig. 34 Homogenization temperature versus Density plot for the CO_2 system in the low temperature range, from Roedder, 1984.

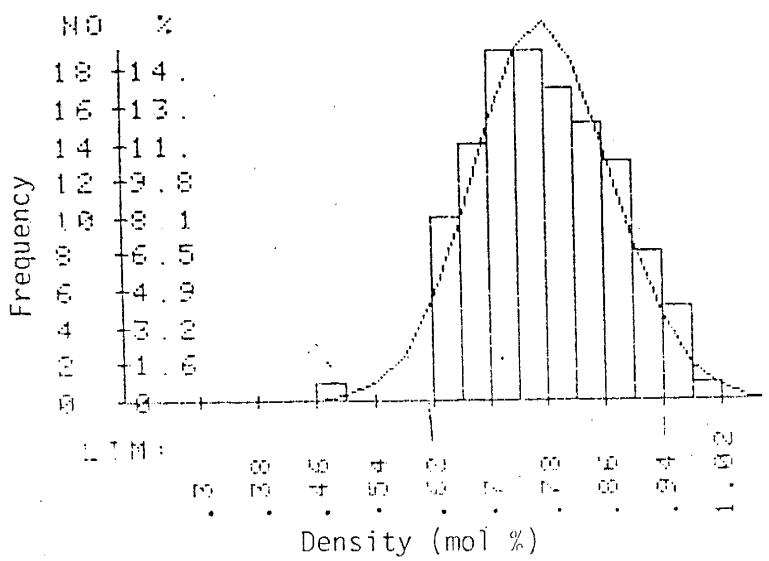

Fig. 35 Histogram of measured densities of type 2 and 3 inclusions.

An approximate bulk composition and molar volume of type 3 inclusions (Appendix D) were determined using estimates of the relative volume % of the CO_2 and H_2O phases at 40°C. Burruss's (1981) approach for estimating these parameters was adopted. The estimation of bulk composition and molar volume in mixed CO_2-H_2O inclusions by this approach relies on three basic assumptions, namely:

1) At temperatures slightly above the critical point of CO_2 (+31.1 < T <50°C), the co-existing phases are pure end members.

2) The bulk molar volume V of an inclusion is a linear combination of the end member components; that is $V = x_{H_2O}v_{H_2O} + x_{CO_2}v_{CO_2}$, where x_{H_2O} and v_{H_2O} are the mole fraction and molar volume of pure H_2O phase respectively, and x_{CO_2} and v_{CO_2} are analogous terms for the CO_2 phase.

3) Up to 40°C the H_2O phase is incompressible. Thus the pressure within a given CO_2-H_2O inclusion is fixed by the isochore for the one phase CO_2 fluid at 40°C (Burruss, 1981).

Burruss (1981) discusses the appropriateness of these assumptions.

Fig. 36 is an isothermal density-internal pressure plot for co-existing CO_2-H_2O fluids at 40°C. The volume % of H_2O in the inclusions is contoured on the plot to allow

estimation of the bulk density of an inclusion for any observed CO_2 phase density. The density of the CO_2 phase is expressed in moles per litre and used on Fig. 36 to determine the internal pressure (ip) of the inclusions at 40°C. From assumption # 3, the pressure inside a given inclusion at 40°C, is determined from the 0% H_2O contour. The value of ip defines the tie line a-b connecting the densities of the co-existing CO_2 and H_2O phases. The intersection c of the tie line a-b and the contour corresponding to the volume % H_2O in the inclusion fixes the bulk density of the fluids in that inclusion. An example from Burruss (1981) is given here to illustrate how Fig. 36 and 37 were used in this study to determine bulk composition and molar volume of inclusions. Suppose an inclusion with 30 volume % H_2O has the two phases within the CO_2 component homogenizing to the liquid phase at 20°C. From Fig. 34, the density of the CO_2 phase in this inclusion would be 0.77gm/cc or 17.5mol/litre. This corresponds to an internal pressure of 140 bars at 40°C. Thus tie line a-b in Fig. 36 is defined. The tie line intersects the 30 volume % contour at a density of 28.8 mol/litre which is the bulk density of the fluids in that inclusion.

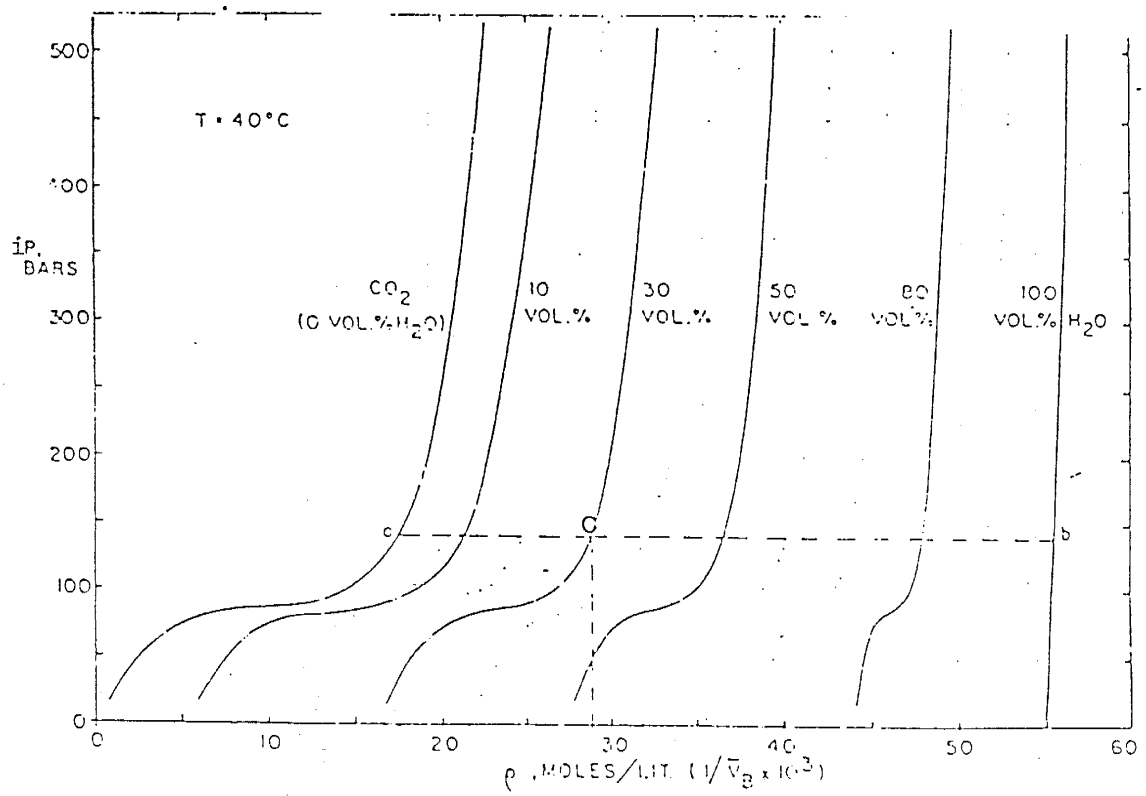

Fig. 36 A quantitative isothermal density - internal pressure diagram for coexisting CO_2 and H_2O fluids at +40°C.

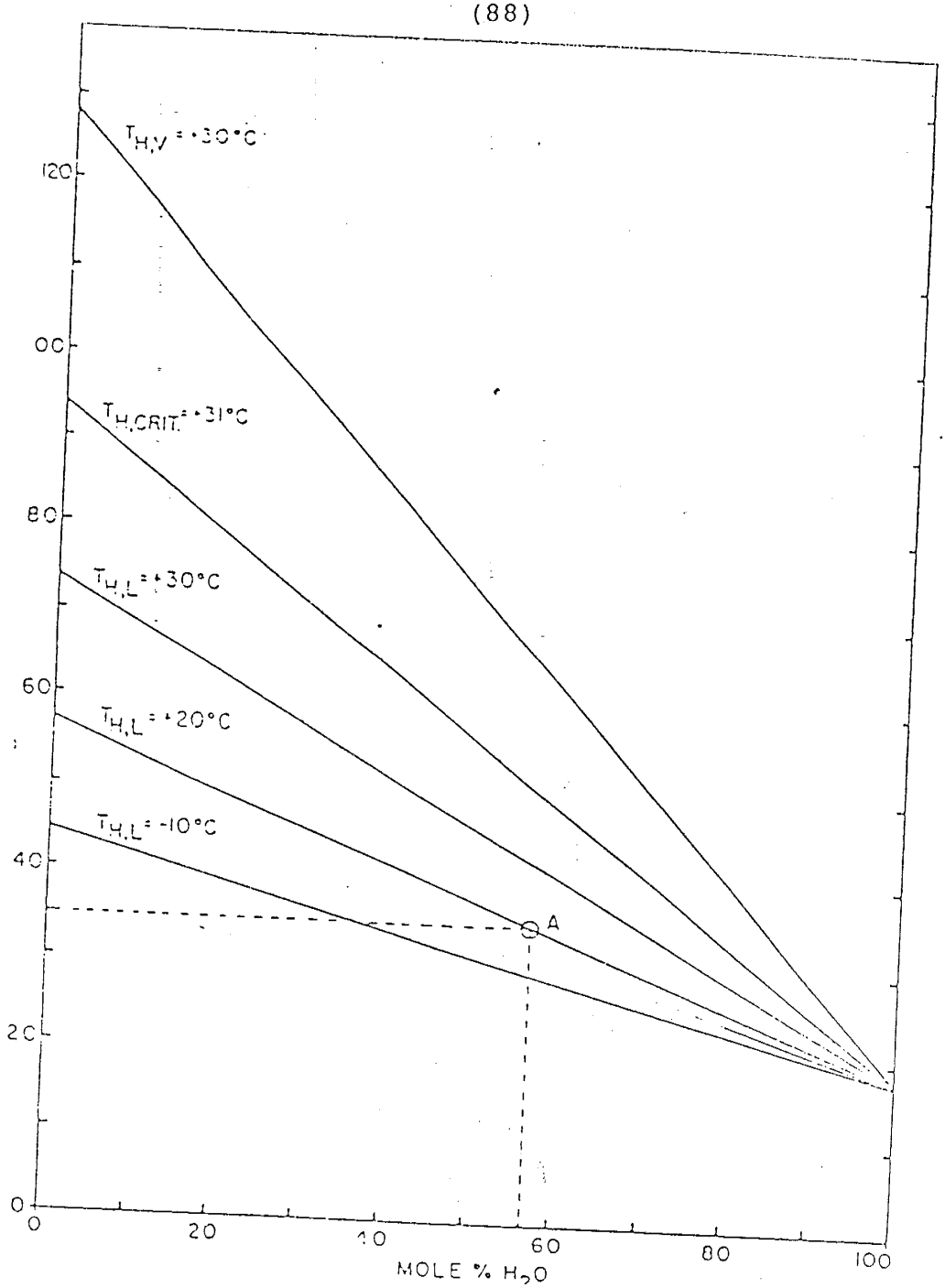

Fig. 37 A polythermal V_B - X_{H_2O} diagram with tie lines for coexisting CO_2 fluids and H_2O-rich liquid for the designated CO_2 liquid - vapour homogenization temperatures (Th., where subscript l or v indicate homogenization to liquid or vapour). After Burruss (1981).

To get the bulk composition, the bulk density is expressed as molar volume and plotted on Fig. 37 using the appropriate curve for the observed homogenization. In this example, the appropriate curve will be Th,l = +20°C and point A fixes the bulk composition of that inclusion at 57.8 mol. % H_2O.

Fig. 38 is a plot of Th versus composition of type 3 inclusions. The data define a solvus, which together with the observation that CO_2- rich and aqueous-rich inclusions co-exist and have variable phase ratios, is interpreted to indicate immiscibility of fluids during entrapment (Roedder, 1984). CO_2-rich and aqueous inclusions which homogenized within the same temperature range were trapped as separate homogeneous phases and their homogenization temperatures represents true trapping temperatures (Hendel and Hollister, 1981; Roedder, 1984).

Salinities of type 3 inclusions were determined from clathrate decomposition temperatures (Collins, 1979). Measured salinities range from 6.8 to 11.9 equiv. wt% NaCl (Appendix D, Fig. 39).

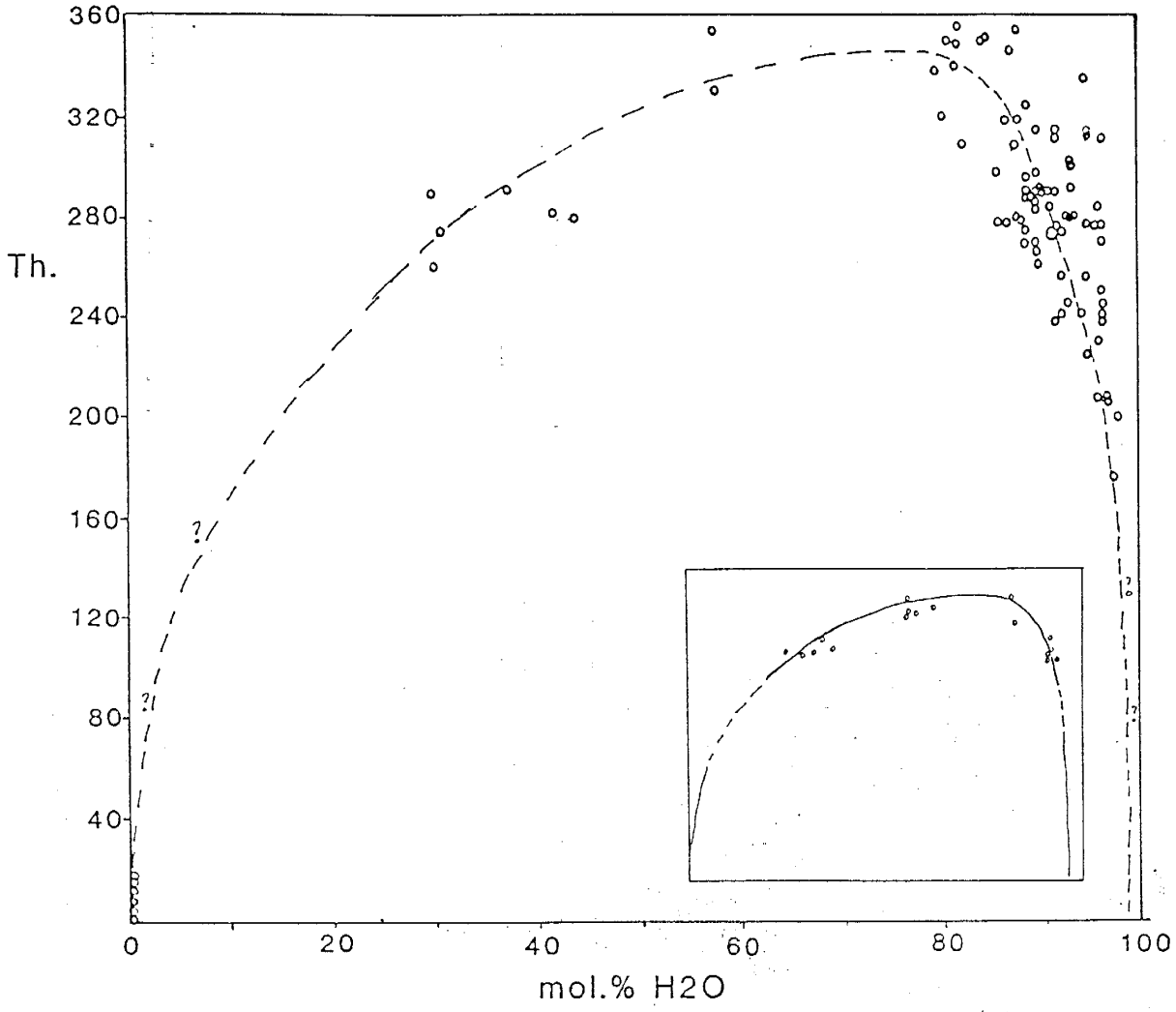

Fig. 38 Empirical solvus plot for CO2 – H2O inclusions with salinities ranging from 7.2 to 11.6 equi. wt. % NaCl (inset : solvus plot of Hendel and Hollister, 1981 for inclusions with 2.6 equi. wt. % NaCl in solution)

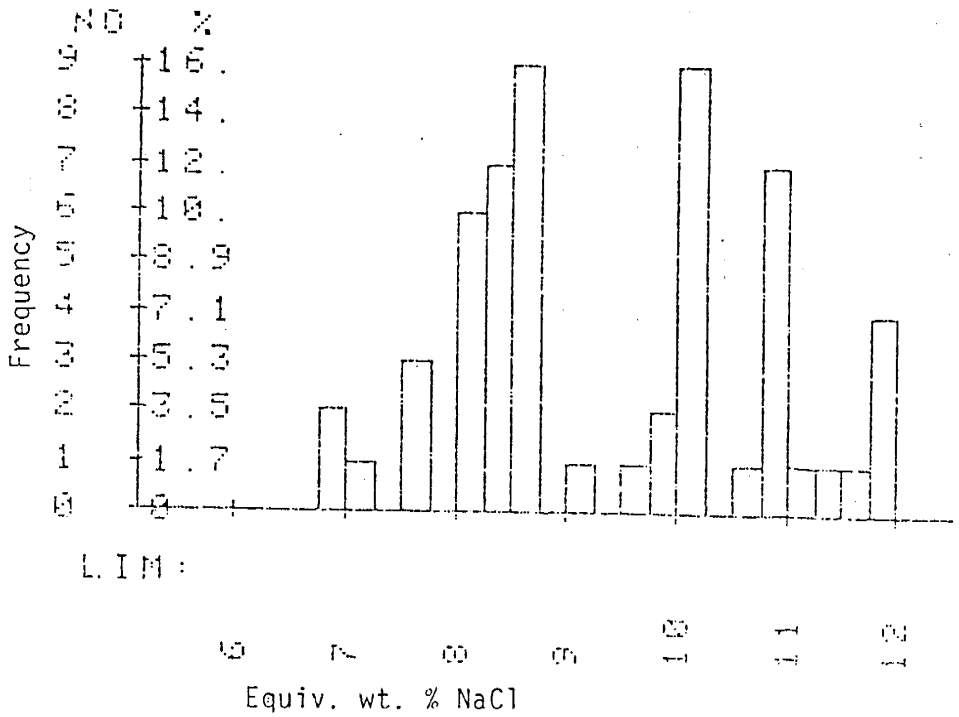

Fig. 39 Histograms of salinities of type 3 inclusions.

Estimation of Pressure of Entrapment

The data of Takenouchi and Kennedy (1965) on solubility of CO_2 in salt solutions at high temperatures and pressures (Fig. 40a and 40b) were curve fit by a computer program and used to determine the trapping pressures of inclusions in this study (Fig. 41). Input data for the computer program which is listed in Appendix C are Th, equiv. wt. % NaCl, and wt. % CO_2.

The pressure values range from 917 to 3000 bars, with a majority of the values falling within the range of 1000 - 2000 bars. The apparent wide range in the pressure values may be attributed, in part, to the variation in the salinities of the inclusions, and also to the inherent error in determining the volume percent of the aqueous and CO_2-rich phases in the inclusions. Inclusions interpreted to have been trapped as homogeneous phases, and defining the solvus curve (Fig. 38) were used in estimating the pressures; pressure values greater than 2500 bars were probably obtained from inclusions that do not quite belong to the population of inclusions which define the solvus. A pressure of 1400 bars was obtained using the average values of Th (290^{o}C), salinity (10.5 wt. % NaCl), and mole % (10 mole % CO_2) of all the aqueous-rich inclusions believed to have trapped a homogeneous phase.

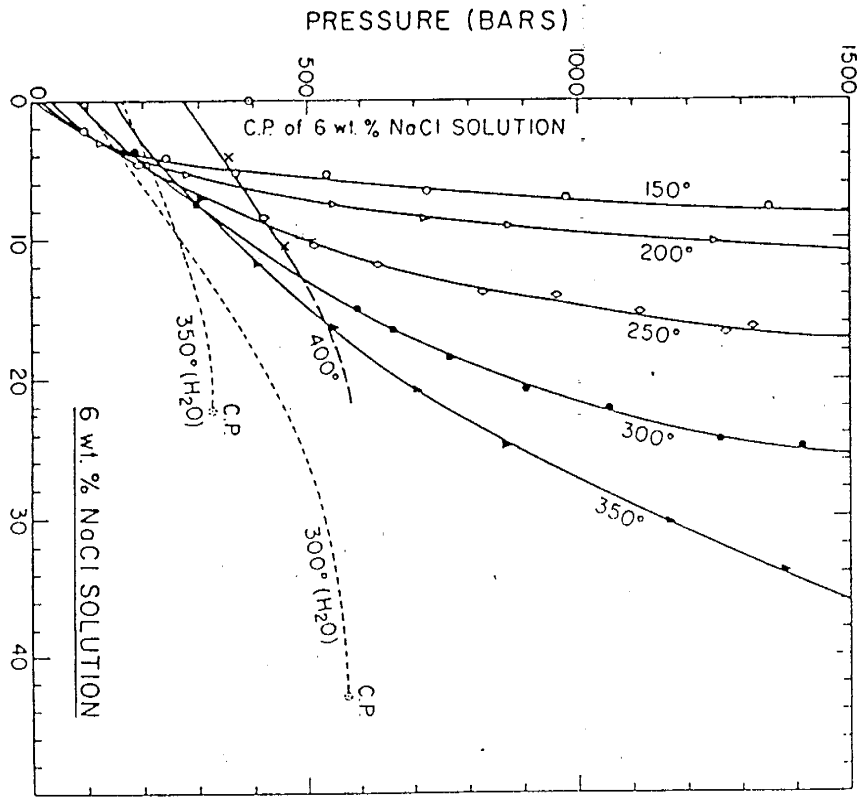

Solubility of carbon dioxide in 6 weight percent NaCl solution.

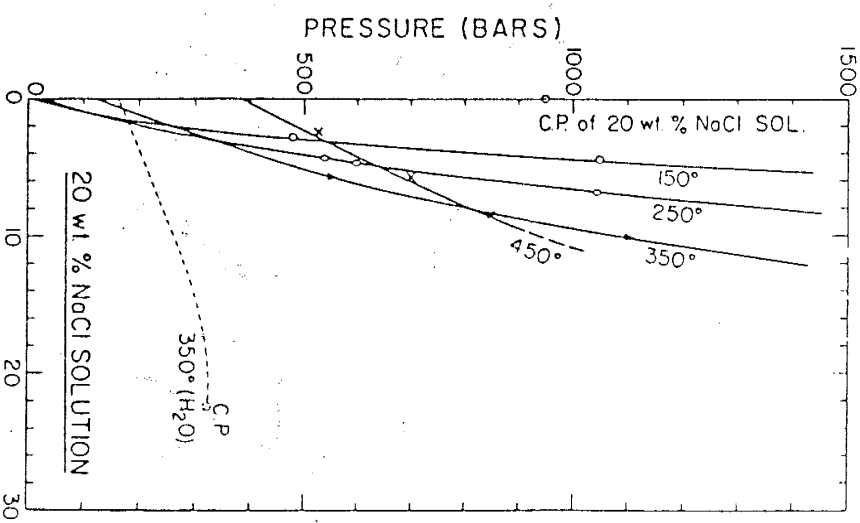

Solubility of carbon dioxide in 20 weight percent NaCl solution.

Fig. 40

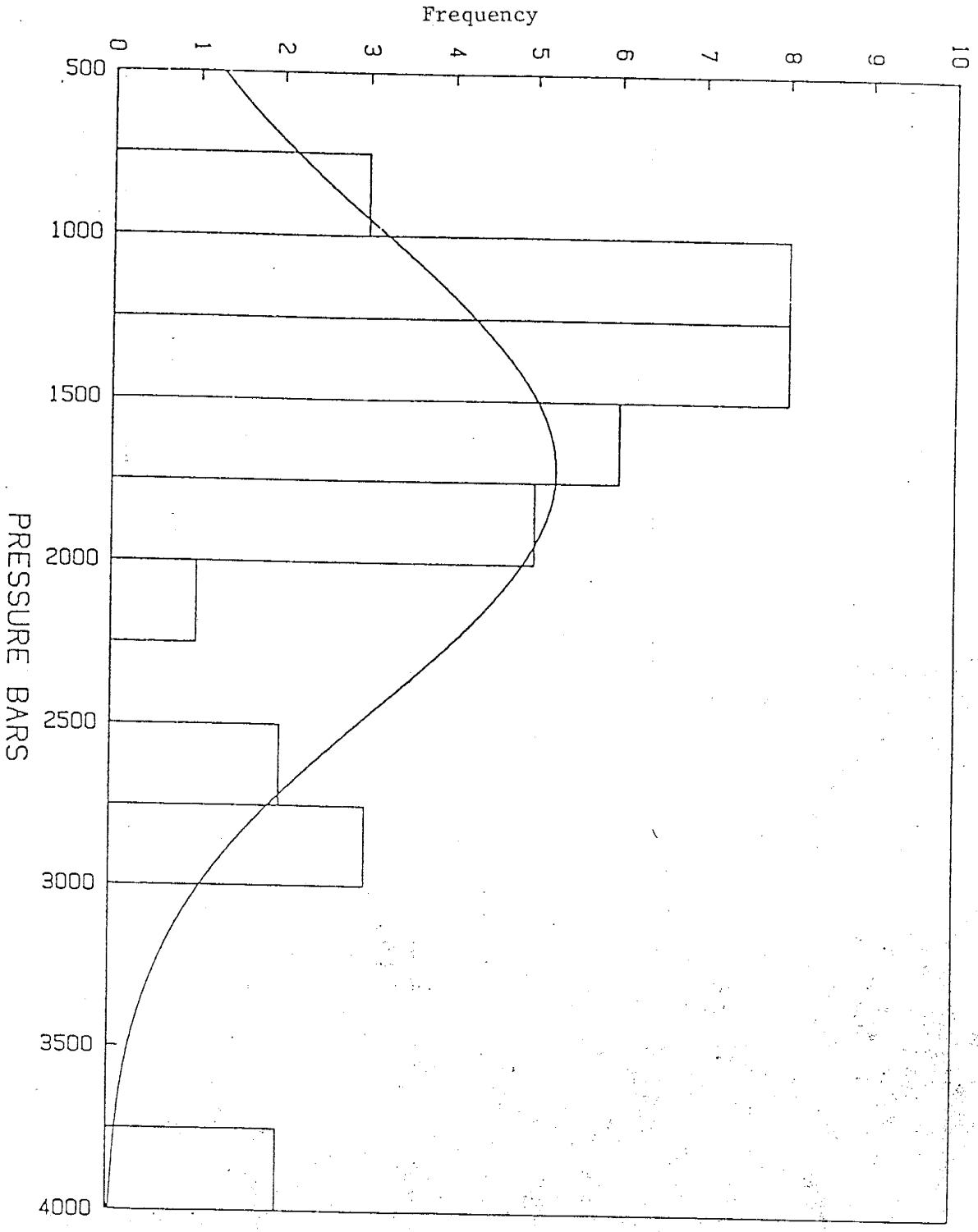

Fig. 41 Histogram of estimated trapping pressures of inclusions in this study.

Since there are no P-X plots for the CO_2-rich component of the ternary system, only the aqueous rich inclusions are used in the pressure estimates. The presence of the CO_2-rich inclusions is nonetheless important in constraining the Th. and composition of the aqueous inclusions that were trapped as homogeneous phases.

Pressure Correction:

The fluid inclusions examined in this study were trapped during boiling or phase separation. The homogenization temperatures are therefore the true trapping temperatures of the inclusions and require no pressure corrections. This is confirmed on isochoric plots by Bowers and Helgeson (1983) for fluids of different CO_2 content and salinities.

DISCUSSION

Protoliths of major rock types and geologic setting

Thin sections of the Moppin Series rocks examined were found to contain relict igneous textures which strongly suggest that rocks of the series are volcanogenic. The mineralogy of the different members of the series suggests that their protoliths range from mafic to felsic volcanic rocks. Trace element data indicate that members of the series form a continuous volcanic suite which range in composition from basalts through andesites to dacites. The series is compared with Phanerozoic calcalkaline volcanic suite and is interpreted to have formed along a converging plate margin.

The age of the Moppin Series is unknown. $T_{bulk\text{-}earth}$ of one sample of the Moppin Series is 1860 Ma. This age conforms with model ages, T_{DM}, from northern New Mexico which indicate that the Precambrian rocks in the area could not have been extracted from the mantle prior to 1900 Ma (Nelson and DePaolo, 1985).

Thin sections of the Burned Mountain metarhyolite contain relict eutaxitic textures diagnostic of welded ash flow tuffs. Its mineralogy and trace element chemistry indicate that it has the composition of a rhyolite. The Burned Mountain metarhyolite is interpreted as a subaerial

flow; marine incursion during the waning stages of volcanism may have resulted in the intercalation of the immature metasediments within the metarhyolite. A long period of quiescence is suggested by the 1 km thick Ortega quartzite.

An Rb - Sr whole rock isochron date of 1467 of samples of the granite of Hopewell Lake is interpreted to represent the emplacement age of the granite. The granite was derived from a depleted mantle and is probably a deep seated eqiuvalent of other 1400 - 1500 Ma granites in New Mexico.

Timing of gold mineralization

The minimum age of the mineralization has been constrained by Bingler (1968) who notes that clasts of mineralized Precambrian rocks are present within the basal Tertiary conglomerate.

Field observation and fluid inclusion studies in the present study indicate that the mineralization post dates all the Precambrian rocks in the Hopewell area. Although the mineralization is limited to the Moppin Series rocks, mineralized veins follow structural discontinuities which are also present in all the other Precambrian successions. Furthermore, unmineralized quartz veins in the quartzite are known, from fluid inclusion studies, to be genetically related to the mineralized veins in the Moppin. It is

evident then that the mineralization occurred when the rocks had been affected by one or more episodes of deformation and had devoloped a fabric which served as channelways for the fluids.

The Sr isotopic composition of the altered granite of Hopewell Lake strongly suggests that the granite was derived from a depleted mantle source or that it has equilibrated with fluids from a depleted mantle. The low initial $^{87}Sr/^{86}Sr$ ratio of the altered granite indicate minimal or no interaction with crustal fluids.

The whole rock isochron date of 1467 +/ 43 Ma is interpreted as representing the emplacement of the granite of Hopewell Lake. Within the limit of the error on the date, it also represents the timing of the alteration. The carbonate alteration present in the granite of Hopewell Lake is present in the metavolcanic rocks also and closely associated with the mineralization. It is thus inferred that the mineralization occurred at 1467 Ma.

Nature of mineralizing fluids and their possible sources

The pervasive carbonate alteration associated with the mineralization and high content of CO_2 in fluid inclusions from mineralized rocks are indicative of mineralizing fluid(s) charged with CO_2. At the great depth at which the mineralization formed, it is unlikely that there was any

significant meteoric input in the ore fluid.

Sr isotopic composition of the altered granite indicate that the fluid responsible for the alteration, which is also the fluid implicated in the mineralization, contained Sr derived from a magmatic source. The mineralizing fluid may have equilibrated with a magma at depth or even exsolved from a magma. Magmas saturated with CO_2 may exsolve a fluid phase at pressures in excess of 2 kb in which CO_2 phase may be dominant relative to H_2O and H_2S (N. Dunbar, personal comm., 1985).

Another possible source of fluid is metamorphic. The date on the mineralization correlates very well with the 1450 Ma date on metamorphism by Grambling and Ward (1985). Therefore metamorphic dehydration and decarbonation reactions may have furnished some fluids too. At the time of metamorphism the metavolcanic rocks were over 300 Ma old and must have contained high radiogenic Sr. Fluids derived from such a source should reflect the high ^{87}Sr content of the rocks. The isotopic data, however, do not indicate any measureable contribution of fluids derived from a high Sr source rock.

The indicated saline nature of the ore fluids and the presence of sulphides in the deposit, indicate that chlorides and sulphides were present in the fluids. The gold could therefore have been transported as Cl^- or HS^-

complex.

Migration of fluids

Alteration and mineralization in the Hopewell area are closely associated with the deformation fabric, principally foliation, within the host rocks. Where rocks are massive and lacking in structural discontinuities, alteration and mineralization are lacking also. The mineralizing fluids must have therefore been funnelled along structural discontinuities to their site of mineralization.

Source of metals

The Sr isotopic composition of the altered granite, which monitors the solute source of the fluids responsible for the alteration (Norman and Landis, 1983), indicate the gold and other metals were derived from a magmatic source. The low initial ratio of the altered granite indicate that the ore fluid had virtually no contact with the metavolcanic rocks, the only alternative for a metal source besides a magmatic source. The gold and other metals were thus introduced into the rocks by magmatic fluids.

Controls of ore deposition

Three main factors may have operated together to cause the deposition of the ore.

The deposition of quartz in the area of mineralization suggests that the ore fluid was cooling (Truesdell, 1984; Fournier and Potter, 1982). Experimental data from Fyfe and Henley (1973) indicate a major decrease in the the solubility of gold transported as $Au-Cl^-$ complex within the temperature range of 300 and 400°C. Gold and other metals which were mobilized as Cl^- complexes, along with quartz, would therefore precipitate out of solution as the ore fluid cooled to the appropriate temperature range.

The data from fluid inclusion studies indicate a marked phase separation at the site of mineralization. Dissolved CO_2 exsolved out of the ore fluid due to a sudden drop in pressure as the fluid encountered low pressure environments such as fracture cleavages and tension fractures formed by earlier deformation events. Loss of CO_2 from the fluid medium would lead to an increase in the pH of the residual aqueous phase. $Au-Cl^-$ complexes are unstable in alkaline media (Henley, 1984); thus a significant increase in pH would result in the breakdown of the $Au-Cl^-$ complexes and hence the deposition of the gold. An increase in pH would also facilitate the deposition of carbonates (Hedenquist and Henley, 1985; Higgins, 1985), while the drop in pressure

will result in the deposition of quartz (D. Norman, personal comm., 1985). In addition, the phase separation may cause the partioning of H_2S into the CO_2 phase. A depletion of H_2S in the aqueous phase will result in the breakdown of Au-HS^- complexes to replenish lost H_2S and therefore cause deposition of gold. Thus, regardless of the species responsible for mobilizing the gold, the unmixing of CO_2 out of the ore fluid would play a major role in causing the deposition of gold. Pb, Zn and Cu may also be decomplexed of Cl^- and HS^- and would similarly be expected to precipitate.

Wall rock interaction with the ore fluid may have resulted in the fixation of CO_2 to form the carbonates associated with the mineralization. Such depletion in dissolved CO_2 would lead to deposition of the ore, as discussed above. Also hydrolysis reactions, such as alteration of potash feldspar and plagioclase to sericite and paragonite respectively, will deplete the fluid of H^+ resulting in an increase in the pH of the ore fluid (Henley, 1984). Alteration assemblages in rocks associated with the mineralization at Hopewell suggest that such reactions did occur and may have played an important role in causing the deposition of the ore.

Genetic Model

The data assembled in this study suggest that a large proportion of the fluids involved in the mineralization at Hopewell was derived from a magma related to a depleted mantle source. Although the mineralization is coeval with metamorphism, the Sr isotopic data on the altered granite and the trapping temperature of the ore fluid argue against any significant metamorphic component in the mineralizing fluid. The isotopic data strongly suggest that the fluid was pristine and had no contact with the metavolcanic rocks prior to the deposition of the ore.

The metallic constituents were derived from a magmatic source, probably the same source from which the magmatic fluids were derived. It is also possible that the gold was leached out of the granite of Hopewell Lake. The gold and other metals may have been mobilized as Cl^- and HS^- complexes.

The following mechanisms operated together to cause deposition of the ore: a) cooling of fluids down a geothermal gradient as the fluids ascended; b) unmixing of CO_2 phase as the fluids encountered low pressure environments in deformed rocks, and c) interaction of fluids with wall rock. The last two mechanisms would both lead to an increase in pH which will results in the breakdown of the Au - complex. The uncomplexed Au co-precipitated with

metallic species, quartz and carbonate to form the deposit.

Type comparison

The mineralization at Hopewell shares similar characteristics with many Precambrian and Phanerozoic deposits described world wide. Archean gold deposits in Australia are hosted by metavolcanic rocks and intrusive rocks associated with the metavolcanics (Groves, 1985). The deposits are characterized by pervasive carbonate alteration and are postulated to have formed by CO_2 - H_2O fluids at pressures between 1 and 2 kb and temperatures which range from 300 to 400^{o}C. Kerrich and Fyfe (1981) report intense carbonate alteration enveloping auriferous veins within the Campbell, Con and Giant shear zone at Yellowknife, NW Territories, Canada. The deposits are estimated to have formed at a pressure of 2 kb and temperature of 400^{o}C (approx.). Colvine et al. (1984) describe a number of lode gold deposits in the Abitibi Subprovince which include the Mecassa, Kerr, Addison, Sigma, Detour, and Dome mines. All of these deposits are either hosted by, or spatially associated with intrusives which range in composition from syenites to granites. The gold is also hosted by metavolcanic rocks into which the plutonic rocks intrude. Carbonate alteration is present in the rocks and is closely associated with the mineralization. Colvine and others interpret the early carbonate phase to indicate an evolving

hydrothermal system initially CO_2-dominated, and later CO_2 + H_2O-dominated, with gold-mineralization associated mainly with the latter. Petrovskaya et al. (1973), and Lyakhov and Popivnyak (1978) report unmixing of CO_2 out of ore fluids involved in the mineralization of the Buryatia deposit and several other gold deposits in the Soviet Union (see Bowers and Helgeson 1983). The authors postulate that pressure drop and associated degassing of CO_2 out of the Au-bearing fluids contributed to the breakdown of complexes responsible for transporting gold. Reinthal et al. (1985) note a zone where CO_2 boiling or unmixing occurred during deposition of Au-Ag in the Cracker Creek district, NE Oregon. Zones immediately beneath the zone of unmixing are reported to host ores whose grade are substantially higher than ores obtained from elsewhere in the area. The deposits formed between 300 and 350^{o}C. Harris (1978) describe carbonate and sodic alteration in granodiorite stock which host the Salave gold deposit in Austurais, Spain.

The Australian and Canadian deposits are postulated to have formed by metamorphic processes (Groves, 1985; Kerrich, 1977), in contrast to the magmatic origin that this study proposes for the gold mineralization in the Hopewell area.

CONCLUSIONS

1) The Moppin metavolcanic series represent a compositionally continuous suite of mainly subalkaline volcanic rocks analogous to those present in Phanerozoic converging tectonic settings.

2) The gold mineralization which is hosted by the Moppin Series rocks is coeval with the emplacement of the granite of Hopewell Lake and was formed by deuteric fluids which flushed through the granite and adjacent volcanic rocks. The fluids and the granite of Hopewell Lake were both derived from a depleted mantle or from the partial melting of an older rock with a depleted mantle source.

3) The mineralization formed at a depth equivalent to a pressure of 1.5 kb and a temperature of about 300^{o}C (approx.).

4) Whole rock Rb - Sr isochron date of 1467 Ma obtained on the granite represents the time of the emplacement of the granite and that of the deuteric alteration. Since the alteration is closely associated with the gold mineralization, the date also gives the age of the mineralization. The granite was emplaced during metamorphism and therefore is syntectonic.

5) The mineralization at Hopewell shares many of the features of lode gold deposits described world wide. These features include a close association with granitic intrusives, ubiquitous carbonate alteration, the presence of CO_2 in fluid inclusions which commonly indicates a phase separation, sodic alteration, and P - T of formation of 1 to 2 kb and 300 to 400^{o}C respectively.

REFERENCES

Barker, F., 1958 Precambrian and Tertiary Geology of the Las Tablas Quadrangle, New Mexico: New Mexico Bureau of Mines and Mineral Resources Bulletin 45, 104p.

----------, 1979, Trondhjemites: Definition, Environment, and Hypotheses of origin; in Barker, F., ed., Trondhjemites, Dacites and Related Rocks: El Sevier publishing, New York.

Bell, D. A., and Nielsen, K. C., 1985, Intrusion and Deformation Sequence of the Embudo Granites, Northcentral New Mexico. (abs.) Geol. Soc. Am. with Programs, 17, 3, 151.

Best, G. M., 1982 Igneous and Metamorphic Petrology. Publishers: W. H. Freeman and Co. 630p.

Bingler, E. C., 1968 Geology and Mineral Resources of Rio Arriba Co. New Mexico: New Mexico Bureau of Mines and Mineral Resources Bulletin 91, 158p.

Bowers, T. S., and Helgeson, H. C., 1983. Calculation of the Thermodynamic and Geochemical Consequences of Non Ideal Mixing in the System H_2O - CO_2 - NaCl on Phase Relations in Geologic Systems: Metamorphic Equilibria at High Pressures and Temperatures. Am. Mineral., vol. 68, 1059 - 1075.

Brookins, D. G., and Majumdar, A., 1982, The Sandia Granite, New Mexico: Biotite Metamorphic and Whole Rock Rb - Sr ages: Isochron/West, n. 33 p 19 - 21.

Burruss, R. C., 1981 Analysis of Phase Equilibria in C-O-H-S Fluid Inclusions. Mineral. Assoc. Canada Short Course Handbook 6, 39 - 74.

Butler, A. P., Jr., 1946 The Tertiary and Quaternary Geology of Tusas - Tres Piedras Area, New Mexico, Ph.D dissertation, Havard Univ.

Collins, P. L. F., 1979 Gas Hydrates in CO_2- Bearing Fluid Inclusions and The Use of Freezzing Data for Estimation of Salinity. Econ. Geol. vol. 74, pp 1435 - 1444.

Colvine, A. C., et al. 1984 An Integrated Model for the Origin of Archean Lode Gold Deposits. Ontario Geological Survey Open File Report 5524 98p.

Condie, K. C., 1982a, Early and Middle Proterozoic Supracrustal Successions and Their Tectonic Settings. Am. J. Sc. vol. 282 pp 341 - 357.

----------, 1982b, Plate Tectonics and Crustal Evolution 2nd ed. Pergamon Press 310p.

Fournier, R. O., and Potter,R. W., 1982 A Revised and Expanded Silica (quartz) Geothermometer: Geothermal Research Council Bulletin, vol. 11, pp 3 - 9.

Fyfe, W. S., and Henley, R. W., 1973 Some Thoughts on Chemical Transport Processes, With Particular Reference to Gold. Miner. Sc. Engng.,vol. 5 No. 4 pp 295 - 303.

Gibson, T. R., 1981 Precambrian Geology of The Burned Mountain - Hopewell Lake Area, Rio Arriba Co., New Mexico. MS thesis New Mexico Inst. of Mining and Technology, 105p.

Gramling, J. A., and Ward, D. B., 1985 Crustal Thickening during Proterozoic Metamorphism and Deformation in New Mexico: Proceedings of the 6th International Conference on Basement Tectonics.

----------, and Williams, M. L., 1985 The Effects of Fe^{3+} and Mn^{3+} on Aluminum Silicate Phase Relations in North - Central New Mexico, U. S. A Jour. of Petrology. vol. 26 Part 2, 324 - 354.

Graton, L. C., 1910, in Lindgren, W. et al. The Ore Deposits of New Mexico: USGS Prof. Paper 68, 361p.

Groves, D. I., 1985 The Geological Setting and Genesis of Archean Gold Deposits of Australia. Geological Society of America Abstracts with Programs vol. 17 No. 7, 1985 Annual Meeting.

Harris, M., 1978 Mineralization at the Salave Gold Prospect, Austurias, Spain (abstr.): in mineral deposits genesis (Evans, A. M., compiler), Inst. Min. Metall., Trans., sect. B, vol. 87 p. 34

Hedenquist, J. W., and Henley, R. W., 1985 The Importance of CO_2 on Freezing Point Measurements of Fluid Inclusionos: Evidence from Active Geothermal Systems and Implications for Epithermal Ore Deposition. Econ. Geol. vol. 80 pp 1379 - 1406.

Hendel, E. M., and Hollister, L. S., 1985 An Empirical Solvus for CO_2 - H_2O - 2.6 wt. % Salt. Geochim. Cosmochim. Acta 45, 225 - 228.

Henley, R. W., 1984a pH Calculations for Hydrothermal Fluids. Reviews in Econ. Geol. vol. 1: Fluid - Mineral Equilibria in Hydrothermal Systems (series ed., J. M. Robertson) pp 83 - 98.

----------, 1984b Metals in Hydrothermal Fluids. Reviews in Econ. Geol. vol. 1: Fluid - Mineral Equilibria in Hydrothermal Systems (series ed., J. M. Robertson) pp 115 - 127.

Higgins, N. C., 1985 Wolframite Deposition in Hydrothermal vein system: The Grey River Tungsten Prospect, New Foundland Canada. Econ. Geol. vol. 80, pp 1297 - 1327.

Kent, S. C., 1980 Precambrian Geology of The Tusas Mountain Area, Rio Arriba Co., New Mexico: MS thesis New Mexico Inst. of Mining and Technology 151p.

Kerrich, R., 1977, Yellowknife Gold Mineralization: the Product of Metamorphic Degassing. Geol. Soc. Am. Abstr. Programs, 9 1048 - 1049

Kerrich, R., and Fyfe, W. S., 1981 The Gold Carbonate Association: Source of CO_2 and CO_2 Fixation Reactions in Archean Lode Deposits. Chemical Geol., 33, pp 265 - 294.

Krauskopf, K. B., 1979, Introduction to Geochemistry 2nd ed. McGraw - Hill Book Company 617p.

Lyakhov, Y. V., and Popivnyak, I. V., 1978 Physiochemical Conditions of Development of Gold Mineralization in Northern Buryatia. International Geol. Review, 20, pp 955 - 967.

Miyashiro, A., 1973 Metamorphism and Metamorphic Belts: George, Allen, and Unwin, London. 492p.

Nelson, B. K., and DePaolo, D. J., 1985 Rapid Production of Continental Crust 1.7 to 1.9 b.y ago: Nd Isotopic Evidence from the Basement of the North American Mid. Continent. GSA Bulletin , vol. 78, pp 746 - 754.

Norman, D. I., and Landis, G. P., 1983 Source of Mineralizing Components in Hydrothermal Ore Fluids as Evidence by $^{87}Sr/^{86}Sr$ and Stable Isotope Data from the Pasto Bueno Deposit, Peru. Econ. Geol. vol. 78 pp 451 - 465.

Petrovskaya, N. V., et al., 1973 Composition and Conditions of Formation of Gas Inclusions In Native Gold. COFFI, 7, 167.

Reinthal, W. A., et al., 1985 CO_2 Unmixing and Mineralization Controls for a Au - Ag Vein System in The Blue Mountains of NE Oregon. Geological Society of America Abstracts with Programs vol. 17 No. 7, 1985 Annual Meeting.

Roedder, E., 1984 Fluid Inclusions: Reviews in Mineralogy vol. 12 (series ed. P. H. Ribbe). Min. Soc. Am. 644p.

Silver, L., in Robertson et al., Precambrian of New Mexico, in Prep.

Smith, S. S., 1986, Precambrian Geology of the Jawbone Mountain Area, Rio Arriba County, New Mexico: MS thesis New Mexico Inst. of Mining and Technology.

Takenouchi, S., and Kennedy, G. C., 1965 The Solubility of CO_2 in NaCl Solutions at High Temperatures and Pressures. Am. J. Sc. 263, 445 - 454.

Truesdell, A. H., 1984 Geothermometers for Geothermal Exploration. Reviews in Econ. Geol. vol. 1: Fluid - Mineral Equilibria in Hydrothermal Systems (series ed., J. M. Robertson) pp 31 - 43.

Turner, F. J., 1968 Metamorphic Petrology; Mineralogical and Field Aspects. McGraw - Hill Book Company, 403p.

APPENDIX A

ANALYSIS FOR GOLD BY FIRE ASSAY AND ATOMIC ABSORPTION

Sample preparation

Between 1.5 and 3 kg of rock sample were crushed and pulverized in a swing mill to minus 80 mesh size. The powdered sample was thoroughly mixed and split using a Jones riffle.

Fire Assay

Appropriate fluxes composed of litharge, sodium carbonate, borax and flour in different proportions were prepared for the rocks which varied considerably in their compositions. For samples in which silica content was suspected to be low, some calcium fluoride and standard quartz were added to the flux.

An assay ton of powdered sample (about 29.2 gm) and 128.3 gm of the flux were mixed and fused at 1830^{o}F. Gold-free silver "in-quartz" were added to the sample before fusion. The "in-quartz" and also the litharge serve as a sink and concentrate the gold into a "lead button" that is recovered after the fusion. The button was cupelled in a furnace at about 1650^{o}F to give a tiny gold-silver bead. Usually from the color of the bead and its size, it is possible to tell which samples contained high gold values to be determined gravimetrically. The beads were parted in

warm dilute nitric acid (HNO_3); the silver readily dissolves in HNO_3 and leaves an amorphus black residue - gold. Samples which contained sufficient gold residue were assayed gravimetrically. The black residue was rinsed, heated to high temperatures to anneal and weighed on a mettler balance upon cooling.

Analysis for gold by atomic absorption spectrometry

Reagents

HNO_3, HCl, MIBK (metyl-iso-butyl-ketone), equilibrated dilute HCl (ED HCl) and a standard gold solution (1000 ppm). ED HCl was prepared by adding 19 parts of water to 1 part HCl, and shaking in a separatory funnel with excess MIBK.

Procedure

About 40ml of aqua regia with excess HCl were added to the samples whose gold content could not be determined by the gravimetric method and heated without sputtering for an hour with glass cover. The glass covers were removed and the samples heated until all the HNO_3 evaporated; AgCl precipitated at this point. Upon cooling, 20ml of ED HCl were added to the solutions of the various samples, swirled gently and tranferred into 100ml volumetric flasks.

Extraction of gold into MIBK

Fifteen millilitres of MIBK were pipetted into each flask. The flasks and their contents were shaken for about 15 mins. to ensure equilibration of the gold between the MIBK phase and aqueous phase. Enough ED HCl was then added to the flasks to bring their contents to the neck of the flasks. Standard solutions were prepared by pipetting 0.1, 0.2, 0.3, 0.4, and 0.5ml of 100ppm gold solution were pipetted into 5 separate 100ml volumetric flasks each of which contained 15ml MIBK and 20ml ED HCl. The flasks were shaken for 15 mins., and topped with ED HCl to the neck.

Atomic absorption

The standards were first aspirated into a flame and their absorbances determined on a Perkin and Elmer atomic absorption spectrophotometer. The absorbances for the various samples were then similarly determined.

The standards contained 0.01 to 0.05 mg of gold respectively. The gold content of the samples were determined from an absorbance - concentration curve plotted for the standards.

A milligram of gold in the sample translates as a troy ounce of gold per avoir dupois tonne of rock or 34.3 ppm. Precise measurements of all kinds are therefore essential if reliable values are to be obtained.

Appendix B

Analyses of rock samples from the Hopewell Area by fire assay and atomic absorption spectrometry

Sample #	Element						
	Au (ppm)	Ag (oz/ton)	Cu (%)	Pb (%)	Zn (%)	Sb ( )	As ( )
1A	0.22	--	--				
1B	0.15	<0.6	0.004	--	0.0026		
1E	<0.15*						
2	--						
3	--	--	0.005	0.0036	0.013		
4A	0.15	--	--	--	0.007		
4B	--						
4D	<0.15	0.64					
5	--						
5C-1							
5C-2	<0.15	--	0.01				
5C-3	3.11	4.11	0.148				
5C-4	12.75	--	0.015	0.16	0.1		
5C-5	<0.15						
5D	<0.15	--	0.006	0.004	0.022		
5F	<0.15	0.64	0.002	0.005	0.028		
5G-1	<0.15	--	0.002				
5G-2	3.42	--	0.017				
5H	0.31	--	0.009	0.003	0.016		
6C	0.23						
7D	--						
11D	--						
12C	--						
13B	0.15	--	0.007				
14	<0.15						

Sample #	Element						
	Au (ppm)	Ag (oz/ton)	Cu (%)	Pb (%)	Zn (%)	Sb ( )	As ( )
14B(+QTZ)	--						
14C	--						
16A-1	--	1.25	0.006	0.004	0.027		
16A-2	<0.15						
16A-3	--						
16	--	--	0.003				
17	--						
17E							
17G	<0.15						
17G-2	<0.15						
20D	12.5						
20D(ORE)	52.57						
20D-1	1160	8.45	2.37	--	0.016		
20D-3	0.31	--	0.065				
20D-4	2.8						
20D-7	1.24	--	0.54				
20D-8	515	13.7	2.06	--	0.019		
20D-9	<0.15	--					
20D-10	--						
22A	24.26						
22B	0.61						
22C	<0.15						
27E	1.87	--	0.005				
28C	--	--	--	0.002	0.009		
31	<0.15	--	--	0.0027	0.007		
35A	7.78	<0.6	0.045	0.003	0.007		

Sample #	Element						
	Au (ppm)	Ag (oz/ton)	Cu (%)	Pb (%)	Zn (%)	Sb ( )	As ( )
35B	--	--	--	--	0.006		
41B-1	0.28	--	0.006				
41B-2	<0.15						
41B-3	0.26	--	0.018				
41B-4	0.62	<0.6	0.012	0.013	0.015		
47A	<0.15						
47B							
52	--	1.13					
57A	<0.15						
57B	--	--	0.005	--	0.013		
58	--						
62A	--	<0.6	0.002	--	0.003		
62B	--	<0.6	--	--	0.003		
63B	--						
63D	5.6	--	0.22	0.003	0.007		
64A	0.15						
64B	0.31	--	0.02				
66	--	--	--				
68	0.22						
68B	0.22						
68C	0.39	<0.6	0.023				
68D	4.35	<0.6	0.095				
68E	0.31						
69	0.15						
73	--						
75B	0.33	--	0.014				

Sample #	Element Au (ppm)	Ag (oz/ton)	Cu (%)	Pb (%)	Zn (%)	Sb ( )	As ( )
76	4.9	4.07	0.114	3.80	6.26		
76E	2.8	1.8	0.130				
77	<0.15						
78B-2	--	--	--				
78B	--	<0.6	<0.002	--	0.006		
78E-2	<0.15						
79B	--	--	0.006	--	0.006		
79C	--						
80C	1.4						
80C-2	5.31	<0.6	0.121	0.007	0.008		
82	2.3	<0.6	<0.002	--	0.009		
82B	0.28	--					
82B-2		--	0.014				
83C	--						
85C	0.65	--	0.069				
88B	<0.15						
89	0.15						
89(+QTZ)	0.42	--	0.012				
89C-2	0.31	--	0.005				
91A	<0.15	--	0.01	0.019	0.016		
91B	0.15	--	0.02	0.012	0.084		
91C	7.78	<0.6	0.016	0.008	0.028		
92	0.75	1.53	0.276	0.015	0.019		
92B							
94	--						
95B	--						

Sample #	Element						
	Au (ppm)	Ag (oz/ton)	Cu (%)	Pb (%)	Zn (%)	Sb ( )	As ( )
95E	--						
101	--						
102	0.26	--	0.008				
102B	--						
105	2.15	4.10	0.134	7.32	2.25		
105B	0.31						
105C	1.37	1.0	0.067				
106D	0.19						
107							
108	--						
108B	--		<0.002	0.005	0.019		
110	--						
110B	--	--	--				
114	--						
115	<0.15	--	0.003				

-- not detected

** Detection limits

Au 0.15ppm

Ag 0.60oz/ton

Cu,Pb,Zn .. 0.002%

Appendix B (continued)

Nuclear Activation Analyses of Samples from the Hopewell Area

Sample	As (ppm)	Sb (ppm)	Au (ppb)
CG-5B*	4	0.5	6.7
1ZK-82	6	4.2	10
BMR-16*	240	29	3.5
1ZK-5F	5	7.7	8.7
S-131*	3	2.8	0.6
ADIT #3	30	18	12000
1ZK-4A	6	4.8	0.6
S-75D*	1	5.0	20
1ZK-133	2	4.3	2.5
BMR-20*	20	3.8	0.8
1ZK-14A	5	17	4.7
1ZK-129B	14	18	3.7
1ZK-78B-2	4	8.2	<0.1
CG-5A*	4	0.5	0.4
1ZK-127B	4	4.3	0.9
1ZK-14B	5	5.7	9.6
1ZK-126B	14	4.2	1.1
1ZK-66	8	0.7	0.5
BMR-18*	160	11	0.2
S-112A*	4	4.2	4.8
S-59*	4	1.1	1.5
1ZK-136	2	2.6	0.7
S-73*	5	1.3	0.5
1ZK-31B	88	4.3	0.4
1ZK-35B	5	4.3	16
1ZK-41B-4	23	9.9	630
BMR-13*	28	4.6	0.6
1ZK-5	7	6.8	1.0
1ZK-5G-1	3	5.5	0.6
1ZK-1A	4	2.8	0.9

* sample obtained from areas adjacent to the study area

APPENDIX C

COMPUTER PROGRAM FOR ESTIMATING OF PRESSURE OF ENTRAPMENT

```
  1 DIM A(10,10)
  2 N=0
  3 CLEAR
 10 REM PROGRAM TO CALC PRESSURE
        GIVEN NACL, CO2, & T
    OF          THE SOLUTION
 20 DISP "ENTER T(DEG C), NACL(E
    Q. WT %), & CO2(WT %)"
 30 INPUT T,S,C
 35 IF N=1 THEN GOTO 155
 40 DATA 412.3229,7080.396,-3682
    .125,734.265,-58.89981,2.907
    367,-.0518376
 50 DATA -5.93686,-80.29987,42.1
    8668,-8.575728,.6607719,-.03
    176085,.0005663473
 60 DATA .03014514,.2741394,-.14
    77382,.03155945,-.00226249,.
    0001060833,-.000001911892
 70 DATA -.00005813489,-.0002033
    297,.0001252059,-.0000325211
    8,.000001805746,-7.988915E-8
    ,1.536529E-9
 80 DATA 1.680884E-8,-.000000325
    895,1.553996E-7,-2.517086E-8
    ,2.480923E-9,-1.207413E-10,2
    .042959E-12
 90 DATA 7.200292E-11,2.014488E-
    10
100 DATA -1.301214E-10,3.296728E
    -11,-1.8774455E-12,8.581649E
    -14,-1.658716E-15
110 FOR Y=1 TO 6
120 FOR X=1 TO 7
130 READ A(X,Y)
140 NEXT X
150 NEXT Y
155 P=0
160 FOR Y=1 TO 6
170 FOR X=1 TO 7
180 P=P+A(X,Y)*C^(X-1)*T^(Y-1)
190 NEXT X
200 NEXT Y
202 F=.93*EXP(.09*S)/1.596
210 P=P*F
215 IF N=1 THEN GOTO 240
220 PRINT " T    CO2    NACL    PRE
    SSURE"
230 PRINT "(C)   WT%    EQ.WT%    B
    ARS"
235 N=1
236 PRINT
240 PRINT USING "DDD.,3X,DD.D,3X
    ,DD.D,3,DDDDDD." ; T,C,S,P
250 GOTO 20
260 STOP
```

Appendix D

Tf CO_2	Tm ice	Tm clath rate	Equiv Wt. % NaCl	Th CO_2 v-l (l-v%)	V % H_2O	ρ CO_2 (g/c^3)	(m/l)	Bulkρ m/l	Molar Vol (c^3/m)	Bulk Comp Mol% H_2O	Th CO_2:H_2O
-59.0				9.0	0	.86	19.6				
-60.0				1.7	0	.90	20.7				
-58.5				14.4	0	.81	18.4				
-56.5	-17.5	5.3	8.5	22.2	80	.75	17.0	46.7	21.4	90.7	
	-8.3			24	85	.72	16.4	49.5	20.2	93.7	
	-7.8	3.4	11.4	25	80	.71	16.1	47.6	21	92	
				19.1	25	.78	17.7	26.8	37.3	48.7	
-56.8	-15.5	5.3	8.5	25.6	80	.70	15.9	47.5	21.1	92.3	
				25.8	65	.70	15.9	41.4	24.2	86	
-56.5				16.7	25	.80	18.2	27.2	36.8	50	
					65						322
					70						320
				22.1	75	.75	17.0	45.7	21.9	90	
				19.4	80	.79	18	48	20.8	91	
				20.0	80	.77	17.5	47.8	20.9	91	
				27.9	75	.67	15.2	45	22.2	90.7	
				19.2	70	.79	18.0	44.2	22.6	86.7	
	-10.6			29.1	60	.63	14.3	38.3	26.1	83.3	
				23.3	85	.73	16.6	49.5	20.2	93.7	
				24	85	.72	16.4	49	20.4	93	
				24	85	.72	16.4	49	20.4	93	
				21.2	80	.76	17.3	47.8	20.9	91.7	
				19.9	90	.78	17.7	51.7	19.3	95	
				16.4	70	.81	18.4	44	22.7	86	
				21	80	.76	17.3	47.8	20.9	92.5	
				22.5	70	.74	16.8	44	22.7	88.3	236(D)
				16.5	80	.81	18.4	48	20.8	90.5	
				21.5	85	.75	17.0	49.5	20.2	93.7	
				16.4	60	.81	18.4	40.8	24.5	79	260(D)
					92.5						265
				26.7	50	.68	15.5	35	28.6	77	
				27.5	70	.67	15.2	42.9	23.3	88.5	
-56.6				13.9	0	.83	18.9				
				16.0	50	.81	18.4	37	27	73.1	
-56.6				17.0	50	.80	18.2	36.2	27.2	73	
-56.6				7.0	0	.87	19.8				
-56.6				1.8	0	.90	20.7				
-56.6					0						
-56.6				8.9	25	.86	19.6	28	35.7	53	
				18	25	.79	18.0	27.2	36.8	50.5	
-56.6				-3.8	0	.93	21.1				
-56.6				0	0	.92	20.9				
				18.9	20	.78	17.3	25.5	39.2	44	
-56.6				-3.8	0	.93	21.1				
				8.5	0	.86	19.6				
				7.9	0	.86	19.6				
				8.9	0	.85	19.3				

Appendix D

Tf CO_2	Tm ice	Tm clath rate	Equiv Wt. % NaCl	Th CO_2 v-f (l-v*)	V % H_2O	CO_2 ρ (g/c^3)	CO_2 (m/l)	Bulk ρ m/l	Molar Vol (c^3/m)	Bulk Comp Mol% H_2O	Th CO_2:H_2O
-56.9				9.1	0	.85	19.3				
				10.3	0	.85	19.3				
				11.5	0	.84	19.1				
-56.9				9.6	0	.85	19.3				
-56.9					0						
-56.9					0						
-56.9					0						
-56.9					0						
-56.9					0						
	-9.0	5.1	9.0	12.3	80	.84	19.1	48	20.8	90	
	-9.3	5.1	9.0		90	.77	17.5	51.4	19.5	95	
		5.1	9.0	25.7	75	.70	15.9	45.6	21.9	90	
-59.3					0						
-59.3					0						
	-10.5			27.8	90	.66	15.0	51.2	19.5	96.5	312
				9.7	0	.86	19.6				
				28.6	90	.65	14.8	51.2	19.5	96.5	
				17.9	80	.79	18.0	47.9	20.9	90	
				24.9	85	.71	16.1	49.5	20.2	94	
				23.7	85	.73	16.6	49.5	20.2	93	206(D)
-57.6				7.1	0	.87	19.8				
-57.4				-11.3	0	.97	22.1				
				25	90	.71	16.1	51.2	19.5	96.5	270
		4.1	10.5	24.6	85	.71	16.1	49.5	20.2	94	280
-60		5.3	8.5	21.8	70	.75	17.0	44	22.7	87	278
-60				7.3	0	.88	20.0				
-60				8.4	0	.87	19.8				
		5.3	8.5	22.5	70	.74	16.8	44	22.7	88.5	278
-60.5				2.4	0	.90	20.5				
				18.5	50	.79	18.0	36.8	27.2	73	225(D)
				-1.5	0	.93					
-59.7				-12.1	0	.97	22.1				
-59.7				-13	0	.98	22.3				
-59.7				3.1	0	.90	20.5				
-59.7				5.9	80	.89	20.2	48	20.8	90	
-59.7				3.1	0	.90	20.5				
				-11.8	0	.97	22.1				
				7.6	0	.87	19.8				
				8.8	0	.86	19.5				
		3.3	11.6	25.8	85	.70	15.9	49	20.4	93.5	302
-55				28.3	90	.66	15	51.4	19.5	96	
-56.1		4.1	10.5	5.5	80	.89	20.2	48	20.8	90	260
		3.7	10.9	4.4	80	.89	20.2	48.3	20.7	90	286
				5.5	85	.89	20.2	50.5	19.8	93	
		4.0	10.6	28.3	75	.66	15.0	45	22.2	90.5	290
		3.6	11.2	25	75	.71	16.1	45	22.2	90	298
		4.5	9.8	25.8	80	.70	15.9	47.2	21.2	92	274
				18.6	90	.79	18.0	51.7	19.3	96	
		5.3	8.5	22.6	70	.74	16.8	44	22.7	88	280

Appendix D

Tf CO_2	Tm ice	Tm clath rate	Equiv Wt. % NaCl	Th CO_2 v-l (l-v%)	V % H_2O	ρ CO_2 (g/cc^3)	ρ CO_2 (m/l)	Bulk ρ m/l	Molar Vol (cc^3/m)	Bulk Comp Mol% H_2O	Th CO_2:H_2O
		3.1	11.8	26.1	80	.70	15.9	47.2	21.2	92	276
		5.1	9.0	21.3	75	.76	17.3	45.6	21.9	90	265
		3.1	11.8	26.9	75	.68	15.5	45	22.2	91.5	284
				21.4	75	.76	17.3	45.6	21.9	89.5	
				13.9	10	.83	18.9	22.5	44.4	27.5	216(D)
				16.2	25	.81	18.4	27.4	36.5	51.5	
				18.6	25	.79	18.0	27.5	36.4	51.5	
				24.0	80	.72	16.4	47.6	21	92	
				26.9	70	.68	15.5	43.2	23.2	89	
				22.8	60	.74	16.8	40	25	82	236(D)
				12.6	25	.84	19.1	24.7	40.5	36	238(D)
				20.0	75	.77	17.5	42.4	23.6	84	
				19.4	60	.78	17.3	40	25	80	
				10.4	50	.85	19.3	37.8	26.5	73	
				15.5	60	.82	18.6	41	24.4	80	
				21.4	50	.76	17.3	36.5	27.4	76	
				26.5	85	.69	15.7	49.5	20.2	95	
-56.5		4.0	10.6	25.7	75	.70	15.9	45.5	22	90	260
-57.5				27.0	85	.68	15.5	49.5	20.2	95	335
	-14.1			30.1	85	.58	13.2	49	20.4	95	255
	-12.6			27.9	90	.66	15	51	19.6	96	230
				27	80	.68	15.5	47	21.3	90	
-55.5				28.2	80	.66	15.0	47.5	21.0	93.5	
-56.5				11.6	80	.85	19.3	48	20.8	90.5	
				15.5	0	.82	18.6				
				-5.4	0	.94	21.4				
				18.8	30	.79	18.0	29.4	34	58	
	-12.6			25	75	.71	16.1	45.7	21.9	90	283
	-15.0			23	70	.74	16.8	44	22.7	89	288
	-17.5			21.6	70	.76	17.3	44	22.7	88	
				22.4	80	.74	16.8	47.6	21	92.5	
				25.8	75	.70	15.9	45.6	21.9	90	225
	-16.0	5.5	8.4	21.8	85	.75	17.0	49.5	20.2	94	
	-16.0	5.5	8.4	25.6	80	.70	15.9	47.5	21.1	92.4	
	-14.4	5.7	8.0		90						
	-16.1	5.9	7.8	22.9	85	.74	16.8	49.5	20.2	94	
	-15.5	6.0	7.6								
	-16.0	5.2	8.7		85	.75	17.0	49.5	20.2	94	
		5.5	8.4	26.8	93	.68	15.5	52.8	18.9	97.5	
				9	70	.86	19.6	45	22.2	86.5	279
				6.8	20	.88	20.0	27	37.0	43.5	246(D)
				12.3	35	.85	19.3	32	31.3	61.5	218(D)
				16.4	65	.82	18.6	42.5	23.5	78.5	222(D)
				22.3	85	.75	17.0	49.5	20.2	93.5	209
				25.0	90	.72	16.4	52	19.2	97	206
				24.6	85	.72	16.4	49	20.4	93.5	291
				19.0	90	.79	18.0	51.8	19.3	96	276
				19.6	85	.78	17.7	49.5	20.2	96.5	276
				18.7	90	.79	18.0	51.8	19.3	95	276

Appendix D

Tf CO_2	Tm ice	Tm clath rate	Equiv Wt. % NaCl	Th CO_2 v-l (l-v*)	V %	H_2O	ρ CO_2 (g/c^3)	ρ CO_2 (m/l)	Bulk ρ m/l	Molar Vol (c^3/m)	Bulk Comp Mol% H_2O	Th CO_2:H_2O
				10.4	25		.85	19.3	24.6	40.7	31	274
				25.1	90		.72	16.4	52	19.2	97	208
				25.8	85		.70	15.9	49	20.4	92	290
				24.4	65		.72	16.4	42	23.8	88	246
				22.2	85		.75	17.0	49.5	20.2	93.5	300
				20.8	90		.77	17.5	51.5	19.4	96	208
				25.6	85		.7	15.9	49	20.4	93.5	280
				11.0	40		.85	19.3	23.4	42.7	30	290
				22.3	80		.75	17.0	48	20.8	92	210(D)
				16.4	25		.82	18.6	27.6	36.2	50	325(D)
				28.6	80		.65	14.8	47.3	21.1	92.5	256
				28.8	70		.65	14.8	43	23.3	88	355
				19.0*	50		.20	4.6	30	33.3	82	355
				19.0*	60		.20	4.6	35	28.6	87.5	345
				21.3*	25		.21	4.8	17.5	57.1	58	354
				28.7*	50		.30	6.8	30	33.3	85	351
				28.8*	80		.30	6.8	45.5	22.0	95	321
				11.7	80		.85	19.3	48.5	20.6	91	205(D)
				18.8*	25		.18	4.1	17	58.8	57.8	330
				21.5	90		.77	17.5	51.5	19.4	96	284
				19.1*	50		.20	4.6	30	33.3	84.5	350
				25.6	50		.70	15.9	35.5	28.2	84	246(D)
				23.4	65		.73	16.6	41.8	23.9	87	318
				19.0	70		.79	18.0	44	22.7	86.5	220
				10.5	65		.85	19.3	42.5	23.5	82.3	250(D)
				15.5	75		.83	18.9	42.5	23.5	85	238(D)
				11.0	60		.85	19.3	41.7	24	81.4	
				20.0	93		.78	17.7	53	18.9	97.5	176.8
				12.5	60		.85	19.3	41.7	24	81.2	350
				18.5	80		.79	18.0	48	20.8	90	238(D)
				23.6	80		.73	16.6	48	20.8	92	255(D)
				21.0	60		.77	17.5	40.3	24.8	83	189.6
				23.0	70		.75	17.0	43.8	22.8	87	254(D)
		3.8	10.8	23.8	75		.73	16.6	45.5	22	90	290
				24.0	50		.73	16.6	36	27.8	76.5	288(D)
		5.2	8.7	25.9	80		.70	15.9	47.5	21.1	91.5	273
				16.6	25		.82	18.6	27.6	33.2	58.5	290(D)
				28.6	90		.65	14.8	51.2	19.5	96.5	245
		5.5	8.4	29.0	70		.66	15.0	43	23.3	88	318
				21.6	50		.77	17.5	36.6	27.3	77	378
				27.2	80		.69	15.9	47.5	21.1	92	311
		3.3	11.6	27.5	80		.69	15.9	47.5	21.1	92	280
				25.0*	95		.25	5.9	53	18.9	98	200
				13.1	75		.83	18.86	28	35.7	44	238(D)
				20.8	75		.77	17.5	45.5	22		218(D)
				13.1	80		.83	18.9	48.5	20.6		215(D)
				17.5	85		.80	18.2	50	20		220(D)
				1.6	70		.91	20.7	45.5	22		301
				3.0	80		.90	20.5	48.8	20.5		305

Appendix D

Tf CO_2	Tm ice	Tm clath	Equiv Wt. % NaCl	Th CO_2 v-l (l-v*)	V % H_2O	ρ (g/c^3)	CO_2 (m/l)	Bulk ρ m/l	Molar Vol (c^3/m)	Bulk Comp Mol% H_2O	Th CO_2:H_2O
				20.8	80	.77	17.5	48	20.8		200(D)
				23.7	90	.73	16.6	51.5	19.4		240
				13.4	90	.83	18.9	52	19.2		310
				11.5	80	.85	19.3	48.5	20.6		200(D)
				23.0	85	.75	17.0	49.5	20.2		248
				26.2	85	.71	16.1	49.4	20.2		200(D)
				23.0	90	.75	17.0	51.6	19.4		215(D)
				21.0	85	.77	17.5	49.5	20.2		207(D)
				20.8	80	.77	17.5	48	20.8		215
				23.7	90	.73	16.6	51.5	19.4		195
				-13.8	20	1.08	24.6	31	32.3	40	191(D)
				0.7	20	.90	20.9	28	35.7	47	190(D)
				-9.0	25	.96	21.8	31	32.3	45	235
				-3.5	60	.94	21.3	42	28.3	63.5	190(D)
				-2.5	90	.93	21.1	52.5	19.1		190(D)
				1.0	5	.92	20.9	23	43.5	24	218(D)
		5.3	8.5	22.4	15	.76	17.3	22.5	44.4	37	250(D)
				28.5	50	.65	14.8	35	28.6	79.5	445
	-14.8	5.6	8.1	20.5	85	.77	17.5	49.5	20.2	93.5	
	-16.0	5.2	8.7	27.7	80	.67	15.2	47	21.3	92.5	
		5.3	8.5	25.8	75	.70	15.9	46.5	21.9	90	
		5.5	8.4								
		5.3	8.5	27.3	50	.68	15.5	35.6	28.1	79	
		5.7	8.0	26.7	90	.68	15.5	51.4	19.5	96	
		5.3	8.5	26.6	90	.68	15.5	51.4	19.5	96	
		5.7	8.0	20.0	85	.78	17.7	50	20	93	
		4.2	10.1	23.4	80	.74	16.8	47.6	21	92.5	
		4.2	10.1	25.5	80	.70	15.9	47.5	21.1	92.5	
		6.0	7.6	28	90	.66	15.0	51.4	19.5	97	
		4.7	9.7	25.2	85	.70	15.9	49.5	20.2	94	
		5.5	8.4	22.2	85	.76	17.3	49.5	20.2	93.5	
		3.7	10.9		90						
		4.5	9.8		95						
		4.3	10.0								
		3.8	10.8	29.9	70	.59	13.4	42.5	23.5	90	315
		3.7	10.9	17.7	60	.80	18.2	40.8	24.5	80.5	320
		3.0	11.9	17.4	85	.80	18.2	49.5	20.2	93	245(D)
	-14.3	3.6	11.2	22.0	75	.75	17.0	45.6	21.9	89.5	287(D)
		3.7	10.9	24.4	40	.72	16.4	31	32.3	69	285(D)
				24.4	75	.72	16.4	46	21.7	91	290
-57.1	-15.0			14.7	93	.82	18.6	52.8	19.0	96.5	240
-57.1				15	95	.82	18.6	52.9	18.9	96.5	250
		4.2	10.1								265
		4.2	10.1								260
-56.8	-15.3	5.6	8.1	27.3*	75	.29	6.6	44.2	22.6	90	290
-56.8	-15.3	5.4	8.4	25.5*	80	.25	5.7	45	22.2	90	269
-59.8	-14.8			25.9	80	.70	15.9	47.5	21.1	92	315
-59.8	-15.4										300
	-14.1				95						230

Appendix D

Tf CO_2	Tm ice	Tm clath rate	Equiv Wt. % NaCl	Th CO_2 v-l (l-v*)	V % H_2O	ρ CO_2 (g/c^3)	CO_2 (m/l)	Bulk ρ m/l	Molar Vol (c^3/m)	Bulk Comp Mol% H_2O	Th CO_2:H_2O
					95						230
	-16.8	6.1	7.2	26.5	85	.68	15.5	49.5	20.2	95	315
	-17.0				90						290
	-19.7	3.8	10.8	23.5	60	.73	16.6	44	22.7	89	265
		3.7	10.9	25.7	90	.70	15.9	51.3	19.5	96.5	238
		4.0	10.6		80						
	-20.0	3.1	11.8	19.9	70	.78	17.7	44	22.7	86.5	
		5.6	8.1	8.0	80	.87	19.8	48.5	20.6	90.5	200(D)
		4.5	9.8	8.0	70	.87	19.8	45	22.2	87	200(D)
	-20.1	4.2	10.1	28.3	70	.66	15.0	43.9	22.8	89.5	235(D)
		3.4	11.4	25.0	85	.70	15.9	49	20.4	93	238(D)
				15.0	10	.82	18.6	22.2	45	26	200(D)
		3.3	11.6	24.1	85	.72	16.4	49.5	20.2	94.5	241
				23.2	30	.74	16.8	28.3	35.3	60	190(D)
				24.0	60	.73	16.6	40	25	82	330
	-18.3	4.2	10.1	26.3	80	.69	15.7	47.5	21.1	92	238
	-18.3	4.2	10,1	25.7	80	.70	15.9	47.5	21.1	92	193(D)
				24.8	75	.71	16.1	45.5	21.9	89	229(D)
		3.1	11.8	30.5	70	.62	14.1	43	23.3	89	325
		3.1	11.8		95						250
				29.5	80	.63	14.3	47	21.2	92.5	241
		3.3	11.6	29.8	80	.63	14.3	47	21.2	92.5	274
					80						291
					80						270
				22.4	50	.75	17.0	36.5	27.4	76	280
				17.8	20	.80	18.2	25.5	39.2	44	280
				26.0	60	.71	16.1	39.5	25.3	82	349
				22.1	85	.75	17.0	49.5	20.2	93.5	245
		3.9	10.7	27.8	70	.69	15.7	43.7	22.9	89	290
				26.6	50	.71	16.1	36	27.8	78	310(D)
				27.4	50	.69	15.7	35.5	28.2	80	342(D)
				27.3	50	.69	15.7	35.5	28.2	80	260
				0.5	15	.91	20.7	25.8	38.8	37.5	291
				12.2	65	.85	19.3	43.2	23.1	83	263(D)
				9.2	70	.86	19.6	45	22.2	86.5	257(D)
				10.9	65	.85	19.3	43.2	23.1	83	274(D)
				13.5	75	.83	18.9	46.5	21.5	89	274(D)
				10.5	65	.86	19.6	44.1	22.7	86	298
				8.1	15	.88	20.0	25	40	36	
				12.8	20	.85	19.3	26.3	38	42	282
		4.0	10.6	14.1	75	.83	18.9	46.2	21.6	89	296
				18.5	50	.79	18.0	36.5	27.4	72.5	260(D)
				2.3	10	.92	20.9	24.6	40.7	30	261
				12.6	40	.84	19.1	33.8	29.6	68	274(D)
				23.3	70	.73	16.6	44	22.7	88	210(D)
				18	15	.80	18.2	24	41.7	38.5	204(D)
				14.4	50	.83	18.9	37.5	26.7	75	
				21.9	35	.75	17.1	34	29.4	72	206(D)
				25	40	.71	16.4	31	32.3	68.5	280(D)

Appendix D

Tf CO_2	Tm ice	Tm clath rate	Equiv Wt. % NaCl	Th CO_2 v-l (l-v*)	V % H_2O	ρ CO_2 (g/c^3)	ρ CO_2 (m/l)	Bulk ρ m/l	Molar Vol (c^3/m)	Bulk Comp Mol% H_2O	Th CO_2:H_2O
		4.2	10.1	22.7	70	.74	16.8	44	22.7	88	308
				23.6	40	.73	16.6	31	32.3	66.5	228(D)
				25.3	60	.70	15.9	39	25.6	82.5	
				29.6	50	.63	14.3	35	28.6	80	338
				25.8	50	.70	15.9	35.7	28.0	77.5	283(D)
				25.9	60	.70	15.9	39	25.6	82.5	309(D)
				29.6	30	.63	14.3	30	33.3	68	294(D)
				13.7	35	.84	19.1	31.8	31.4	62.5	239(D)
				7.7	20	.87	19.8	26.8	37.3	43.5	243(D)
				11.8	10	.85	19.3	23.2	43.5	27.5	225(D)
				16.8	70	.80	18.2	44.5	22.5	86.5	
				14.0	40	.84	19.1	32.8	30.5	65.5	225(D)
				15.3	25	.82	18.6	45.6	21.9	87.5	218(D)
				23.8	55	.73	16.6	38.2	26.2	80	232(D)

D = Decrepitate

* = Homogenization to vapor phase

This thesis is accepted on behalf of the faculty of the Institute by the following committee:

David A. Norman — Co-Advisor — James M Robertson

D. Norman — J. Robertson

Andrew R Campbell

A. Campbell

10 Jan - 1986

Date

Plate 2

CROSS SECTION

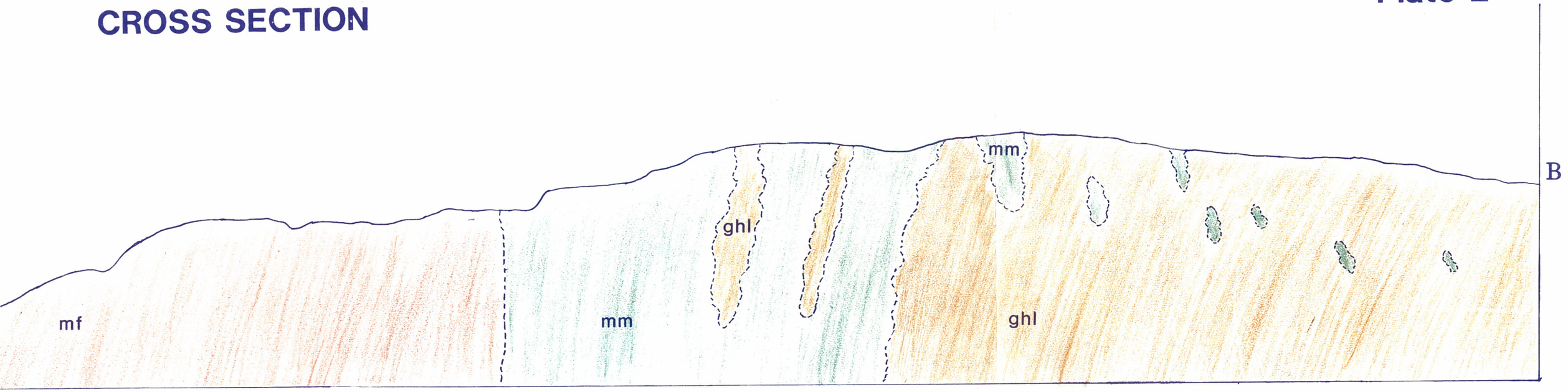

Scale 1:3000

CROSS SECTION

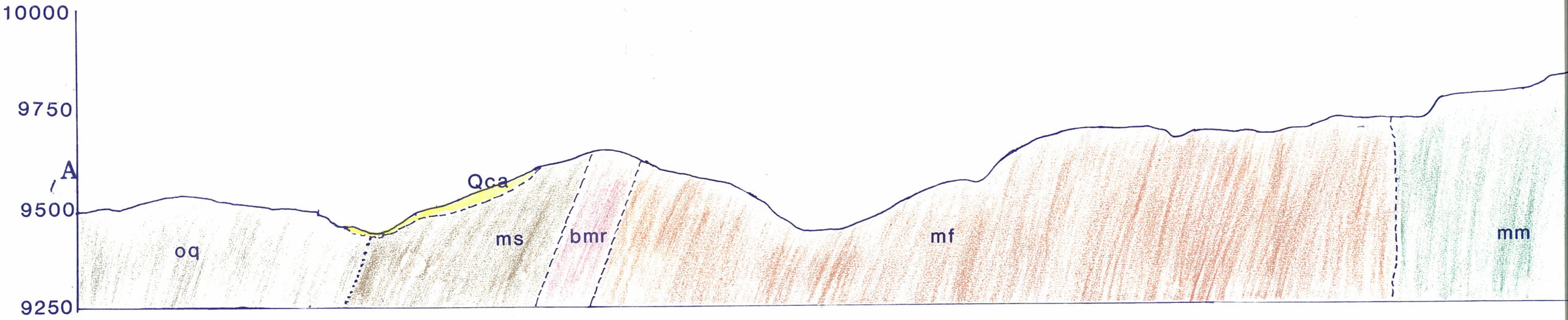

Scale 1:3000